

High Power High Energy Ytterbium-doped Fiber Amplifier System

Submitted in partial fulfillment of the requirements for

the degree of

Doctor of Philosophy

in

Electrical and Computer Engineering

Jinxu Bai

B.S., Electrical Engineering, Tianjin University

M.S., Electrical and Computer Engineering, Carnegie Mellon University

Carnegie Mellon University
Pittsburgh, PA

Dec, 2016

© Copyright by Jinxu Bai 2016

All Rights Reserved

Acknowledgement

My first and foremost thanks go to Prof. Elias Towe, my academic advisor and the mentor of my life. I still can remember the first day I come to US and met him. Even since then, he not only guides me how to do the research but also how to live in a new country. Being a CMU PhD student is very challenging, especially as a non-native speaker of English. Prof. Towe always helped me through the most difficult time of my research and my life. I will leave CMU soon, but CMU feels like another home to me and Prof. Towe is like my family member.

I would like to thank Dr. Jim Zhang and Dr. Manoj Kanskar from nLight, Inc, and Dr. Xiuquan Ma from University of Michigan, for proving us with the chirally-coupled-core fibers. Their intelligence and kindness helped me to build a fantastic new laser system. I appreciate their valuable suggestions and useful discussions.

I want to thank all my committee members, Prof. Ozan Tonguz, Prof. Maysam Chamanzar, and Prof. Randall Feentra, who helped me during my defense at an awkward time of the year. I appreciate their valuable suggestions, critiques, advice and feedback on my research and thesis. I want to thank Prof. David Greve, my former committee member, who also provided enlightenment on semiconductors.

I would like express my sincere thanks to the following CMU staff: Nathan Snizaski, Patricia L. Grieco, and Kevin Bosle for helping about my PhD life at CMU.

I had a surgery recently, and I want to thank my surgeon Dr. Matthew Holtzman and his team at UPMC for helping me to quickly recover from the disease.

During my stay at CMU I met a group of intelligent friends. I want to thank Xiaoyu Bai, Min Xu, Yu-Han Liang, Ellen Reifler and so many more for their help about my life and research. I would like to express my thanks to Zhengkun Dai for useful discussions about my experiments.

Here, I want to express my special thanks to my parents and the whole family. No matter how far I go, no matter what choices I made, no matter how difficult life is, they are always my strongest supporters and protectors.

Finally, I want to thank my wife Chang Yang, who is also a PhD student of Prof. Towe. She is not only my dear wife, but also my best friend, my best research collaborator, and my soul-mate. Through happiness and difficulties in life, we will always have each other.

The financial support for the work contained in this PhD dissertation was provided by DARPA Grant N66001-12-1-4202 and Grant HR0011-15-1-0009.

My thesis committee:

Prof. Elias Towe, advisor

Prof. Ozan Tonguz

Prof. Maysam Chamanzar

Prof. Randall Feenstra

Abstract

Fiber amplifiers with high power and high pulse energy are strongly in demand for both scientific research and industrial applications. Ytterbium-doped fiber has been an outstanding choice for its broad-gain bandwidth and excellent power conversion efficiencies. In this dissertation, we introduced a compact high power high pulsed energy laser system with chirally coupled core (3C) Yb-doped fibers as the gain media.

Traditional standard fibers and photonic crystal fibers are not suitable for compact high power high pulse energy laser systems because of poor higher order modes (HOMs) management and complicated air-hole structure. Newly invented 3C silica fibers solve these problems. A helical side-core around the Yb-doped central core extracts the HOMs from the central core. By adjusting this chirally structure, the core of the 3C fiber can be enlarged and the transverse mode of the fiber can be single mode at certain wavelengths.

To simulate the amplification process with high power high pulse energy better, a new modeling method based on a combination of the rate equations and the nonlinear Schrödinger equations is invented. The gain was calculated from rate equations and the pulse evolution was analyzed using nonlinear Schrödinger equation. The simulation provided a good guidance for building compact high power high pulse energy laser systems.

To achieve high power and high pulse energy, the system is designed as a two-stage structure. The laser system provides 1064 nm pulsed laser beam with

excellent beam quality ($M^2 < 1.2$). Achieved average power is 121.4 W. The pulse energy is as high as 1.2 mJ with 25 ns pulse width and 100 kHz repetition rate. The total gain of the amplification system is 39 dB, which is outstanding among the high power high pulse energy lasers. The slope efficiency of the gain fiber is 82 %, which is exceptionally remarkable compared with other types of large mode area fibers. This high pulse energy high power laser system can be applied in different areas, like medical instruments, material processing and other industrial applications.

Table of Contents

Acknowledgement	III
Abstract	V
Table of Contents	VII
List of Figures	IX
List of Tables	XII
1. INTRODUCTION	1
1.1 Rare Earth Doped Fiber Amplifiers	1
1.2 Thesis Statement	6
2. YTTERBIUM-DOPED FIBERS	10
2.1 Fiber Gain Media	10
2.1.1 Standard fibers	13
2.1.2 Photonic Crystal Fibers	15
2.1.3 Chirally Coupled Core Fibers	17
2.2 Core Pumping and Cladding Pumping	21
2.3 Fiber Safety and Thermal Management	23
2.4 Summary	25
3. MODELING OF RARE-EARTH DOPED FIBER AMPLIFIERS	26
3.1 Traditional Modeling	26
3.1.1 Power, gain, and pulse energy	26
3.1.2 Dispersion, nonlinearity, and pulse profile	29
3.2 New Approach	29
3.2.1 Gain saturation	29
3.2.2 The unified model equation	30
3.3 Reliability of the New Model	32
3.4 Advantages of the New Model	34
3.4.1 Classic multi-stage structure for high power laser system	34
3.4.2 Analysis of pulse amplification process with different modeling methods	36
3.5 Summary	47
4. YTTERBIUM-DOPED AMPLIFIERS CONSTRUCTED FOR STANDARD FIBER	48
4.1 Ytterbium-doped Standard Fiber Amplifiers	48
4.1.1 Continuous-wave and pulsed seed lasers	48
4.1.2 Design and configuration considerations for the multi-stage fiber amplifiers	53
4.1.3 Analysis of amplification in standard fiber amplifiers	56
4.2 Issues of Amplification	60
4.2.1 Coupling and slope efficiency	60
4.2.2 Amplified spontaneous emission	62
4.3 Summary	70
5. HIGH POWER HIGH PULSE ENERGY YTTERBIUM-DOPED LASER	

SYSTEMS.....	72
5.1 Seed Laser	73
5.2 Two-stage High Power Chirally-Coupled-Core Fiber Amplification System	76
5.2.1 System design and configuration.....	77
5.2.2 Analysis of pulse amplification in high power laser systems.....	82
5.3 Applications of the high power laser system.....	94
5.4 Summary	95
6. CONCLUSION AND OUTLOOK.....	97
6.1 Summary of the Dissertation.....	97
6.2 Outlook.....	99
REFERENCE	101

List of Figures

Figure 1.1 Structure of high power high pulse energy Yb-doped amplification system.	5
Figure 1.2 Gain and slope efficiency in one level amplifier with different types of fibers.....	8
Figure 2.1 Slope efficiency of rare earth doped fibers.....	10
Figure 2.2 Absorption and emission of Ytterbium doped fiber.....	12
Figure 2.3 Fiber core diameters and fiber modes.....	12
Figure 2.4 Yb-doped standard fiber.....	13
Figure 2.5 Number of linearly polarized modes supported by fibers with different core sizes and NAs. LMA is nLight Yb1200-25/250DC (core diameter 25 μm , NA 0.07); PCF is NKTPhotonics DC-200-40-PZ-Yb (core diameter 40 μm , NA 0.03); 3C is nLight Yb700-34/250DC-3C (core diameter 34 μm , NA 0.065).....	14
Figure 2.6 Structure of Photonic Crystal Fibers.....	16
Figure 2.7 (a) Structure of standard fiber; (b) Structure of 3C fiber; (c) TEM photo for fiber ends of nLight Yb700-34/250DC-3C fiber.....	18
Figure 2.8 Mode loss vs fiber core diameter in 3C fiber.....	20
Figure 2.9 (a) Single cladding fiber & pumping method; (b) Double cladding fiber & pumping method.....	21
Figure 2.10 Damaged fiber end surface.....	23
Figure 2.11 (a) Laser beam leaking at junction part; (b) Thermal management and fiber protection.	24
Figure 3.1 A two-stage fiber amplifier system.	31
Figure 3.2 Compressed output power as a function input pump power launched into the amplifier system.	34
Figure 3.3 Structure of Pre-amplifier.....	35
Figure 3.4 Structure of Main Amplifier.....	36
Figure 3.5 Average output power for the (a) pre- and (b) main amplifier as a function of propagation length.....	38
Figure 3.6 Output power for the (a) pre- and (b) main amplifier as a function of pump power. ...	39
Figure 3.7 Pulse evolution in the main amplifier.....	41

Figure 3.8 Gain of the (a) pre- and (b) main amplifier as a function of propagation length.....	42
Figure 3.9 Time domain comparison of the input and output pulse envelopes in the main amplifier for (a) 2-ns pulse input, and (b) a 2-ps pulse input.....	44
Figure 3.10 Frequency domain comparison of the spectral content of a pulse in the (a) pre- and (b) main amplifier.	45
Figure 3.11 B-integral, a measure of fiber nonlinearity, as a function of normalized length along pre- and main amplifier.....	46
Figure 4.1 Configuration of continuous-wave seed laser.	49
Figure 4.2 Actual size of continuous-wave seed laser.	50
Figure 4.3 Configuration of pulsed seed laser.	51
Figure 4.4 Actual size of pulsed seed laser.	52
Figure 4.5 Spectra of continuous-wave and pulsed seed lasers.....	52
Figure 4.6 Configuration of the whole amplification system.	54
Figure 4.7 Configuration of the pre-amplifier.	54
Figure 4.8 Configuration of the main amplifier.	56
Figure 4.9 Spectra of the continuous-wave laser amplification process.....	56
Figure 4.10 Spectra of the pulsed laser amplification process.....	58
Figure 4.11 PD signal of the pulse with 3 ns pulse width.....	59
Figure 4.12 Electrical spectrum of the pulsed laser output.	59
Figure 4.13 Comparing between theoretical and experimental results for backward ASE generated in 2 m long Yb-doped fiber with 2 W pumping.	63
Figure 4.14 Amplified spontaneous emission generation in Yb-doped fiber.	64
Figure 4.15 Amplified spontaneous emission spectra in Yb-doped fibers (0.3, 2, & 8 m) reaching saturation.....	65
Figure 4.16 Amplified spontaneous emission and lasing wavelength shifting in Yb-doped fibers with different fiber lengths and threshold pump powers.....	66
Figure 4.17 Energy level diagram of Yb ³⁺	67
Figure 4.18 Lasing peak instability spectra comparison in 0.3, 2 & 8 m long fibers.....	69
Figure 5.1 3C Yb-doped high power high pulse energy laser system.....	72

Figure 5.2 Configuration of seed laser.....	74
Figure 5.3 Actual size of seed laser.....	75
Figure 5.4 Spectra of the pulsed seed laser.....	75
Figure 5.5 Electrical spectra of the pulsed seed laser.	76
Figure 5.6 Configuration of the whole amplification system.	77
Figure 5.7 Configuration of the pre-amplifier.	78
Figure 5.8 Configuration of the main amplifier.	79
Figure 5.9 Configuration of testing system for (a) average power and (b) spectra, pulse width and repetition rate.	80
Figure 5.10 Simulated average power of the pre-amplifier.....	82
Figure 5.11 Simulated total gain and unit gain of the pre-amplifier.	83
Figure 5.12 Simulated pulse energy and peak power of the pre-amplifier.....	84
Figure 5.13 Simulated average power of the main amplifier.	85
Figure 5.14 Simulated total gain and unit gain of the main amplifier.	86
Figure 5.15 Simulated upper level population in both pre- and main amplifiers.	87
Figure 5.16 Simulated pulse energy and peak power of the main amplifier.....	88
Figure 5.17 Tested output power and slope efficiency in main amplifier.	89
Figure 5.18 Tested spectra of the pulsed laser amplification process in the whole amplification system.	90
Figure 5.19 PD signal of the pulse with 3 ns pulse width.....	91
Figure 5.20 Electrical spectrum of the pulsed laser output.	92
Figure 5.21 Intensity distribution of the single mode seed beam.	93
Figure 5.22 Simulated B-Integrals of the pre- and main amplifiers.	94
Figure 6.1 Potential output power from the current laser system.	99
Figure 6.2 Potential output power and gain saturation with 400 W coupled pump power.....	100

List of Tables

Table 3.1 Amplifier parameters.....	33
Table 3.2 Design parameters.....	37

1. INTRODUCTION

Even since 1960 when the first functioning laser was built by Theodore Maiman, lasers have widely affected modern society. As a valuable technology, lasers are applied in different areas such as in communications, manufacturing industry, biomedical industry, and scientific research. The theoretical framework of the laser was established by Charles Townes and Arthur Schawlow, who were recognized by the award of Noble Prize for their contributions. Hundreds of thousands of people are working in this area and many different types of lasers have been invented over decades. In 1964, Elias Snitzer and colleagues constructed and operated the world's first optical fiber amplifier. Also in the 1960s, Charles Kao and his group provided the foundational theory of optical communication based on the optical fiber. This has become one of the most important technologies in modern society and Kao was awarded Noble Prize in 2010. Research on fiber lasers and fiber amplifiers has changed the world. In the 1980s, rare earth doped fibers were invented at Southampton University; these were quickly made part of the fiber amplifier.

1.1 Rare Earth Doped Fiber Amplifiers

The invention of silica fibers doped with rare-earth elements such as erbium, neodymium, and ytterbium has provided a new and versatile solid-state gain medium that simplifies thermal management, packaging, and control in a number of laser system configurations. When pumped with appropriate light sources, doped fibers can

be used as components of high conversion efficiency amplifiers. Rare earth doped fiber amplifiers have a wide range of applications in, for example, optical communications, spectroscopy, and fundamental quantum optics studies [1], [2]. The erbium-doped fiber amplifier (EDFA) is one of the foundations of today's advanced optical communication systems that power the internet. However, in most non-communication high power applications, ytterbium-doped fiber amplifiers (YDFA) are a better choice for their broad-gain bandwidth and excellent power conversion efficiencies [2]. Compared to high power solid-state lasers and amplifiers like Nd:YAG, Yb-doped fiber amplifiers are more compact and can be made in all-fiber systems. Removing the lenses and mirrors, the Yb-doped fibers can function robustly outside the laboratory. The main limitation of Yb-doped fiber lasers are lack of reliable mode control and the dependency of modal structure on the size of doped-core diameter. The invention of the photonic crystal fiber (PCF) brought additional properties that enhance design flexibility and mode control to fiber amplifiers [3]. Many researchers are building high power fiber lasers and amplifiers with PCFs [4], [5]. However, PCFs still have some problems due to their complicated structure and the fact they are very difficult to use in an all-fiber system. There is a new fiber based on a chirally-coupled-core (3C) scheme that solves some of the problems associated with the other fiber types. In the following Chapters, we will discuss three different types of Yb-doped fibers in detail.

While progress is being made in advancing and improving the practical fabrication of the fiber gain medium, the theoretical guidance necessary for their design is being

limited by the available quantitative models. In general, a rate equations (REs) approach and a nonlinear Schrödinger equation (NLSE) method are used to model and simulate the gain and pulse evolution processes, respectively, in the appropriate regime of operation [2], [6], [7]. Each approach has advantages and disadvantages; each is limited to a special regime of operation. As the diversity of fiber amplifiers has increased, traditional methods are becoming inadequate.

Fiber amplifiers can be divided into two broad classes: a continuous-wave type amplifier and a pulsed light amplifier. Continuous-wave amplifiers are attractive because of their wide range of industrial applications. Pulsed light amplifiers on the other hand are convenient for generating large pulse energies for special applications, for example, in providing access to large peak electric fields. These types of amplifiers, however, are usually dogged with undesirable dispersive and nonlinear effects that must either be controlled or avoided. Depending on the electronic energy level structure of the rare-earth doped fiber, one may use rate equations to model and simulate the light amplification process in the fiber [2], [6]. However, rate equations alone cannot be used to calculate the evolution and propagation of pulsed light in a fiber. Pulse evolution and propagation in amplifiers inevitably lead to dispersive and nonlinear effects; these must be accounted for. One is therefore forced to resort to a nonlinear wave equation to model the pulse propagation. Beginning from Maxwell's equations, where the dielectric constant (or index of refraction) is affected by extraordinarily high optical electric fields, one arrives at a nonlinear wave equation that is identical to the nonlinear Schrödinger equation [7]. While the nonlinear

Schrödinger equation provides an acceptable model for the evolution of a pulse, the gain of the amplifier cannot be calculated from this model. On the other hand, pulse evolution cannot be determined from the rate equation model. Neither of the models alone provides satisfactory guidance for design considerations in high peak power fiber amplifiers. Thus, a comprehensive theoretical method for modeling and simulating fiber amplifiers under diverse regimes of operation is needed for high power pulsed fiber laser design and modeling. In Chapter 3, a new type of modeling method for rare earth doped fiber amplifiers is introduced in detail. This new method can obtain the precise gain and simulate the pulse evolution at the same time in the gain fibers. This new method can be used to provide a comprehensive analysis of the laser amplification process and it can serve to provide guidance for the design and construction of fiber amplifiers.

A typical high power high pulse energy Yb-doped fiber amplification system may consist of three parts as shown in Figure 1.1: a single seed laser system, several pre-amplifiers, and one or several main amplifier(s). These three major parts are connected by isolators for uni-direction propagation. The seed laser provides the initial signal light, to be amplified. The pre-amplifiers and main amplifier(s) work together to perform a multi-level amplification processes. In general, it is useful to minimize or limit amplified spontaneous emission. Usually, the pre-amplifiers are made to operate at relatively lower power levels (below 5 W). The main amplifier(s) generally are responsible for boosting the power of seed light to values over 100 W.

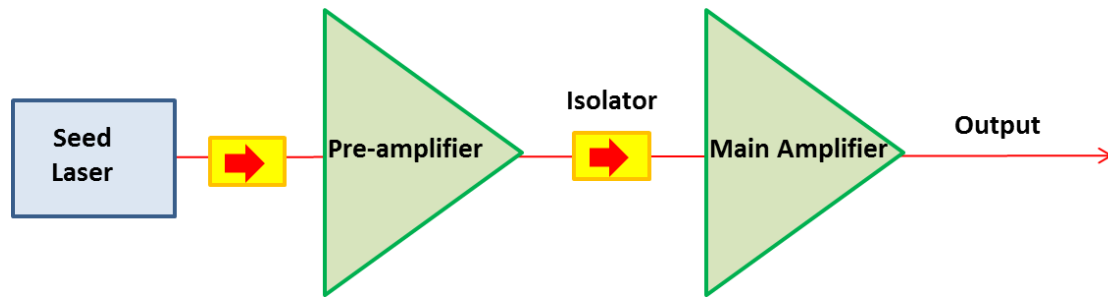


Figure 1.1 Structure of high power high pulse energy Yb-doped amplification system.

High power high pulse energy Yb-doped fiber amplifiers have been developing very rapidly since 2002. Researchers have typically worked on advancing the state-of-the-art of high average power, low pulse energy amplifiers or on low average power, high pulse energy amplifiers. Although standard fibers, with core diameters less than 12 μm , are usually used in the high average power amplifiers, they cannot be used to build high pulse energy amplifiers. The small core diameters of standard fibers cannot withstand the high intensities that are achievable in large pulse energy systems. In such cases one may use large core area PCFs as the gain media in high pulse energy fiber amplifiers. Researchers at the University of Jena have reported successful use of the PCFs in high pulse energy systems [4]. Despite the reported successes, PCFs still have some unavoidable limitations. The air-hole structure of PCFs introduces difficulties in splicing but more importantly, it is almost impossible to build a high efficiency all-fiber system with PCFs. Use of free space optics for light-shaping focusing, and directing ultimately lead to a complex system with reduced efficiency prone to misalignments. Furthermore, large core area PCFs are very difficult to coil tightly. To avoid some of these problems, this work explores use of chirally-coupled-core (3C) Yb-doped fibers. The 3C fibers can maintain single-mode operation in very large core area gain media, which are suitable for high

pulse energy amplifiers. Without the cumbersome air-hole structure, 3C fibers can be easily spliced in an all fiber system. Overall, the 3C fibers have more useful properties for high power, high energy applications than PCFs.

To build a high power, high energy fiber amplifier, many issues need to be considered. Transmission efficiency, one of the issues that has to be considered, is extremely important because both the pump and seed laser power decrease along the propagating length of the fiber, and additional losses are incurred for propagation through lenses, couplers, or deflections by mirrors. To construct a high performance fiber amplifier, the transmission efficiency needs to be high. Furthermore, the slope efficiency (which is the ratio of the output power to the input power) of the fiber needs to be high. Amplified spontaneous emission (ASE) is another important issue that leads to a decrease of useful transmission efficiency in high-gain amplifiers [8]. For a high peak power pulsed laser systems, the considerations for building an amplifier system become even more complicated. Dispersion and nonlinearities, which result from the high peak power, strongly affect the quality of the pulse and decrease its peak value [9]. We have considered and controlled these issues and successfully built a high power, high pulse energy fiber amplification system. We discuss this in Chapter 4.

1.2 Thesis Statement

There are two major objectives for this Thesis; the first is to consider and introduce a viable theoretical approach for modeling and simulating fiber amplifiers under

diverse regimes of operation. The second objective is to experimentally demonstrate operation of a high power, large pulse energy Yb-doped fiber amplification system with high gain and high transmission efficiency in a compact foot print.

In the theoretical approach, we will assume a general upper and lower level energy structure for rare-earth doped fibers with a four-level or a three-level manifold. Furthermore, it will be assumed that non-radiative decays are extremely fast. Transition rates involved in the amplification processes are therefore much faster than upper-level lifetime decay rates, which can then be ignored [6]. Under these circumstances, the model can be considered as a simple two-level system with an upper energy level and a lower energy level. In Chapter 3, the basic equations of the proposed methodology are discussed; based on the need for a comprehensive consideration of the amplification process, the conventional rate equations and the nonlinear wave equation will be modified. Comparisons between simulation results based on the modified model equations and the conventional equations will be discussed.

The high power, large pulse energy Yb-doped fiber amplification system will be discussed in detail in Chapter 4. This amplifier is capable of yielding up to 120 W of average power and pulse energies of up to 1.2 mJ pulse energy, limited by available input pump power. The total gain obtained is ~38.9 dB, with little or limited ASE, which is outstanding among Yb-doped amplifiers. The slope efficiency of our amplifier is as high as ~81 %, as shown in Figure 1.2, this value stands out among other high power amplifiers. This high power Yb-doped fiber amplifier system is a

good solution for generating high pulse energy pulses. Such a system would find applications in medical instruments, high energy physics research, and other high power, high energy laser applications.

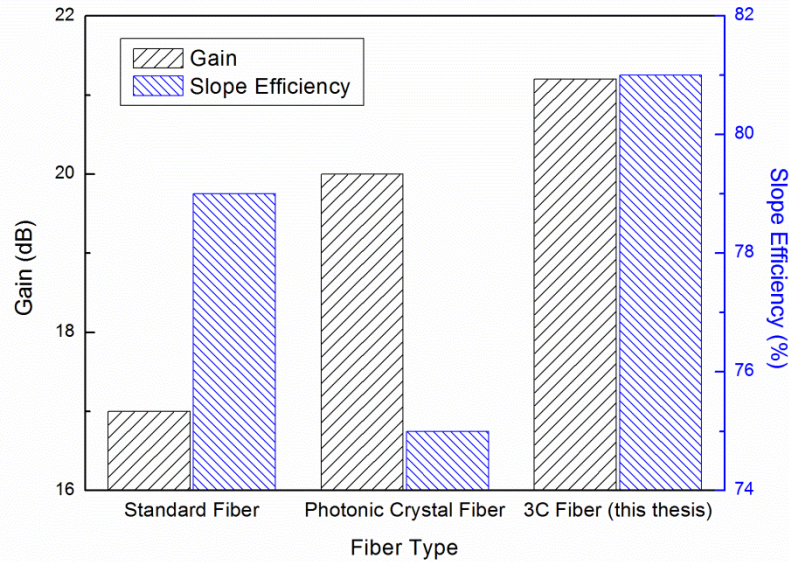


Figure 1.2 Gain and slope efficiency in one level amplifier with different types of fibers.

In this dissertation, the two major contributions are a new comprehensive rare-earth doped fiber simulation model, and a practical demonstration of a high power, high pulse energy Yb-doped fiber amplification system.

In Chapter 2, the three major types of Yb-doped fibers are discussed and compared. This Chapter also discusses the pumping method for double-clad fibers. Safety and thermal management considerations for rare-earth doped fibers are also introduced.

In Chapter 3, the first major contribution of this thesis, the unified model for rare-earth doped fiber amplifiers is introduced. Simulation results based on the new model are compared with the experiment to verify the validity of the new modeling and simulation method. The advantages of the unified model are shown by comparing

it to other existing modeling methods.

In Chapter 4, two types of Yb-doped standard fiber amplifiers are introduced. Both continuous-wave (CW) and pulsed amplifiers are discussed. The important issues typical to amplification systems are presented in preparation for the discussion of high power, high energy amplification systems in Chapter 5.

In Chapter 5, the second major contribution of this thesis, the construction of a high power, high pulse energy amplifier system based on ytterbium-doped fiber is introduced. The configuration and properties of the seed laser system are discussed. We then introduce the structure of a two-level 3C fiber for high power, high energy amplifier system. The analysis of the pulse amplification in the high power laser system is separated into several characterizations: laser power and pulse energy, pulse profile and spectrum, and beam quality. Finally, we briefly introduce potential application areas of the high power, high energy laser system.

Chapter 6 presents the summary of the work of this thesis and a perspective on future work.

2. YTTERBIUM-DOPED FIBERS

2.1 Fiber Gain Media

To build compact high peak power laser systems, the magnitude of the nonlinear effects that arise due to the high intensities in the systems must be controlled. Among other things, this means improving the power conversion efficiency and enlarging the laser mode field diameter, while maintaining the single mode nature of the laser output beam.

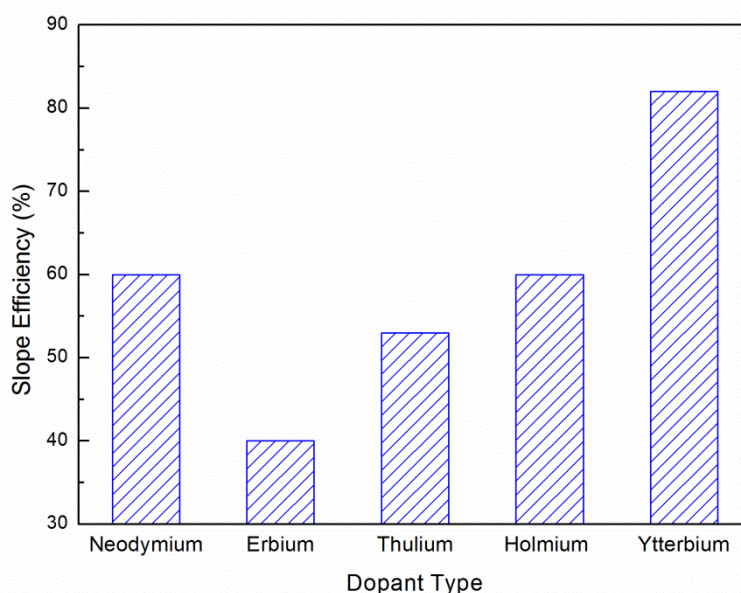


Figure 2.1 Slope efficiency of rare earth doped fibers.

Different rare-earth doped fiber amplifiers generate laser light beams of different wavelengths for different applications. But for high power applications, the highest conversion efficiency is preferred. Among the rare-earth doped fibers, the Yb-doped fiber has the best slope efficiency. With proper doping concentration profile and emission wavelength, the slope efficiency of the Yb-doped fiber can be over 80 % as

shown in Figure 2.1, which is much higher compared to other rare-earth doped fibers. This is the reason why we choose Yb-doped fiber as the gain media for high power amplifiers investigated in this work.

The conversion efficiency is also strongly affected by the absorption and emission wavelengths of the light beams in the fiber. Figure 2.2 shows the two absorption peaks (940 nm, 976 nm) of ytterbium atoms in silica fiber. To avoid strong amplified spontaneous emission around 976 nm, we choose 976 nm as the pump wavelength. The spectral location of 1030 nm is often chosen to be the seed wavelength for the longest emission in Yb-doped fiber. However, a Yb-doped fiber laser emitting at 1064 nm can be used to substitute for high power bulky Nd:YAG lasers because of the better performance and smaller size of the fiber system. The energy level structure of Yb atoms in silica can be represented as a quasi-three level system. A quasi-three-level laser medium is one with a kind of intermediate state, where the lower laser level is so close to the ground state that an appreciable population in that level occurs in thermal equilibrium at the operating temperature [2]. As a consequence, the unpumped gain medium causes some re-absorption loss at the laser wavelength, and transparency is reached only for some finite pump intensity. For higher pump intensities, there is gain, as required for laser operation. The quasi-three level system may cause wavelength shifting of amplified spontaneous emission. Amplified spontaneous emission will be discussed in Chapter 4 in detail.

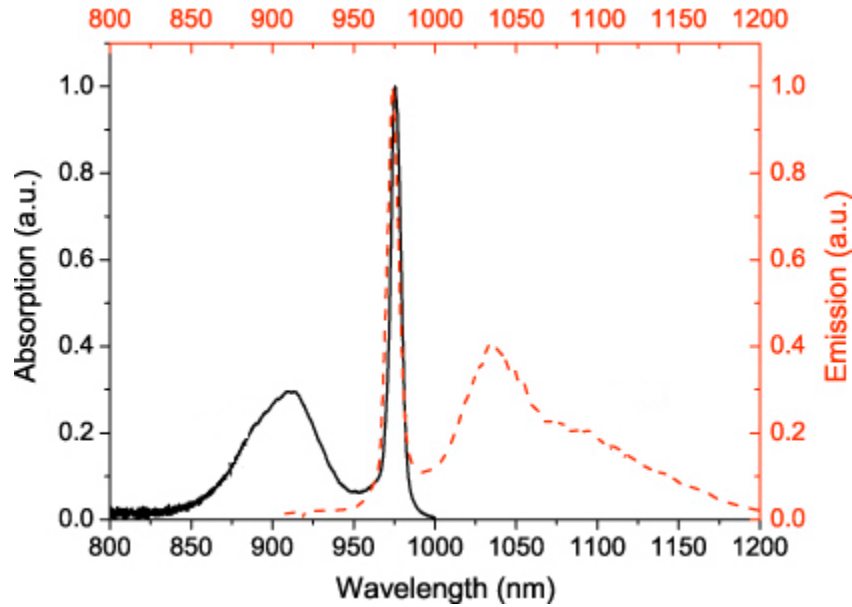


Figure 2.2 Absorption and emission of Ytterbium doped fiber.

For high powers, a large core diameter fiber is preferred in order to limit the power intensity. However, the increase of core diameter leads to higher order modes as shown in Figure 2.3. Higher order modes cause gain reduction and thermal modal instability. So another important aspect for the high power fiber is to increase the mode-field diameter of the beam, while keeping it single mode. Because of this requirement, different types of fibers have been designed to meet this requirement.

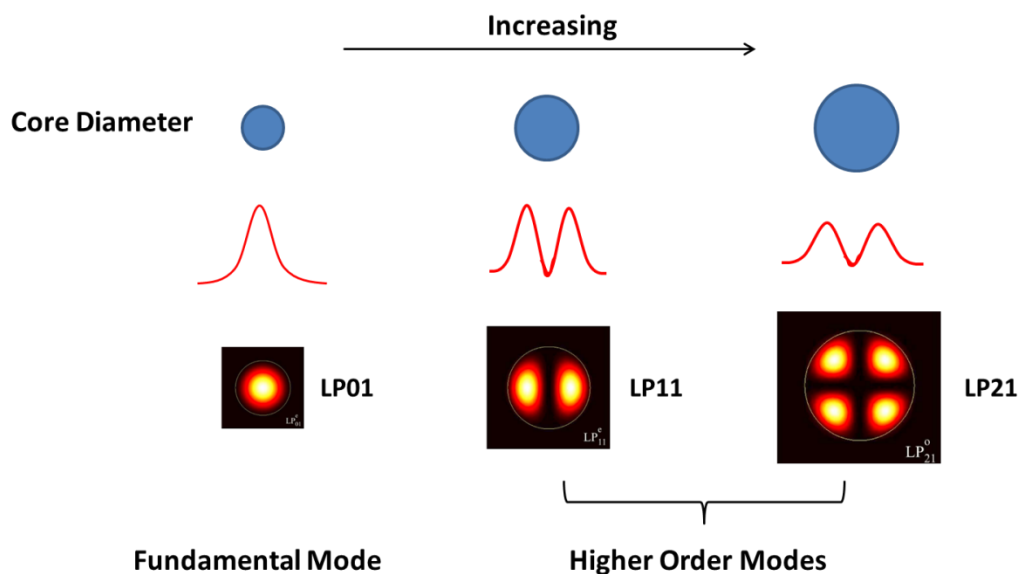


Figure 2.3 Fiber core diameters and fiber modes.

2.1.1 Standard fibers

Power conversion efficiency can be increased by enlarging the core area of the gain medium and increasing the dopant concentration of the medium [13]. A larger core area can obviously lower the optical power intensity, thus protecting the fiber from strong nonlinearity and damage. The typical structure of the standard fiber is very simple and is shown in Figure 2.4. Here, a high index Yb-doped core is surrounded by a silica cladding of lower refractive index. The index difference, which results in total internal reflection, leads to confinement of the seed light in the core region of the fiber, while the pump laser propagates in the cladding region. Large core areas provide better conversion efficiencies and are also easier to couple signal light into.

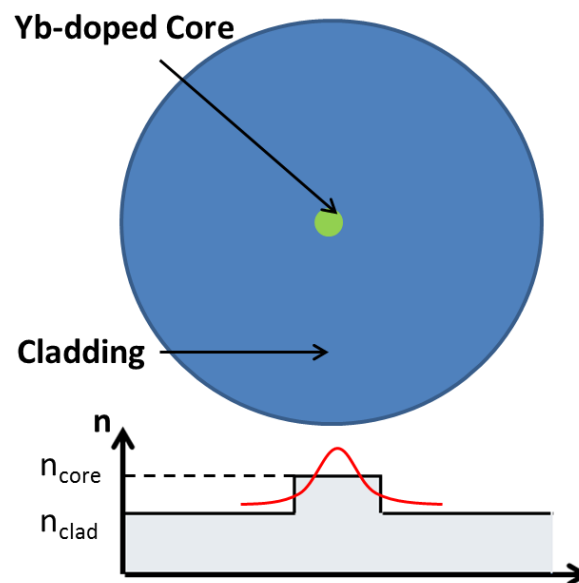


Figure 2.4 Yb-doped standard fiber.

However, a standard fiber with a large core cannot maintain single mode operation. The so-called large mode area (LMA) fibers are optical fibers with relatively large mode areas and yet offer the possibility to operate the fiber with a single transverse mode or only a few modes. To avoid excitation of higher-order modes (HOMs) in a

large mode area fiber, one needs to coil the fiber tightly to introduce selective loss for the higher-order modes (HOMs). In comparison, the fundamental mode suffers very little loss in coiled fibers, leading to operation of the fiber as a single mode guide. One cannot, however, completely avoid the higher-order modes with this method. To determine the number of linearly polarized modes, the normalized frequency, or V-parameter of the fiber is introduced; the standard formula for the V-parameter is

$$V = \frac{2\pi d}{\lambda} \frac{d}{2} \sqrt{n_{core}^2 - n_{clad}^2} = \frac{\pi d NA}{\lambda} \quad (2.1)$$

where $NA = \sqrt{n_{core}^2 - n_{clad}^2}$ defines the numerical aperture of the fiber; d is the core diameter; λ is the operating wavelength, and n_{core} and n_{clad} are, respectively, the index of refraction in the core and cladding.

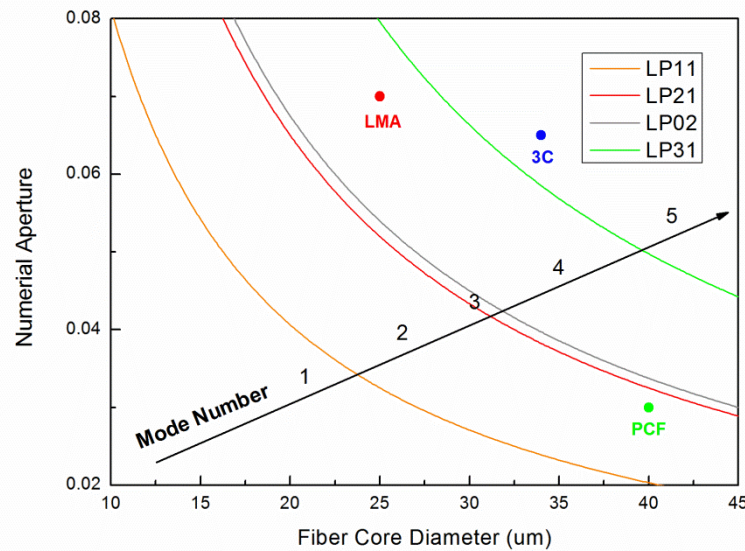


Figure 2.5 Number of linearly polarized modes supported by fibers with different core sizes and NAs. LMA is nLight Yb1200-25/250DC (core diameter 25 um, NA 0.07); PCF is NKTPhotonics DC-200-40-PZ-Yb (core diameter 40 um, NA 0.03); 3C is nLight Yb700-34/250DC-3C (core diameter 34 um, NA 0.065).

Figure 2.5 illustrates the number of modes supported by fibers with different core

diameters and NAs. As the NA and/or the core diameter increase, the V parameter and the number of modes within the fiber increase. The number of linearly polarized (LP) modes supported by fibers with specific core size and NA tolerances can be determined from plots such as that in Figure 2.5.

From Figure 2.5, we determine, for example, that a large mode area fiber with a 25- μm core diameter and NA of 0.07, can support four LP modes. Although this large mode area fiber can be coiled to limit the number of higher-order modes, it turns that this solution does not work well for high power amplifiers. To resolve this issue, other fiber types must be considered.

2.1.2 Photonic Crystal Fibers

Use of photonic crystal fibers with their unique properties in the design of optical amplifiers offers some advantages in resolving these problems [3]. The simplest and most common type of photonic crystal fiber is a wave-guide type fiber. This has a solid core surrounded by an array of air holes. The guiding properties of this type of fiber are similar to those of the standard fiber. The region surrounding the core can be analyzed and understood within an effective index model. The core of the fiber has a higher refractive index. In this case, light is confined within the core area [14]. As a gain media, the core of the photonic crystal fiber should be doped with rare-earth Yb atoms. For high-power fiber amplifiers, double-clad photonic crystal fibers are used.

Figure 2.6 shows the common structure of the double-clad photonic crystal fiber. The pump area is surrounded by an inner air cladding. Due to the large contrast in the

index of refraction, the pump area can have a very high numerical aperture. This property makes the pump laser coupling process easier. Such photonic crystal fiber designs also have large mode areas in the core [3] and yet maintain a relatively single mode characteristic at the same time [13]. By carefully adjusting the design of the fiber structure, a suitable effective index would be obtained for lower NA. Thus the fiber can maintain a single mode nature with a lower NA and a larger core diameter. Figure 2.5 also shows the supported LP modes in a common photonic crystal fiber. This fiber represents a compromise among the number of the LP modes, NA, and core diameter. If the NA is too small, it becomes very difficult to couple light into the core. Finally, this example of a photonic crystal fiber operates in a relatively single mode regime that supports both the fundamental mode and the LP11 mode. This structure is can be used for high output powers with acceptable beam quality. If the fiber is made of fused silica construction with no polymer coatings anywhere in its structure, melting from overheating can be avoided.

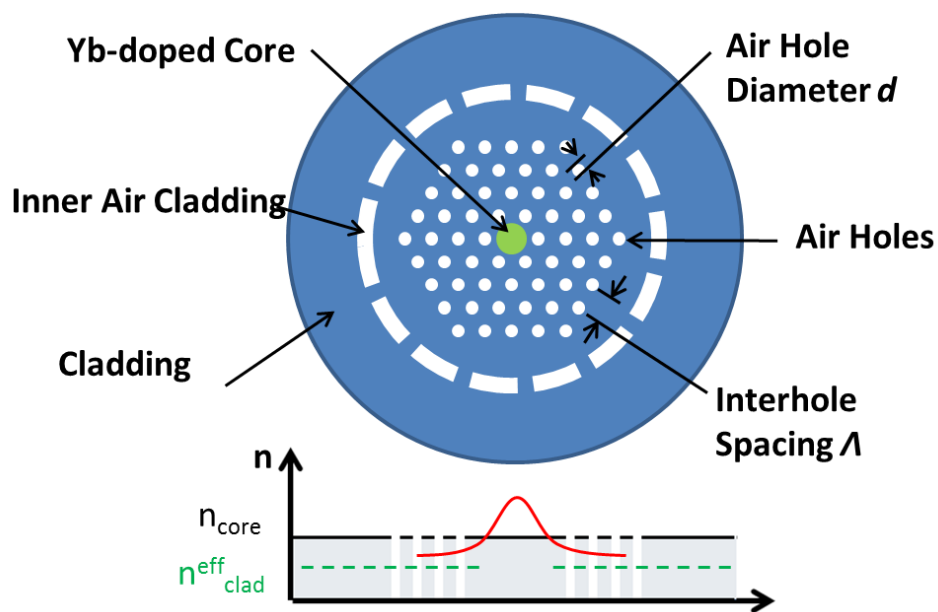


Figure 2.6 Structure of Photonic Crystal Fibers.

Although photonic crystal fibers have desirable properties, they still have some problems when used in high power laser systems. Since there are air-holes and air cladding in the photonic crystal fibers, they cannot be coiled tightly. In the case of the photonic crystal rod, the cladding diameter is very large, making the rod difficult to bend. High power photonic crystal fiber lasers are difficult to construct in a compact manner; they end to occupy very large foot prints. To build compact high power laser systems, an all-fiber structure is a better choice because of excellent coupling efficiency and more compact configuration. Because of the air holes in photonic crystal fibers, it is very difficult to splice photonic crystal fibers and to join them to standard fibers for an all fiber systems. If attempted, there would be unacceptably large power losses at the splicing points. In addition, for high power amplification in photonic crystal fibers, there is thermal mode instability (TMI) that generates high-order modes that dance around the fundamental single mode [15].

To avoid some of the problems of the standard fibers and the photonic crystal fibers, a new type of fiber, the chirally-coupled core (3C) fiber is introduced; this fiber can serve as the gain media for the high power lasers [16].

2.1.3 Chirally Coupled Core Fibers

Chirally-coupled core fibers are a new generation of fibers with unique features for fundamental mode operation when used as gain media in high power fiber lasers [17], [18].

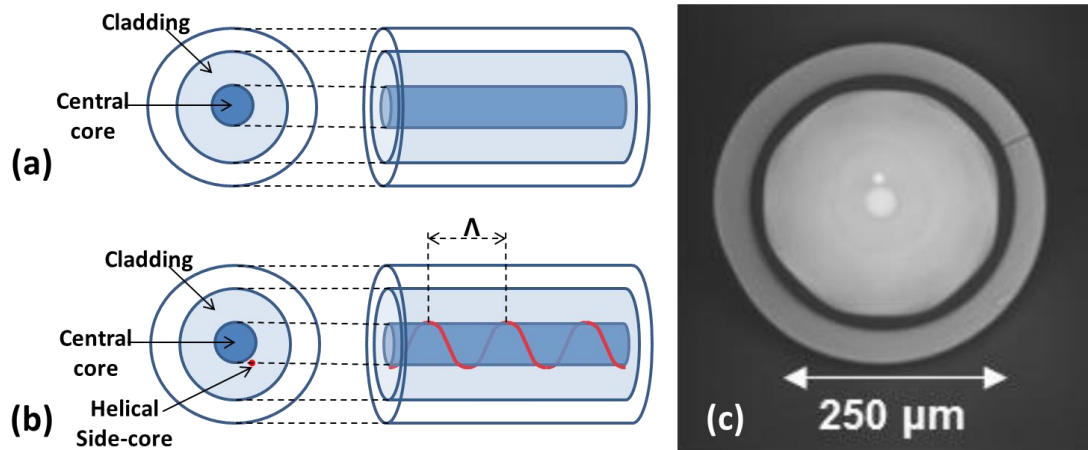


Figure 2.7 (a) Structure of standard fiber; (b) Structure of 3C fiber; (c) TEM photo for fiber ends of nLight Yb700-34/250DC-3C fiber.

From Figure 2.7, we see that the structure of the 3C fiber is quite different from the common standard fiber [16]. With a large central core doped with the desired gain impurities and surrounded by one or several helical side-core(s), 3C fibers are spun during the drawing process at high rates, causing the satellite core to orbit the main core along the fiber length with a pitch of Λ on the order of a few millimeters. This configuration generates an optical angular momentum in the 3C fibers. The fundamental mode has only spin-angular momentum while the higher order LP modes have orbital-angular momentum as well. This leads to symmetry-based distinction between modes. All modes, except the fundamental one, can be radiation modes and do not propagate in the fiber core with proper fiber design [19]. The pitch of the helix period can create a quasi-phase matching condition between the modes of the main core and those of the satellite core where strong coupling between the two occurs. In this case, any higher-order modes generated in the core are coupled to the sidecore so that only the fundamental mode remains in the central core. The quasi-phase matching is given by equation (2.2) as

$$\Delta\beta = \beta_{central\ mode} - \beta_{side\ mode} \cdot \sqrt{1 + R^2 (2\pi / \Lambda)^2} - \Delta m \cdot (2\pi / \Lambda) = 0 \quad (2.2)$$

$\beta_{central\ mode}$ are the propagation constants of fiber modal group in straight central core, while $\beta_{side\ mode}$ are the propagation constants of fiber model group in the side core(s). R is the distance between the central core and side core. $\sqrt{1 + R^2 (2\pi / \Lambda)^2}$ is a helical correction factor for the side core. The parameter Δm represents the mode differences between the two cores. When the propagation constants in the central core and side core conform to the quasi-phase matching condition of equation 2.2, the fundamental mode propagates in the main core, while higher-order-modes (HOMs) are extracted into the side cores and radiated in the cladding. In this way, a 3C fiber can maintain a single mode structure in a large core area.

Figure 2.5 also shows an example of a 3C fiber made by the company nLight; this fiber the model Yb700-34/250DC-3C. This fiber has a large core diameter of 34 μm and a numerical aperture of 0.065. From the figure, such a large core diameter and NA should support higher order modes besides the fundamental mode. However, with careful design, this 3C fiber can maintain a single mode in large core diameter area and NA as shown in Figure 2.8. From the figure, we note that the loss of the fundamental LP01 mode is very small, while the losses of all the higher-order modes are very high. Even the LP11 mode has a loss of under 15 dB/m loss. The usual length for a gain fiber is over 2 m long, so most higher-order modes would suffer severe losses. Large core area 3C fibers offer increased coupling efficiency and lower light intensity, making them ideal for high power fiber amplifiers.

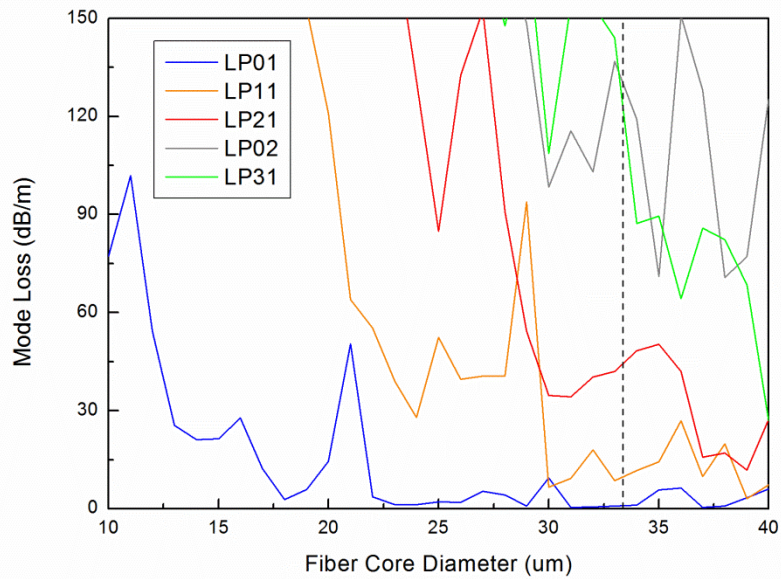


Figure 2.8 Mode loss vs fiber core diameter in 3C fiber.

Compared to standard and photonic crystal fibers, 3C fibers offer more desirable features and advantages. The 3C fiber can maintain fundamental mode operation even with a large NA and a large core diameter. A large NA allows high coupling efficiency; a large core diameter lower the light intensity in the fiber, thus reducing the onset of nonlinearities. To make a compact and robust laser amplification system, an all-fiber structure is desirable. To package and connect all the fiber elements together, the fibers need to be bent and spliced together. This is very difficult to do for the photonic crystal fibers with air-holes while it is easily accomplished for 3C fibers. There is no special splicing method for the 3C fiber; therefore 3C and standard fibers can be spliced together with using a common method. While researchers have found thermal mode instability in the both standard fiber and the photonic crystal fiber, there is no such problem with the 3C fiber. In summary, it appears that the Yb-doped 3C fiber at the present time would be the best choice for the high power high pulse energy

amplifier systems.

2.2 Core Pumping and Cladding Pumping

For a high power pulsed light amplifier, it is generally desirable to have a single-mode fiber as the gain medium. This however, may be disadvantageous during coupling of the pump or signal light.

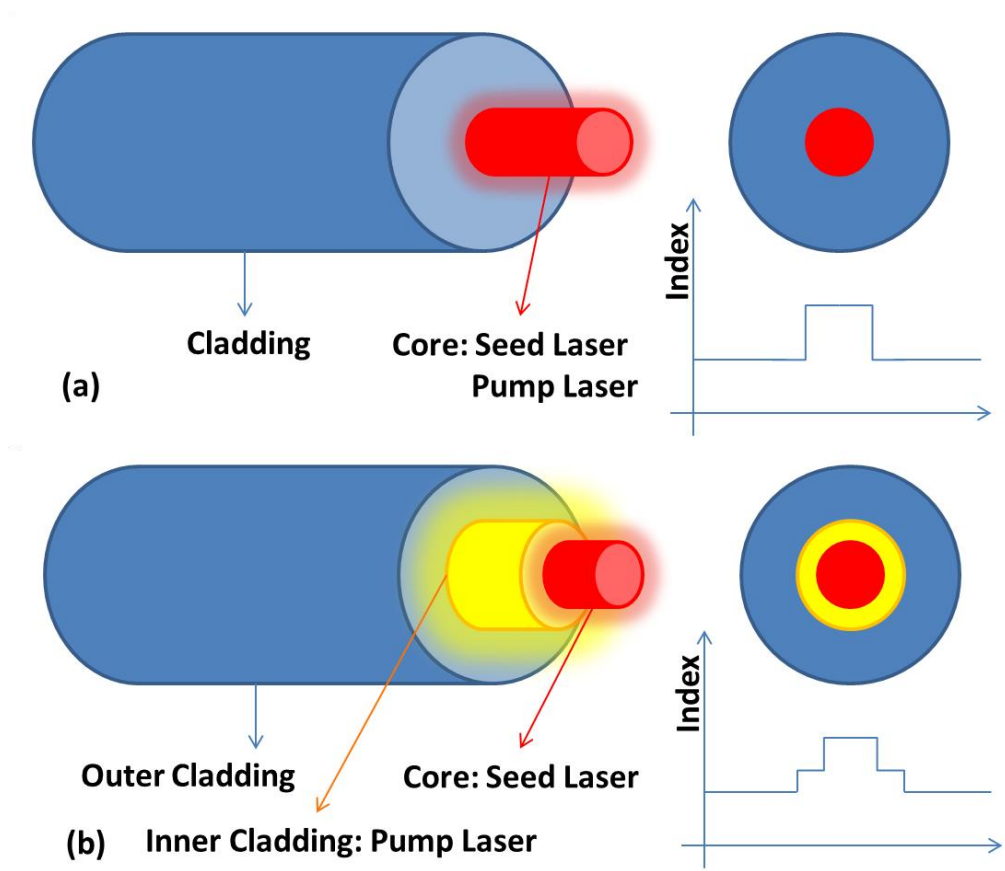


Figure 2.9 (a) Single cladding fiber & pumping method; (b) Double cladding fiber & pumping method.

Figure 2.9 shows two types of fiber cladding designs. The structure of a fiber with common single cladding is shown in Figure 2.9 (a). This type of fiber is widely used in optical communications, lower power fiber laser amplifiers or other low power

fiber-based systems. According to the figure, the refractive index of the cladding is smaller than that of the core, so the beam is confined in the core area. Both the seed light and the pump laser light propagate in the small core, whose typical diameter is below 6 μm . The light intensity in the core area is very high, which is detrimental for high power systems. To build high power, high pulse energy laser systems, a double-clad fiber structure is introduced.

To increase coupling efficiency and lower the light intensity, cladding pumping is usually implemented [29]. The structure of a single-mode fiber with a double-clad configuration suitable for cladding-based pumping is shown in Figure 2.9 (b). The index of the core is typically larger than that of the inner cladding immediately adjacent to it; the index of the inner cladding, in turn, is larger than that of the outer cladding. With a carefully designed index profile, the seed or signal laser light can propagate in the core as it is being amplified while the pumping laser light is confined by the outer cladding. In this case, the light intensity in the fiber core is much lower and the fiber is protected. Also with larger pumping cladding area, the coupling efficiency of the pump light is greatly increased. Under these conditions, the effectively pumped volume is larger than in a standard configuration, thus increasing coupling efficiency [30].

Because of these desirable characteristics, double-clad design is widely used in Yb-doped fibers. The standard large mode area fibers, photonic crystal fibers, and the 3C fibers discussed in this thesis all belong to this class of fibers. This cladding pumping technology is commonly applied in high power laser systems to facilitate

better coupling efficiency and protect the fiber from damage due to high intensities in the core.

2.3 Fiber Safety and Thermal Management

In high power, high pulse energy laser systems, fiber safety and thermal management are always big issues. During the operation of high power laser, there are two parts of the fiber that are easy to damage. The fiber end facet is the most common area that is easily damaged. The other part of the silica fiber that is easy to damage is adjacent to the cladding on the outside and is the polymer jacket (coating) whose role is to protect the fiber from its environment.

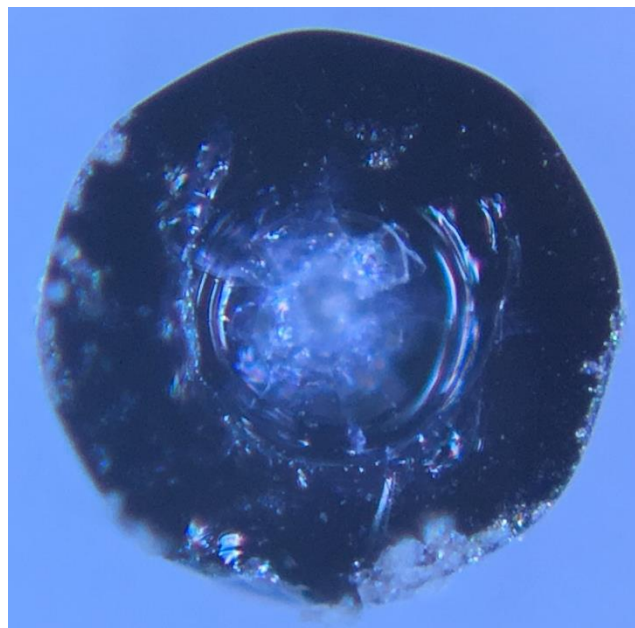


Figure 2.10 Damaged fiber end surface.

Since laser beams need to be coupled through the end facets into or out of the fiber, the end facets usually bear the highest laser intensities. Fiber end facets are easily damaged when the laser beam intensity is higher than the damage threshold. The

small size of fiber end facet is also easy to get dirty if there is dust in the air. Unclean end facets burn. Misalignment and improper fiber end facet angles may also lead to high reflections and amplified spontaneous emission. These effects and factors may cause high energy concentrations at the end facets and thus lead to burn damages. Figure 2.10 shows a damaged fiber end facet of a 3C fiber. Fusion of the silica is clearly evident in the core area because of the high power. To avoid damage to the fiber facets, misalignment must be avoided. Also, the fiber facets should be checked for cleanness before the laser is turned on.

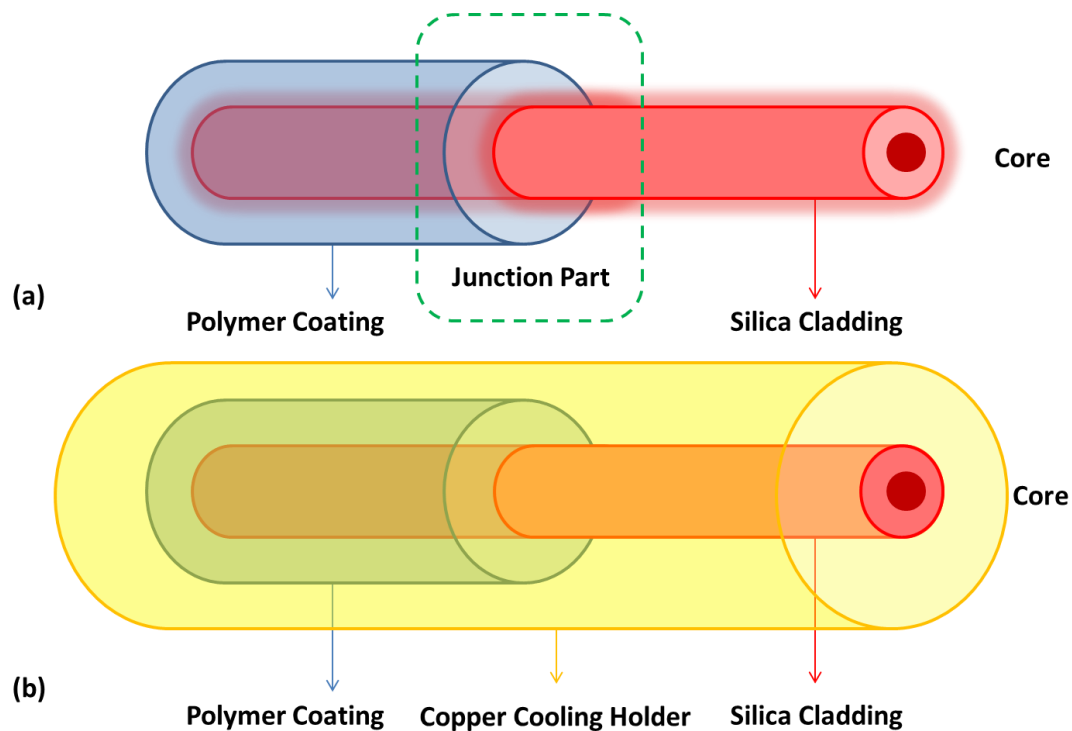


Figure 2.11 (a) Laser beam leaking at junction part; (b) Thermal management and fiber protection.

Another easily damaged point is the junction shown in Figure 2.11 (a). During light coupling, misalignment and mismatching NA can lead to leaking of the beam. The pump beam may propagate into the polymer coating at the junction part. Even several hundred mWs of leaked light lead to damage of the junction part. To avoid this

problem, careful alignment procedures must be followed. If a lens is used to couple the light, its NA must be smaller than the NA of the fiber to confine the laser beam into the cladding area. To better manage thermal problems, we use a copper fixture as a cooling holder for the fiber as shown in Figure 2.11 (b). The copper fixture covers the silica cladding and polymer coating parts. Heat from the fiber is quickly dissipated by the copper fixture which in turn is carried away by air convection currents. This approach protects the fiber from thermal damage.

2.4 Summary

This introduction to fiber gain media for high power, high pulse laser system, including method of pumping has provided the basic background knowledge for understanding fiber amplifiers systems. We have also discussed the issue of fiber safety and thermal management. With this background, we not move on to discuss quantitative modeling of fiber amplifiers.

3. MODELING OF RARE-EARTH DOPED FIBER AMPLIFIERS

In the standard approach to rare-earth doped fiber amplifier modeling, the gain of the amplifier is calculated from rate equations, while any dispersive and nonlinear effects are analyzed within a nonlinear Schrödinger equation (NLSE) picture [2], [6], [7]. However, in the construction of high power fiber lasers, gain saturation becomes an issue and needs to be taken into consideration [20]. In a unified design methodology, the modeling and simulation scheme should consider a simultaneous implementation of the rate equations and the NLSE. In the following, we outline the development of a unified modeling approach.

3.1 Traditional Modeling

3.1.1 Power, gain, and pulse energy

The most common rare-earth elements used for doping a fiber gain medium are erbium and ytterbium. Erbium-doped fiber amplifiers (EDFAs) and Ytterbium-doped fiber amplifiers (YDFAs) can be modeled using rate equations [2], [6]. In silica material, the rare earth elements have a very simple energy level structure that can be thought of as one excited-state manifold within reach from a ground-state manifold when a pump source of appropriate energy is available. To model the transition rates and the amplification process for a CW laser light in the gain medium, the rate equations would normally suffice for the CW amplifier in the steady state. To model

amplification of a pulsed seed laser light however, the pulse width must be considered. For pulse widths that are much shorter than the population relaxation time, the inverted population can be regarded as being in the steady state [21]. In this regime, the pulsed amplifier can be considered to be similar to the CW amplifier: both are in the steady state regime. The basic rate equations for the amplification system in both cases are therefore as follows [2]:

$$\frac{dN_2(z,t)}{dt} = (P_{12} + S_{12})N_1(z,t) - (P_{21} + S_{21} + A_{21})N_2(z,t) \quad (3.1)$$

$$\frac{dN_1(z,t)}{dt} = -(P_{12} + S_{12})N_1(z,t) + (P_{21} + S_{21} + A_{21})N_2(z,t) \quad (3.2)$$

where N_1 and N_2 represent the lower- and upper-level atomic populations; A_{21} is the Einstein coefficient for spontaneous emission, and the upward and downward transition rates are, respectively, P_{12} , S_{12} , and P_{21} , S_{21} ;

$$\begin{aligned} P_{12} &= \frac{\Gamma_p \sigma_{pa} P(z,t)}{h\nu_p A_{core}} & S_{12} &= \frac{\Gamma_s \sigma_{sa} S(z,t)}{h\nu_s A_{core}} \\ P_{21} &= \frac{\Gamma_p \sigma_{pe} P(z,t)}{h\nu_p A_{core}} & S_{21} &= \frac{\Gamma_s \sigma_{se} S(z,t)}{h\nu_s A_{core}} \end{aligned} \quad (3.3)$$

The variables $P(z,t)$ and $S(z,t)$ are the average pump and seed power levels; σ_{pa} , σ_{pe} , σ_{sa} and σ_{se} are the absorption and emission cross sections for the pump and seed laser light, respectively; the parameters Γ_p and Γ_s are the fill factors for the pump and seed laser light in the doped fiber. The fill factors represent the relationships among the inner cladding area, core area and mode field area; the variables ν_p and ν_s are the light wave frequencies; h is Planck's constant, and A_{core} is the area of the doped core. At steady state, the inverted population density N_2 and the ground state population

density N_1 can then be written as:

$$N_2(z) = \frac{(P_{12} + S_{12})N}{P_{12} + S_{12} + P_{21} + S_{21} + A_{21}} \quad N_1(z) = N - N_2(z) \quad (3.4)$$

where N is the dopant concentration of the rare earth element in the fiber. The rate equations for the average powers for the pump and seed laser light are:

$$\frac{dP(z)}{dz} = \Gamma_p [\sigma_{pe} N_2(z) - \sigma_{pa} (N - N_2(z))] P(z) - \alpha(\lambda) P(z) \quad (3.5)$$

$$\frac{dS(z)}{dz} = \Gamma_s [\sigma_{se} N_2(z) - \sigma_{sa} (N - N_2(z))] S(z) - \alpha(\lambda) S(z) \quad (3.6)$$

where $\alpha(\lambda)$ is the spectrally dependent loss. The amplified seed laser light is comprised of two parts: stimulated emission and spontaneous emission. For a comprehensive model, spontaneous emission cannot be ignored. We therefore follow [22] and take spontaneous emission into account. As amply discussed in [23], the rate equation for amplified seed power in Equation (3.6) becomes

$$\begin{aligned} \frac{dS(z, \lambda)}{dz} = & \Gamma_s [\sigma_{se}(\lambda) N_2(z) - \sigma_{sa}(\lambda) (N - N_2(z))] S(z, \lambda) \\ & + \frac{A_{core}^2}{4\pi\Gamma_s(L-z)^2} A_{21}(\lambda) N_2(z) h\nu_0 - \alpha(z, \lambda) S(z, \lambda) \end{aligned} \quad (3.7)$$

where $h\nu_0$ represents a photon of the same wavelength as the seed laser light and L is the fiber length. In the foregoing equation, the first term represents stimulated emission and the second term represents spontaneous emission. The average power can be obtained from Equation (3.5) and (3.7). These are the equations used to calculate the gain, pulse energy, and power.

3.1.2 Dispersion, nonlinearity, and pulse profile

To analyze pulse evolution in an optical amplifier, one must consider the pulse width and atomic population relaxation time in order to select the appropriate model. For most rare-earth doped fiber amplifiers, the atomic population response to the pulses can be neglected [24]. In this case, the pulse amplification process is governed by the nonlinear Schrödinger equation [7], [25]. After including the gain g , which must be known *a priori* in the standard nonlinear Schrödinger equation, the modified light amplitude propagation equation is given as

$$\frac{\partial A(z,T)}{\partial z} + \frac{i}{2} \beta_2 \frac{\partial^2 A(z,T)}{\partial T^2} - i\gamma |A(z,T)|^2 A(z,T) = \frac{1}{2}(g - \alpha)A(z,T) \quad (3.8)$$

where $A(z,T)$ is the pulse amplitude so that $|A(z,T)|^2$ represents the optical power in the pulse, T is relative time in a reference frame moving with the pulse group velocity, β_2 is a dispersion parameter and γ refers to nonlinearity; g is the gain and α is the loss. The evolution of the pulse can be simulated using the modified equation.

3.2 New Approach

3.2.1 Gain saturation

The traditional nonlinear Schrödinger equation can be used to analyze dispersion and nonlinearity in a fiber amplifier as long as the signal laser light to be amplified is small. For large peak powers and pulse energies, gain saturation occurs; in this case the standard nonlinear Schrödinger equation is no longer valid for representing the performance of the amplifier. The saturated gain can generally be calculated from the

average power or the pulse energy. For CW amplification, the saturated gain can be calculated based on the value of the average power [26]. For a pulsed laser, however, gain saturation may not be determined from the average power. As the pulse energy increases, gain saturation becomes dominant. For arbitrarily high gain, the Frantz-Nodvick equation can be used to calculate the gain [27]; but in general, the gain should be written as [21]

$$g(E) = g_0 \left(\frac{E_s}{E} \right) \left[1 - \exp \left(- \frac{E}{E_s} \right) \right] \quad E(z) = \int_{-\infty}^{+\infty} |A(z, T)|^2 dT \quad (3.9)$$

where g_0 is the nominal gain, $E(z)$ is the pulse energy of the amplification system at any position z , and E_s is the saturation energy for the particular rare earth doped fiber. This equation can be used to compute the saturated gain which can then be used to more realistically analyze the performance of the amplifier.

3.2.2 The unified model equation

As discussed, the common approach to analyzing fiber amplifiers is to separately use rate equations for computing the unsaturated gain in the CW regime of operation, and then to use the nonlinear Schrödinger equation to follow the evolution of a pulse in the system. For simple amplifying systems, the two methods can often suffice. However, for classic high power, high pulse energy multistage amplifiers, neither of the two approaches is sufficient. As an example, consider the two-stage amplification system shown in Figure 3.1. This system is comprised of a low power pre-amplifier and a high power main amplifier. To analyze pulse amplification and evolution in this

system, the gain along the length of the fiber must be known. It is unsaturated in the pre-amplifier but becomes saturated in the main amplifier. Clearly, neither the rate equations nor the nonlinear Schrödinger equation alone can fully describe the amplification and pulse evolution process in this system.

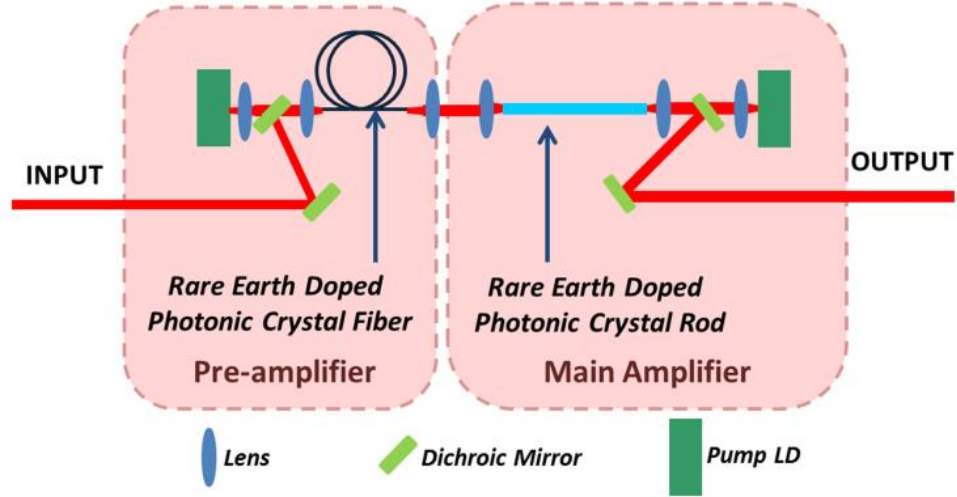


Figure 3.1 A two-stage fiber amplifier system.

However, a unified form of these sets of equations can provide a comprehensive consideration of the amplification and pulse evolution process in the fiber amplifier system. Although the rate equations and the nonlinear Schrödinger equation are derived from different considerations, they are connected by the gain. To obtain the gain along the fiber, the entire length of the amplifier system can be considered to be comprised of short distributed sections of amplifiers. For each short amplifying section, the gain can be taken to be a constant. Furthermore, spontaneous emission will be considered not to contribute much to pulse energy amplification. Therefore, at any position z along the fiber, the nominal gain for the pulse can be written as

$$g_0(z) = \Gamma_s [\sigma_{se}(\lambda)N_2(z) - \sigma_{sa}(\lambda)(N - N_2(z))]. \quad (3.10)$$

For high power amplifiers, gain saturation has a strong influence on the overall gain.

When gain saturation is considered, the unified equation that governs the propagation and amplification of a pulse in a rare earth doped fiber is [23]

$$\begin{aligned}
& \frac{\partial A(z,T)}{\partial z} + \frac{i}{2} \beta_2 \frac{\partial^2 A(z,T)}{\partial T^2} - i\gamma |A(z,T)|^2 A(z,T) \\
& = \frac{1}{2} \left\{ \left[\Gamma_s [\sigma_{se}(\lambda) N_2(z) - \sigma_{sa}(\lambda) (N - N_2(z))] \left(\frac{E_s}{\int_{-\infty}^{+\infty} |A(z,T)|^2 dT} \right) \right] \right. \\
& \quad \left. \cdot \left(1 - \exp \left(- \frac{\int_{-\infty}^{+\infty} |A(z,T)| dT}{E_s} \right) \right) - \alpha \right\} A(z,T) \tag{3.11}
\end{aligned}$$

The left hand side of this unified model equation accounts for dispersive and nonlinear effects that arise due to propagation of short pulses with high energies, while the right hand side accounts for the gain in the presence of gain saturation and loss processes. This unified model gives a better description of pulse evolution in a high power amplification system. With this new method, high power high pulse energy laser system would be easily simulated.

3.3 Reliability of the New Model

The simulation results of the unified model are compared to experimental results in order to assess the fidelity of the model. The experimental results used in the comparison are taken from the work of researchers at the Friedrich Schiller University of Jena in Germany [28]. The simulation parameters are given in Table 1 (taken or estimated from [28]). The gain medium considered in the amplifier is an Yb-doped photonic crystal fiber that has a slope efficiency of about 66%. Pump light absorption

is taken to be 30dB/m at 976 nm. The pulse compressor used is taken to have a throughput of 70%, leading to an overall slope efficiency of 46%.

Table 3.1 Amplifier parameters

Parameter	Numerical Value
Seed wavelength	1030 nm
Pump wavelength	976 nm
Absorption cross sections	Figure 1 of Ref.[2]
Emission cross sections	Figure 1 of Ref.[2]
Lifetime	1 ms
Seed laser power	0.5 W
Pump laser power	230 W
Fiber length	1.2 m
Estimated dopant concentration	$4.5 \times 10^{25} \text{ m}^{-3}$
Mode field area	$4000 \mu\text{m}^2$
Core diameter	80 μm
Inner cladding diameter	200 μm
Repetition rate	200 kHz
Pulse width	2 ns

We show in Figure 3.2, that the data from the new method in the red line have the closest match to the experimental results represented by the black line. Since the rate equations do not account for gain saturation of the pulses, the results obtained via this method do not closely follow experiment and show a pronounced deviation for large input powers where gain saturation becomes important. The anomaly with the nonlinear Schrödinger equation on the other hand is largely due to the fact that the value of the gain used in this method is not valid along the entire length of the amplifier. Results from this method are therefore not expected to faithfully reproduce

experimental data. The results from the unified model on the other hand closely follow experiment because the model accounts for the changing and distributed nature of the gain along the fiber length. Thus the new approach is reliable.

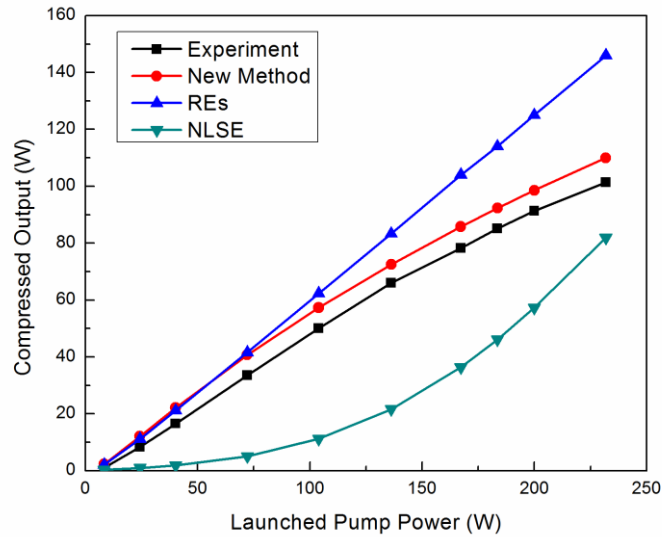


Figure 3.2 Compressed output power as a function input pump power launched into the amplifier system.

3.4 Advantages of the New Model

To achieve high peak power, the gain of an amplification system needs to be very high. A single amplifier is not enough. Consequently the system we discuss in this work is designed with two components that include a pre-amplifier and a main amplifier (Figure 3.3).

3.4.1 Classic multi-stage structure for high power laser system

In this proposed design, the pre-amplifier increases the pulse energy by 100 times in

an Yb-doped photonic crystal fiber. The length of the fiber is 2 m, which is shorter than the nonlinear length to minimize the nonlinearity. This length, however, is long enough to support such a high gain. The wavelength of the pump is chosen to be 976 nm because a Yb-doped fiber has its largest absorption cross section at this wavelength [2]. As shown in Figure 3.3, a pulsed seed laser and a forward pump laser are injected into the Yb-doped photonic crystal fiber via a dichroic mirror and a lens. The output of this system is the amplified pulsed seed laser. Since the average power of the input seed laser is 40 mW, forward pumping has some advantages. With forward pumping, the inverted population is relatively high in the initial region of the fiber. This helps the low power seed light to increase its power. The large gain in the initial region of the fiber increases the power dramatically, thus overcoming fiber loss [31].

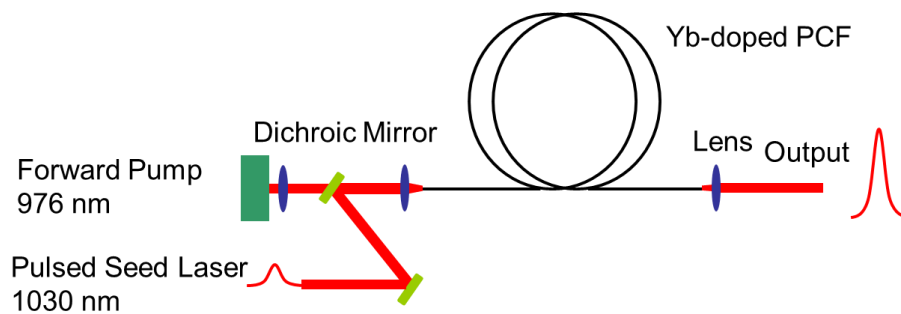


Figure 3.3 Structure of Pre-amplifier.

The main amplifier boosts the pulse energy by 30 times, resulting in over 1 mJ pulse energy. However, such high pulse energies and high peak powers may damage standard photonic crystal fibers. We therefore chose a new rod type photonic crystal as the gain medium for the main amplifier because of its larger gain and higher damage threshold. The photonic crystal rod has a large core area and high doping

concentration. The rod is also good for controlling the nonlinearity [9]. Since the photonic crystal rod cannot bend like a standard fiber, its length should be as short as possible to minimize the size of the amplifier and definitely shorter than the nonlinear length; we choose this to be 36 cm.

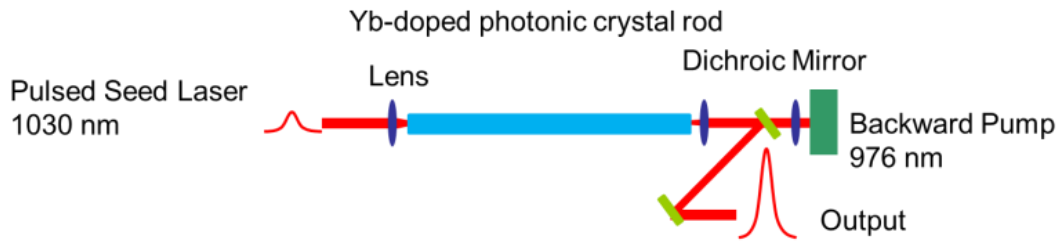


Figure 3.4 Structure of Main Amplifier.

As shown in Figure 3.6, the pulsed seed laser and the backward propagating pump laser are coupled separately from opposite ends of the Yb-doped photonic crystal rod. The output of this system is high energy pulses. In this pumping configuration, the backward pumping should yield higher gains than the other configuration because both the seed and pump lasers are highest in the same region of the photonic crystal rod [31]. The main amplifier, together with the pre-amplifier, should perform as expected.

3.4.2 Analysis of pulse amplification process with different modeling methods

We now discuss numerical simulation results for the designed amplification system based on the unified model discussed in the previous Section. Furthermore, the unified model results are compared to simulations based on the standard models

applied separately. The simulate system, as discussed in the previous Section, consists of a forward-pumped pre-amplifier and a backward-pumped main amplifier. Both pump lasers are continuous-wave. The parameter data set for the design of the pre-amplifier and the main amplifier are given in Table 2.

Table 3.2 Design parameters

Parameter	Numeral Value
Seed wavelength	1030 nm
Pump wavelength	976 nm
Absorption cross sections	Figure1 of Ref. [2]
Emission cross sections	Figure1 of Ref. [2]
Lifetime	1 ms
Repetition rate	40 kHz
Pulse width	2 ns
Pre-amplifier	
Seed laser power	0.04 W
Pump laser power	11 W
Fiber length	2 m
Estimated dopant concentration	$1.4 \times 10^{25} \text{ m}^{-3}$
Mode field diameter	29 μm
Core diameter	40 μm
Inner cladding diameter	200 μm
Main Amplifier	
Seed laser power	4 W
Pump laser power	800 W
Fiber length	0.36 m
Estimated dopant concentration	$4.5 \times 10^{25} \text{ m}^{-3}$
Mode field diameter	76 μm
Core diameter	100 μm
Inner cladding diameter	285 μm

Power and energy

We have chosen to calculate the average power and the gain as functions of distance along the pre-amplifier and main amplifier as determined by each of the methods discussed previously. In addition to output power, pulse energy is the other important variable of an amplification system.

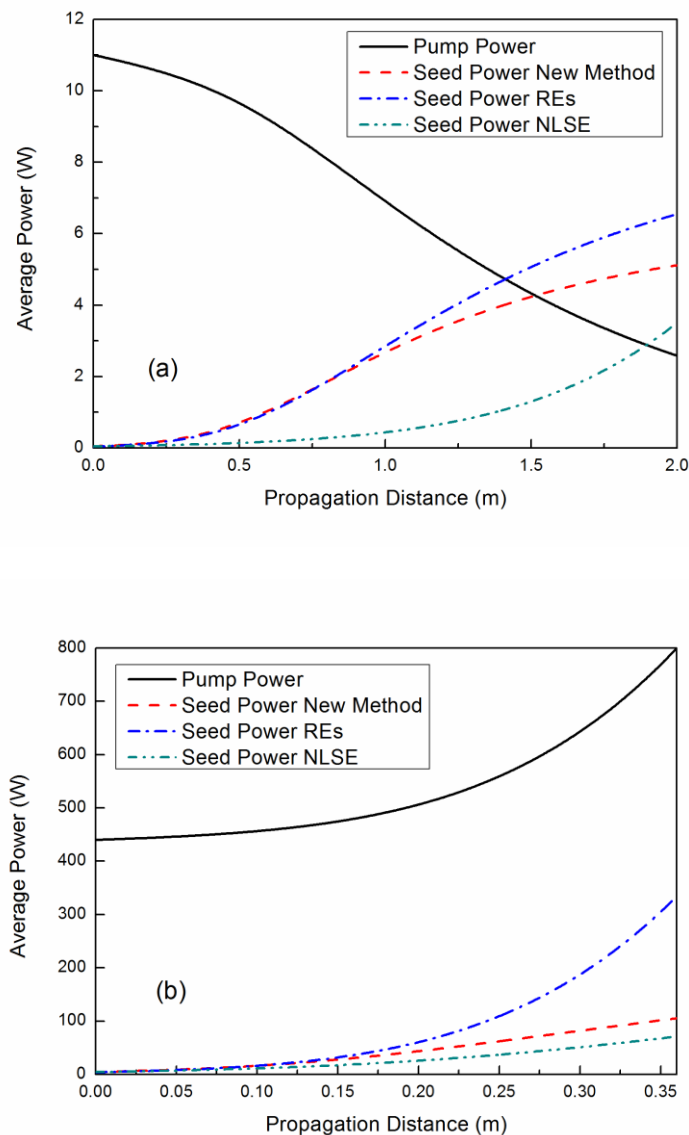


Figure 3.5 Average output power for the (a) pre- and (b) main amplifier as a function of propagation length.

The average power, for a given input, along the pre-amplifier of Figure 3.3 is shown

in Figure 3.5 (a). Note that the average power derived using the unified model is almost similar to that derived from the rate equations. This is so because the two models share a related gain calculated from the inverted population. The value of the average power along the amplifier as calculated from the nonlinear Schrödinger equation is quite different; this is primarily because there is no way of determining an appropriate value for the gain in the standard nonlinear Schrödinger equation.

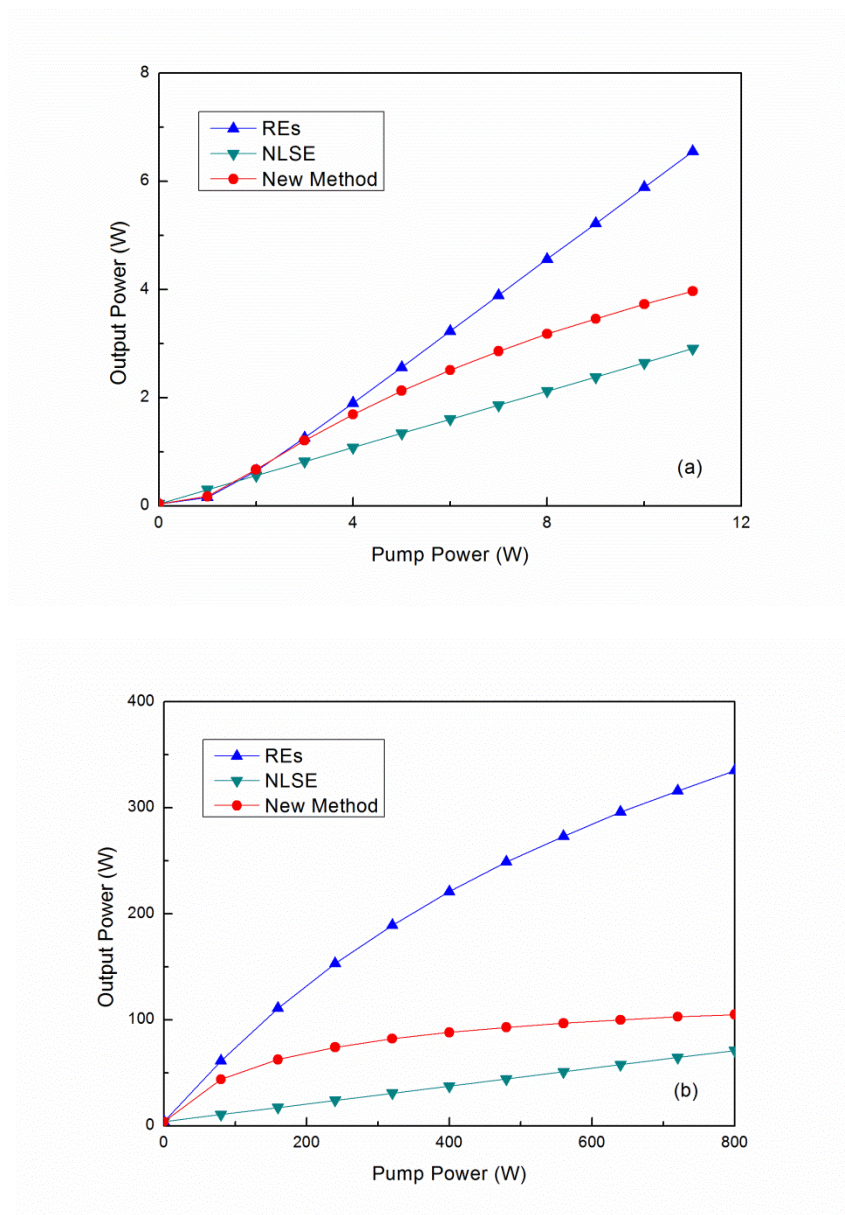


Figure 3.6 Output power for the (a) pre- and (b) main amplifier as a function of pump power.

In Figure 3.5 (b), which shows the behavior of the average power along the length of the main amplifier, one observes that the power calculated using the unified model closely follows the values computed using the nonlinear Schrödinger equation. In both cases, gain saturation is taken into account and because it is sufficiently large, it influences the power along the amplifier. In the blue curve, whose results are calculated using standard rate equation, gain saturation of the pulses is neglected, leading to an unnatural increase in average power with distance along the amplifier. Therefore, only the unified model which intrinsically accounts for all possible regimes of operation appears to give reasonable results.

The relationship between the output power and pump power for the pre- and main amplifiers are shown in Figure 3.6. For the pre-amplifier, the gain saturation is not very obvious. So when the pump power is relatively small, the results from the new method and the rate equations are similar. With the increase of the pump power, the difference occurs for the gain saturation. The result from the nonlinear Schrödinger equation is almost a straight line, which is unlike the real amplification process. For the main amplifier, gain saturation is obvious after the pump power reaches 160 W. The output results from the new method remain around 100 W, though the pump power keeps increasing. The curve from the rate equations increases with pump power showing no effects from the gain saturation. Knowing the repetition rate of the laser, one can determine the pulse energy. It should now be clear that the new method can handle the modeling and simulation of power and pulse energy of an amplifier system operating under different conditions.

Based on the unified model, the evolution of a 2-ns pulse launched into the main amplifier is shown in Figure 3.7. The constancy of the pulse shape is a key attribute of any good amplifier; furthermore, the pulse profile remains steady during propagation through this amplifier. The new method therefore makes simulation of pulse evolution quite straight-forward.

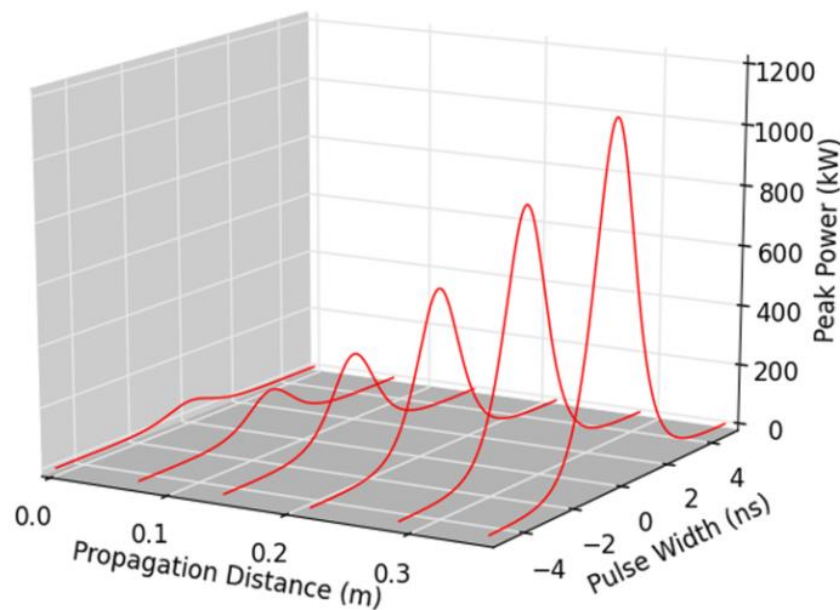


Figure 3.7 Pulse evolution in the main amplifier.

Gain, loss and gain saturation

The pre-amplifier and the main amplifier are operating under different amplification conditions. The pre-amplifier is forward-pumped and operates under unsaturated gain, while the main amplifier is backward-pumped, operating under gain saturation. These conditions and regimes of operation lead to different operating characteristics for each section of the amplifier.

In the pre-amplifier, the forward-pumping scheme concentrates the inverted population in the initial length of the fiber gain medium. The inverted population

dramatically decreases along the fiber. With a smaller inverted population, the gain of the pre-amplifier, as calculated using both the unified method and the rate equations monotonically increases and levels off gradually as shown in Figure 3.8 (a). Because the nonlinear Schrödinger equation approach does not account for changes in the inverted population, the gain calculated by this method is almost a straight line.

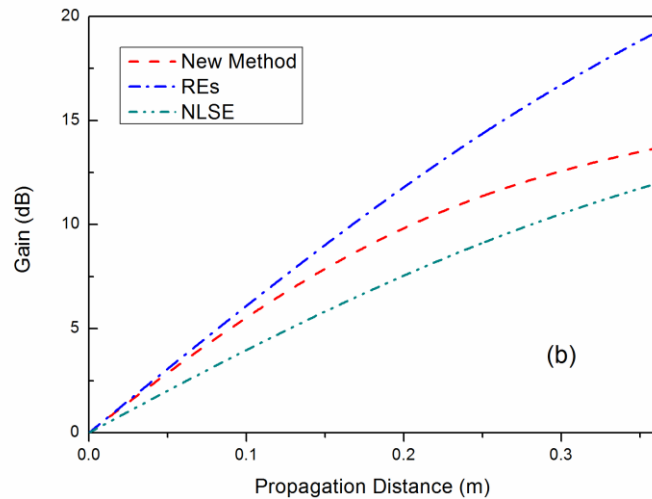
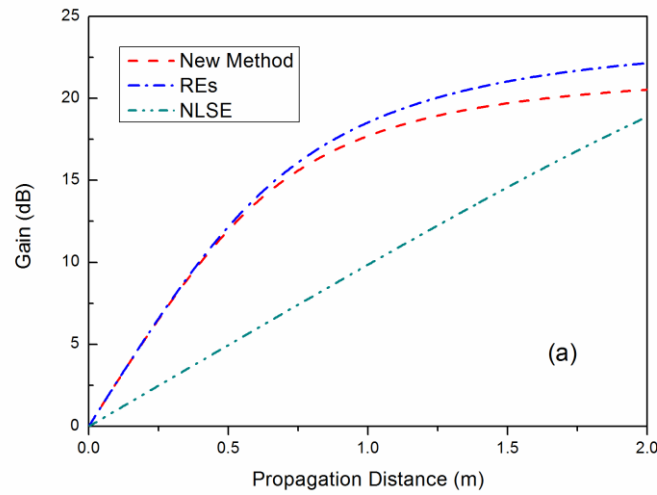


Figure 3.8 Gain of the (a) pre- and (b) main amplifier as a function of propagation length.

In the main amplifier, the effects of gain saturation cannot be ignored because they impact the amplification process. The curves in Figure 3.8 (b), obtained via the

unified method and the nonlinear Schrödinger equation, show an expected decrease in gain along the length of the rod; the curve derived from the standard rate equations on the other hand does not because of the neglect of the influence of gain saturation. Simulations using the unified method reasonably meet most design objectives. The versatility of this new approach in predicting physically reasonable results is also evident.

Dispersion and nonlinearity

In most schemes of light amplification for moderate power outputs, considerations for power and gain are the main objectives. However, in the design of high quality pulsed amplification systems, the impact of dispersion and nonlinearity must be taken into account. Dispersion and nonlinearity influence pulse evolution. A desirable pulse attribute as it propagates along an amplifier has already been alluded to; this attribute is the constancy of the pulse shape shown in Figure 3.7. Thus, one needs to stabilize the amplification process so that it preserves the temporal pulse shape.

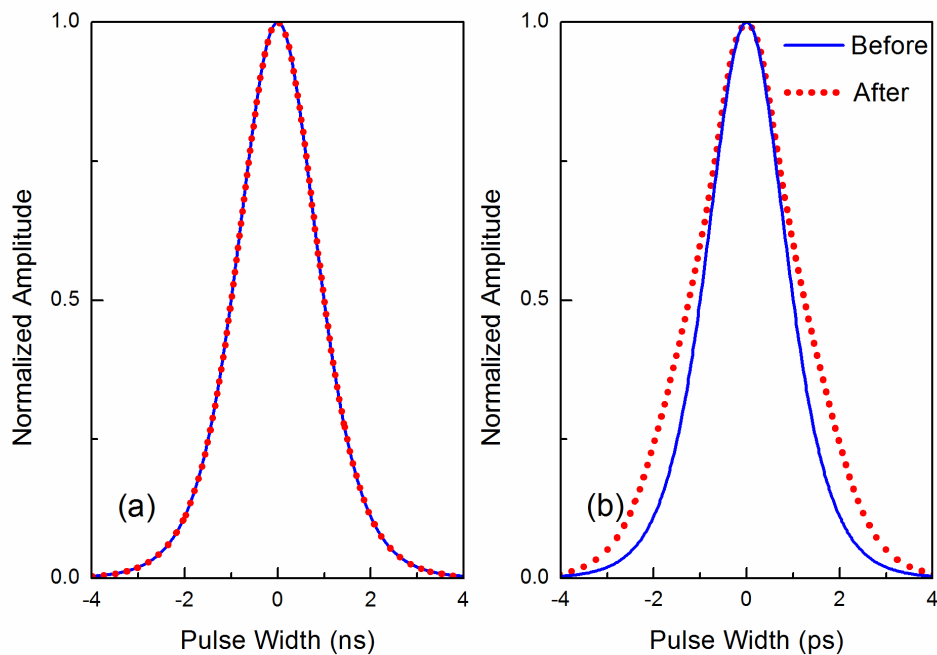


Figure 3.9 Time domain comparison of the input and output pulse envelopes in the main amplifier for (a) 2-ns pulse input, and (b) a 2-ps pulse input.

The normalized pulse envelopes before and after amplification for a 2-ns pulse in the pre-amplifier overlap with each other as shown in Figure 3.9 (a). In our designed case, because the initial pulse width is broad, dispersion can be neglected; the pulse profile remains constant and stable, and the amplification system provides high quality amplification. If all the parameters for the pulse remain the same except that the pulse is now reduced to 2 ps wide, pulse broadening due to spectral dispersion becomes an issue; this is clearly shown in Figure 3.9 (b). For even shorter pulse widths less than 1 ps, the effects of higher-order dispersion become important. These effects cause problems for high power amplification [32]. With this new method, the estimate of the dispersion can be done before building the lasers and amplifiers. In this case, the lasers and amplifiers can be design to enhance or control the dispersion based on the requirements.

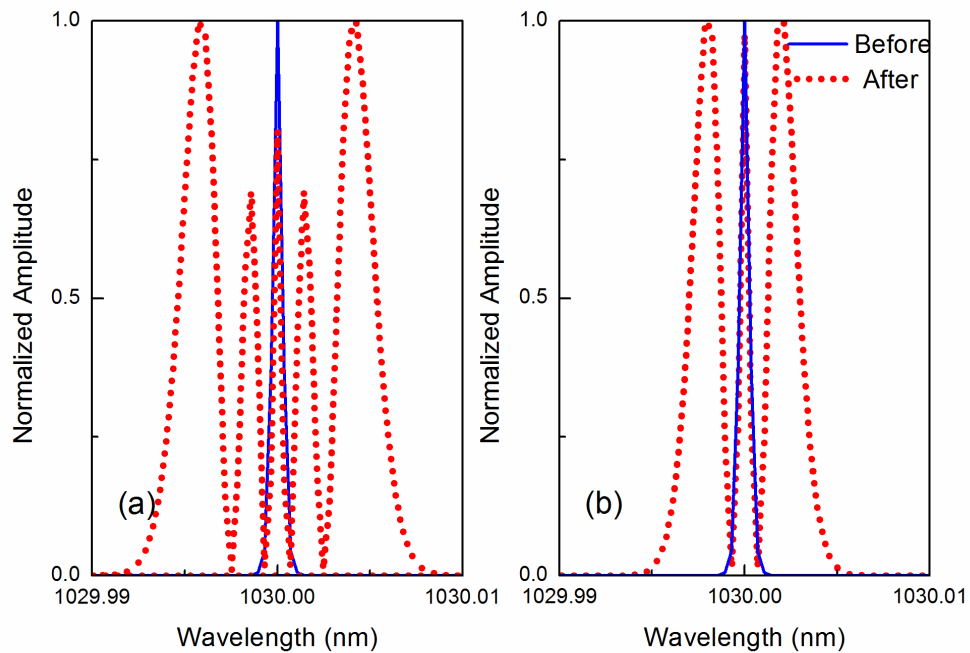


Figure 3.10 Frequency domain comparison of the spectral content of a pulse in the (a) pre- and (b) main amplifier.

Another issue that must be confronted in the design of high power amplifiers is nonlinearity. Generally, to avoid or minimize nonlinear effects, one chooses a fiber length that is shorter than the nonlinear length for the particular fiber in question. The lengths of the gain media in the design discussed here were carefully chosen to control nonlinearity. Another solution for the high peak power is to stretch the pulse width in order to lower the peak pulse amplitude.

Evidence of the impact of nonlinear effects can generally be extracted from the spectral content of a pulse. In Figure 3.10 (a) and Figure 3.10 (b), we show the spectra of the pulse before and after passage through the pre-amplifier and the main amplifier. It is evident that in the pre-amplifier, nonlinearity is very strong.

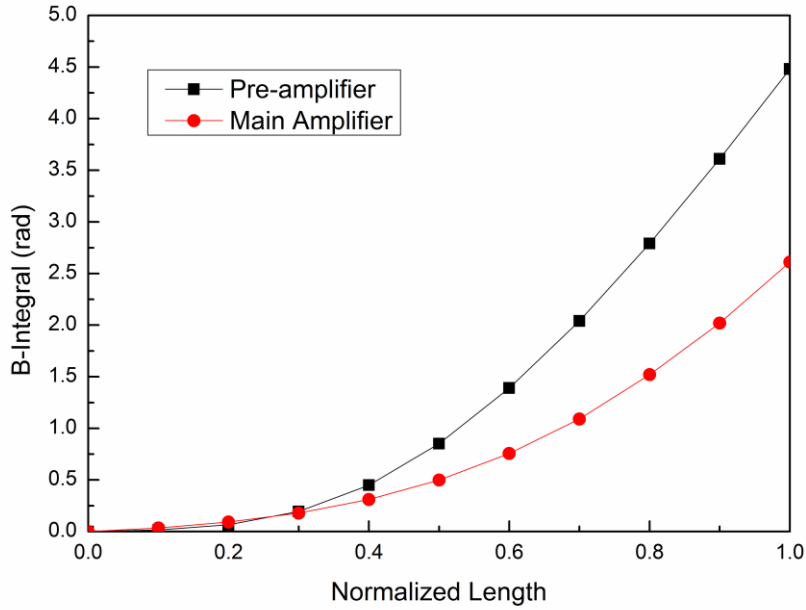


Figure 3.11 B-integral, a measure of fiber nonlinearity, as a function of normalized length along pre- and main amplifier.

A common measure of nonlinearity in fiber amplifiers is the B-integral [34]; it represents the magnitude of the nonlinear effects in the fiber amplification process. We show in Figure 3.11 the B-integral of the pre-amplifier and the main amplifier. The value of the parameter is larger in the pre-amplifier because of the longer path length, and this is consistent with Figure 3.10 (a). The unified model can clearly handle nonlinear effects in the design of fiber amplifiers.

In general, our new modeling method is able to provide insight into the design characteristics and key parameters of high power lasers and amplifiers. In contrast to traditional modeling methods, the new approach can be used to calculate power, gain and pulse energy. Furthermore, it can be used to describe the evolution of the pulse profile during the amplification process. Dispersion and nonlinearity can also be calculated to provide guidance in the design and construction of high power fiber

laser systems.

3.5 Summary

This Chapter introduced a unified approach for analyzing the performance of high-power fiber amplifiers. To provide context, we first discussed the traditional modeling methods that use rate equations and the nonlinear Schrödinger equation. Simulation results from the new method and the traditional methods are compared with experimental results. The new method closely follows the experiments while results based on the rate equations and the nonlinear Schrödinger equation do not.

The unified new method is shown to be capable of analyzing the operation of fiber amplification systems under a wide range of conditions which cannot be analyzed using the traditional methods. Because the method provides a more realistic assessment of the amplification process in both the high- and low-power regimes of operation, we use it to provide design guidance in the construction of rare earth doped fiber amplifiers which are discussed in the following Chapters.

4. YTTERBIUM-DOPED AMPLIFIERS CONSTRUCTED FOR STANDARD FIBER

In this Chapter, we introduce and discuss ytterbium-doped amplifiers constructed from standard fibers. The amplification processes for amplifiers with different types of seed sources are compared and contrasted. This Chapter will serve to highlight the issues important to constructing high power, high pulse energy fiber lasers and provide guidance for designing and building optical systems.

4.1 Ytterbium-doped Standard Fiber Amplifiers

When using standard Yb-doped fibers, the two types of seed laser sources and multi-stage fiber amplifiers are possible. The two types of seed sources are a continuous-wave seed laser or pulsed seed laser: each type leads to a different configuration and characteristic for the amplifier.

4.1.1 Continuous-wave and pulsed seed lasers

As discussed in Chapter 1, three main sub-systems are needed to build a fiber amplifier: the seed laser, the fiber gain media, and the pump laser source. In this Chapter, we discuss use of Yb-doped standard fibers as the gain media. When a continuous-wave (CW) laser beam is used to pump a Yb-doped fiber, it can provide a steady state population inversion condition. Therefore for the systems in this work, all the pump lasers are continuous-wave mode sources. The seed laser, on the other hand,

can be continuous-wave or pulsed, depending on the application. To better understand the amplification process, we have built two seed laser systems: one is continuous-wave and the other is pulsed.

Continuous-wave seed

The most common structure for building a continuous-wave seed laser with a Yb-doped fiber, is the ring structure shown in Figure 4.1.

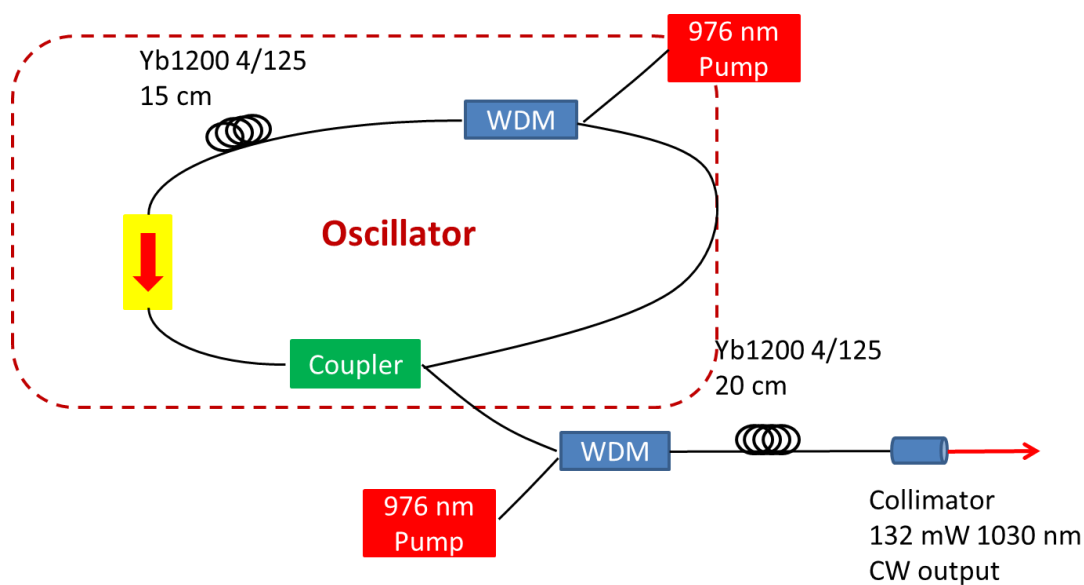


Figure 4.1 Configuration of continuous-wave seed laser.

The all-fiber seed source consists of two sections: a ring oscillator and a low power amplifier. A 15-cm long Yb-doped fiber with a core of 4 μm and a cladding of 125 μm serves as the gain media in the oscillator. The isolator is used to control the beam propagation direction. A coupler provides the output beam from the oscillator, and sends the feedback beam back into the loop. We use a wavelength division multiplexer (WDM) to combine the pump laser and generated seed beam which are then fed into the gain fiber. The oscillator can generate up to 14.8 mW of

continuous-wave output at the wavelength of 1029 ± 1 nm.

Although the output power level from the oscillator is adequate, it is not sufficient for the amplification. So an all-fiber based lower power fiber amplifier is connected to the oscillator. Using a 20-cm length of Yb-doped fiber similar in construction to the one in the oscillator as a gain media, the final seed output can be boosted to over 130 mW, which is large enough as input for multi-stage fiber amplifiers. For flexibility in optimizing the multi-stage fiber amplifiers, we use additional free-space optical components to construct the amplifiers. We use, for example, a collimator at the output of the all-fiber seed laser. The actual size of the continuous-wave seed laser is shown in Figure 4.2. Most parts of the seed laser are fiber-connected, so the laser is very compact. It is portable, collapsible, and robust. It can be operated outside of the laboratory.

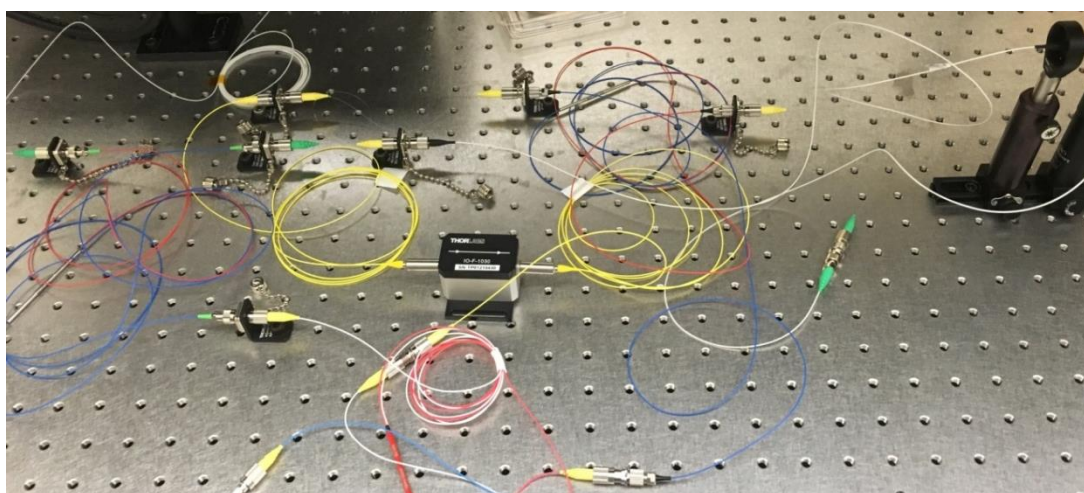


Figure 4.2 Actual size of continuous-wave seed laser.

Pulsed seed

There are two major approaches to building a pulsed seed laser with Yb-doped fibers. One is to construct a mode-locked laser, capable of providing a constant pulsed

stream. Although a mode-locked laser can provide an ultrafast laser beam, the repetition rate and pulse width are difficult to change once the last is built. The other common type of pulsed laser configuration is the master oscillator power amplifier (MOPA) shown in Figure 4.3. This all-fiber seed laser consists of two amplification stages. Stage 1 consists of a computer-controlled laser diode. This is followed with 15-cm long Yb-doped fiber that serves as the gain medium for the oscillator. As before, a WDM component combines the pump laser and generated seed for the input into the gain fiber. An optical (diode) isolator is used to control the beam propagation direction and to connect the two stages together. In the second stage, another WDM component combines the amplified seed and pump for the input into the 20-cm long Yb-doped fiber. The amplified output of laser diode can then be coupled through a free-space collimator to the high power, high energy amplification system.

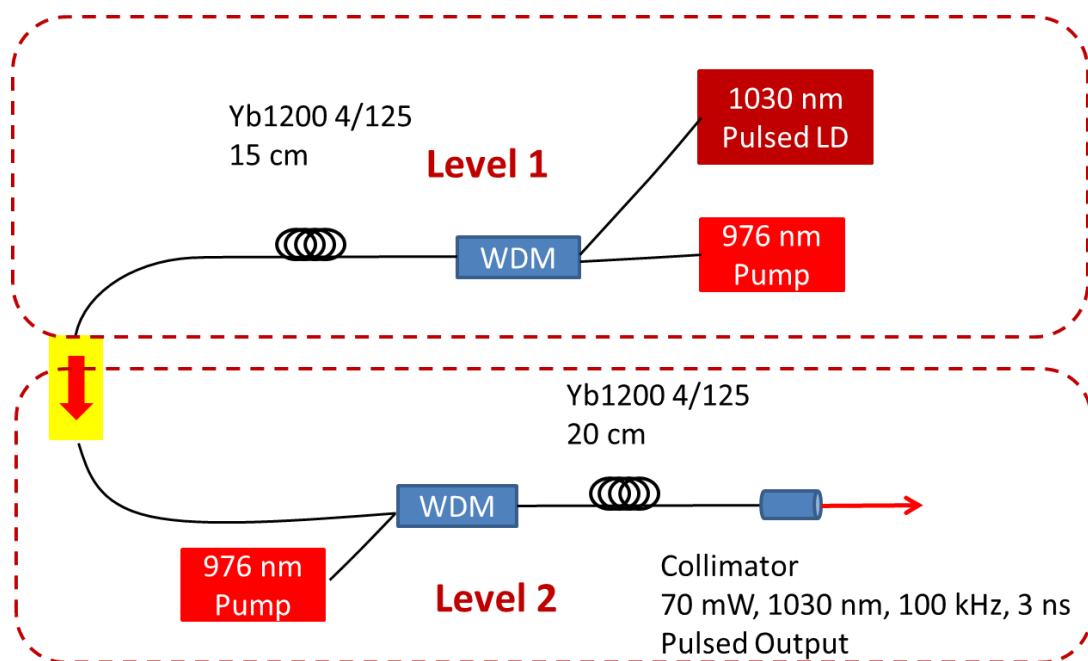


Figure 4.3 Configuration of pulsed seed laser.

The need for the seed amplifier system is because the output of the

computer-controlled laser diode is a mere 10 uW, which is not large enough for the subsequent amplification process. However, after a two-stage amplification process (to 3.7 mW in the first stage, and to 70 mW in the second stage), the output is sufficient for multi-stage high power, high energy fiber amplifiers.

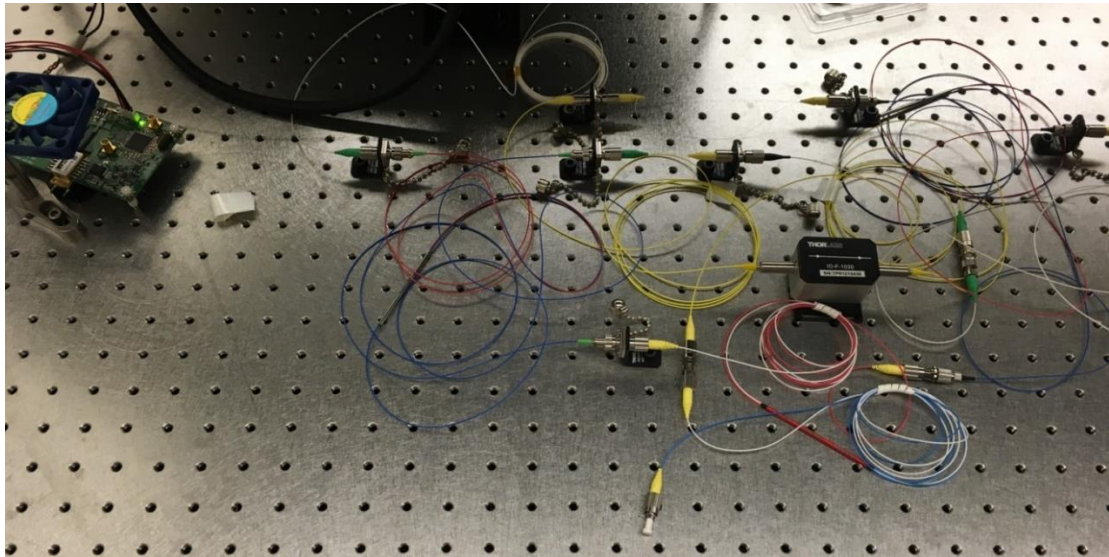


Figure 4.4 Actual size of pulsed seed laser.

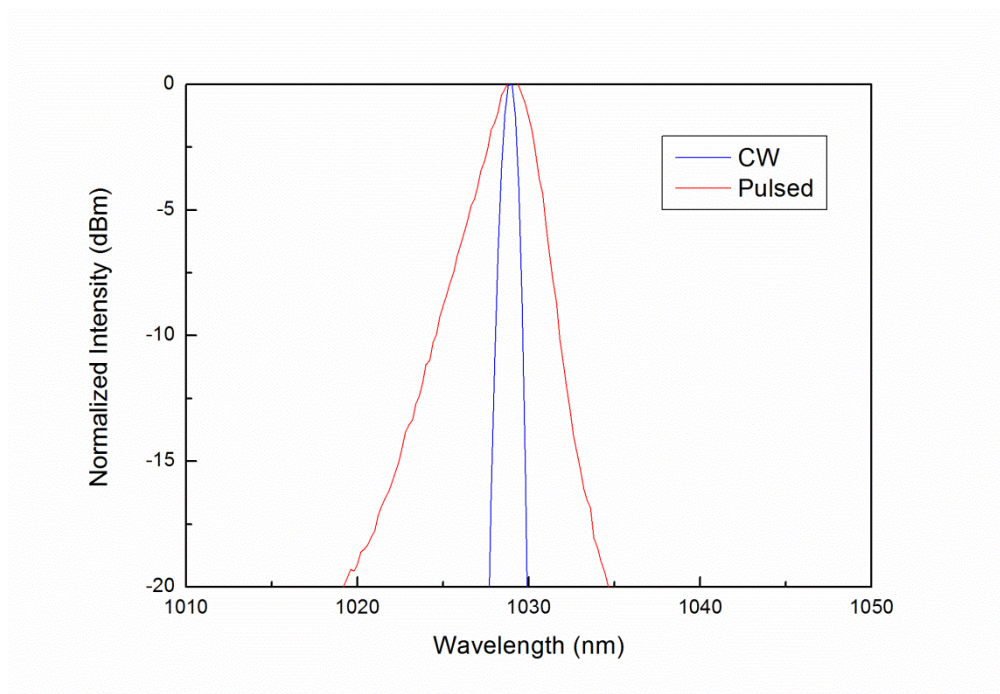


Figure 4.5 Spectra of continuous-wave and pulsed seed lasers.

The selected pulse width for the seed diode laser is 3 ns, and the repetition rate is

100 kHz. Figure 4.5 shows the spectra of the continuous-wave and pulsed seed lasers. Both seed lasers emit around a central wavelength of 1030 nm, but the pulsed laser seed has a broader linewidth. The ring oscillator structure of the cw seed is thought to contribute to the narrowing of its linewidth. Diode lasers generally have broader spectral linewidths.

4.1.2 Design and configuration considerations for the multi-stage fiber amplifiers

The amplification system constructed consists of three sub-systems as shown in Figure 4.6. These are the seed laser source, the pre-amplifier, and the main amplifier. As mentioned earlier, for flexibility and ease in optimization of key system performance parameters, the prototype freely uses free-space optical components. It is envisioned that in product version of the system, the fiber sub-components could be spliced together to form an all-fiber structure.

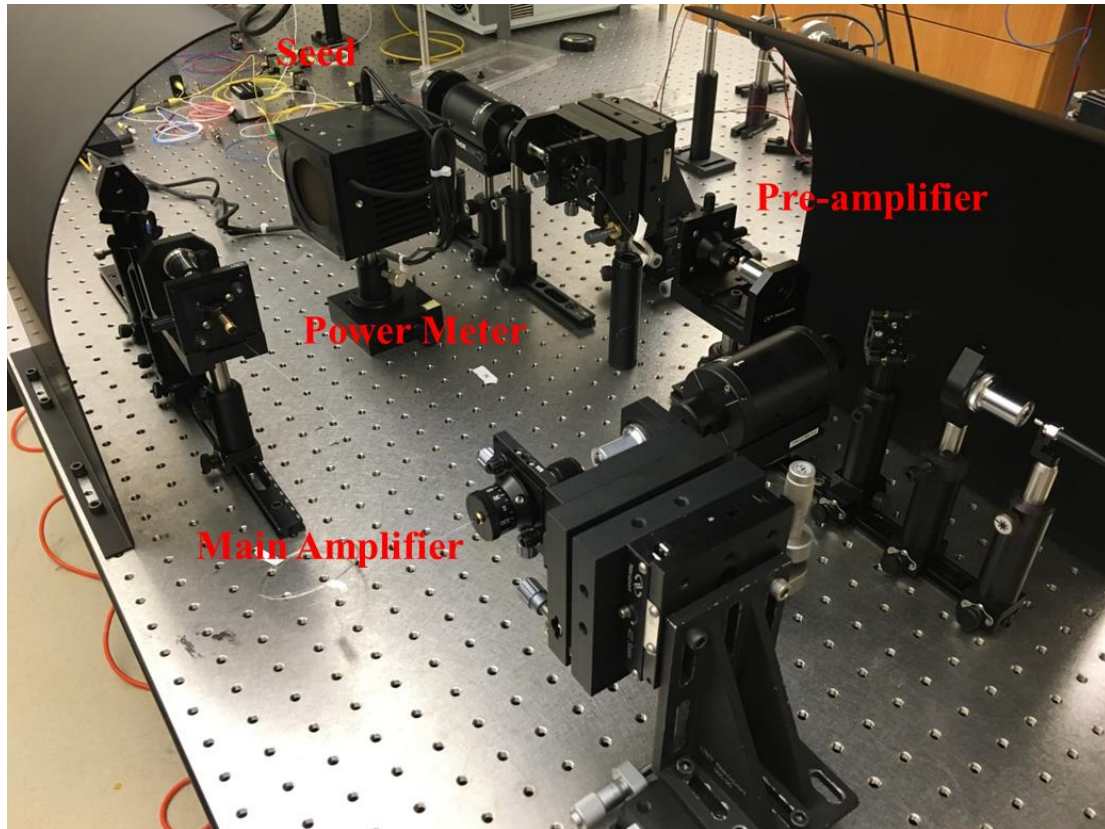


Figure 4.6 Configuration of the whole amplification system.

We now discuss the two-stage amplification system that uses the seed lasers as input. Our chosen configuration of a pre-amplifier and a main amplifier uses a backward-pumping scheme for improve pump absorption.

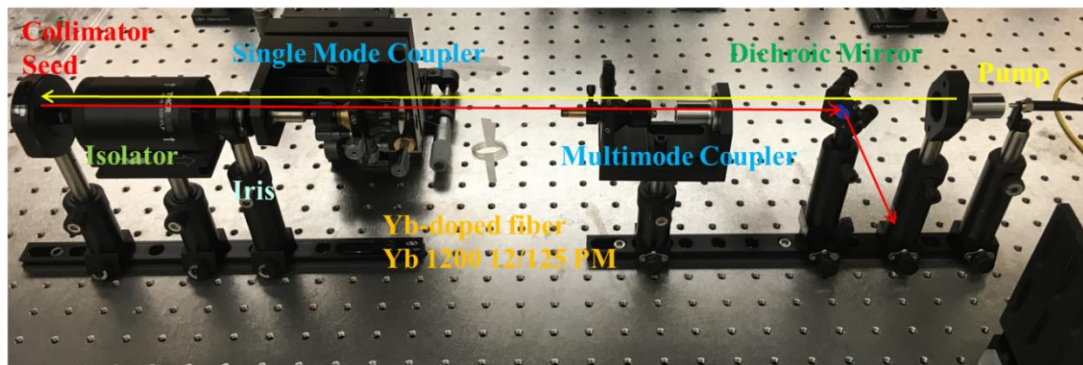


Figure 4.7 Configuration of the pre-amplifier.

The photograph in Figure 4.7 shows the configuration of the pre-amplifier. The red arrow line shows the direction of seed propagation, while the yellow arrow line shows the direction of the pump propagation. The collimator at the output of the all-fiber

seed laser forms a beam with a 0.5-mm beam diameter. The isolator enforces beam directionality in addition to protecting the seed laser. The low initial power level of the seed laser in the pre-amplifier assures that most of the power of backward pump will be fully converted to the power of the seed laser. Since there is a likelihood that the backward residual pump may be sufficient to cause damage the isolator, an iris is used to block any residual pump beam. To couple the single mode seed to the core area of the pre-amplifier fiber, we use a single-mode coupler with a five-axis degree of adjustment mounted on a three-axis platform fixture. The single mode coupler has a rotating adjuster for polarization control. For coupling the backward multimode pump laser into the cladding pumping area, we use a multimode coupler. Because cladding pumping is relatively simple, the three-axis multimode pump coupler can accurately couple the multimode pump into the fiber. To spectrally separate the pump from the seed, we use a dichroic mirror that transmits the pump wavelength of 976 nm from the seed wavelength of 1030 by reflecting the latter. Note that 3-meter long Yb-doped pre-amplifier fiber is coiled to a diameter of 4 cm to suppress high-order modes.

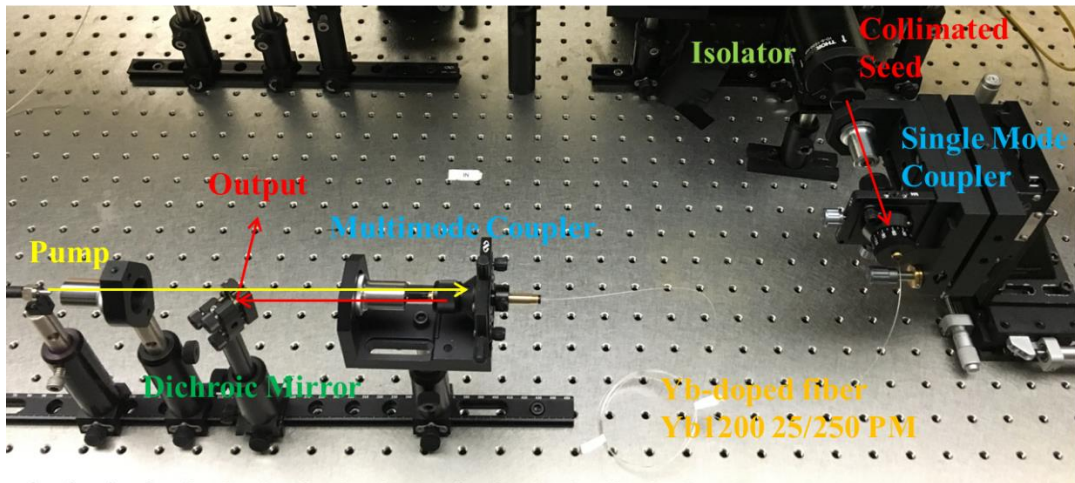


Figure 4.8 Configuration of the main amplifier.

4.1.3 Analysis of amplification in standard fiber amplifiers

Using the two types of seed lasers and the high power, high energy multi-stage fiber amplifiers already discussed, we successfully demonstrated operation of laser amplifier systems in both continuous-wave and pulsed mode. The spectra for the continuous wave mode of amplification process are shown in Figure 4.9.

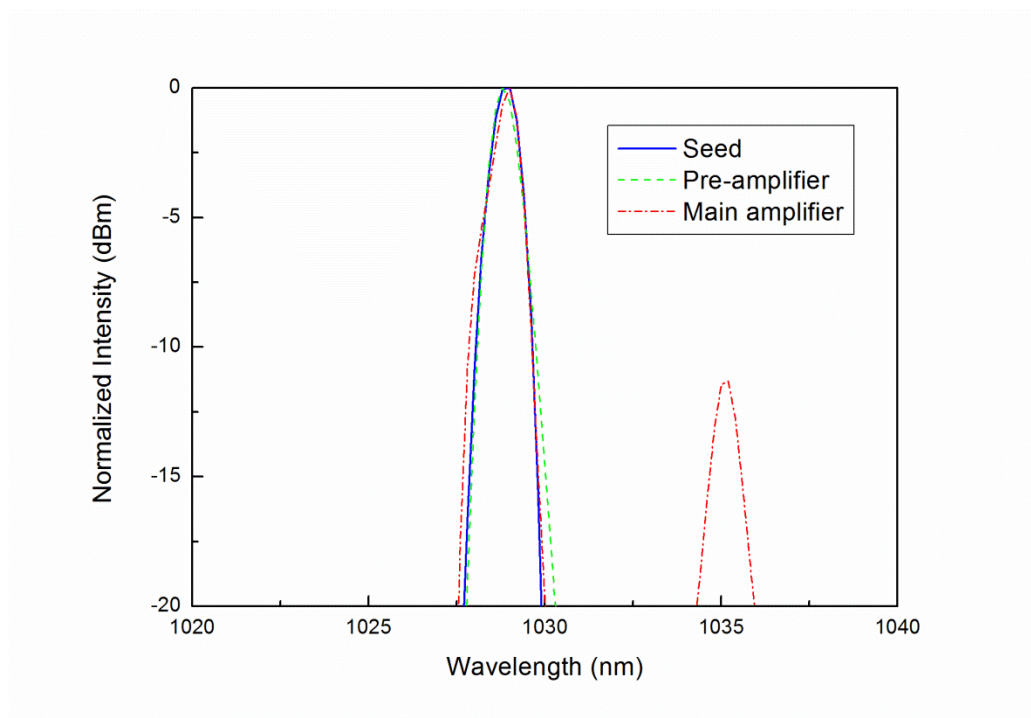


Figure 4.9 Spectra of the continuous-wave laser amplification process.

In particular given experiment, a CW seed power of 60 mW is coupled to a pre-amplifier capable of providing a 12 dB gain. The pre-amplifier boosts the seed laser beam to 900 mW. With a relatively short length for the collimator and a small core diameter for the fiber in the pre-amplifier, we find that there is mismatch between the beam diameter of the seed and that of the core. This mismatch leads to a coupling loss. Furthermore, the isolator probably causes a 70 % power loss. With proper adjustments of the free-space components, one can get an output of 200 mW from the pre-amplifier, which becomes to input to the main amplifier. The gain in the main amplifier is about 11 dB and with this, 3 W can be obtained as final output. Due to the relatively input seed powers, the final output contains amplified spontaneous emission around 1035 nm; this is shown in Figure 4.9. The intensity of the amplified spontaneous emission is below 10 dBm; even though this is low, it still limits the amplification of the seed laser. For increasing pump power, the majority of the added power (energy) is converted to amplified spontaneous emission. Figure 4.9 shows that the amplification process of the two-stage amplifiers is very clean, with no major spectral shape changes during the amplification process. It generates a total gain of 23 dB, but it is not or practical system. The losses in the system are too high, especially coupling losses. The conversion efficiencies in both the pre-amplifier and amplifier fibers are not very large. Finally, since the system shows an obvious amplified spontaneous emission issue, this is likely to develop into a major problem in the quality of the final beam.

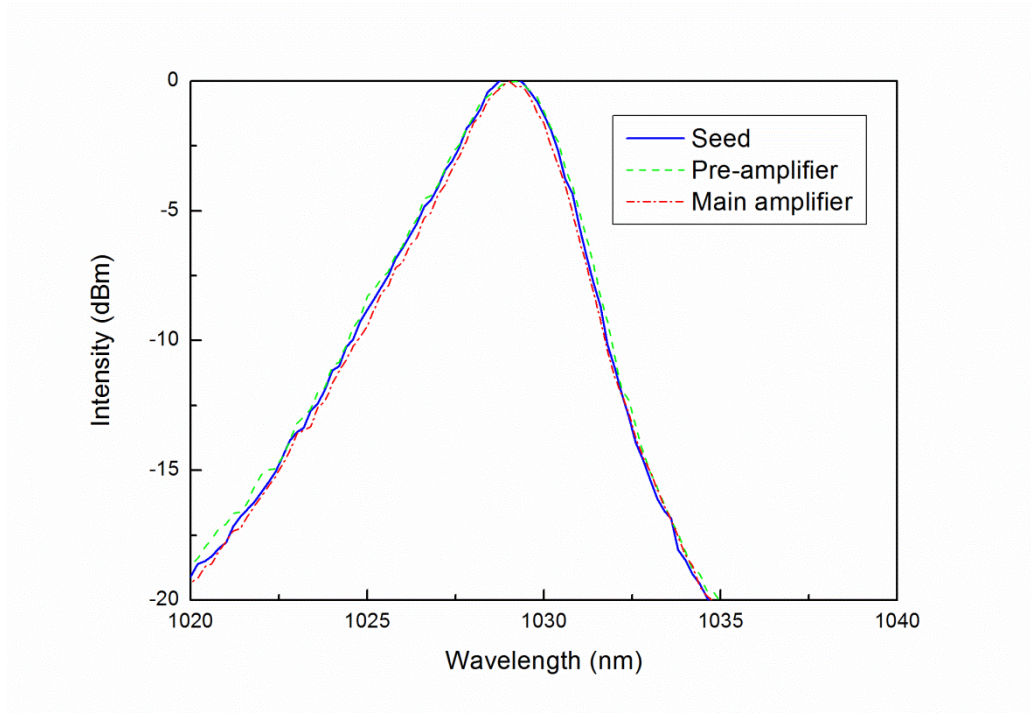


Figure 4.10 Spectra of the pulsed laser amplification process.

We compare the spectra of the continuous wave seed laser at different stages of the system in Figure 4.10. Notice that the spectrum of the seed, pre-amplifier and main amplifier overlap. There are no spectral shape changes. The coupled seed power in this experiment is 40 mW. The pre-amplifier is designed to provide 14 dB of gain which should boost the seed to an amplified level of 1 W. As in the previous experiment, however, beam divergence is large and leads to a mismatch in coupling. The isolator also contributes a significant loss of about 70 %. In the end, the actual measured input to the main amplifier is 500 mW. With a gain of about 10dB in the main amplifier, its actual output is 5 W. With the low gain in the main amplifier, there is no significant amplified spontaneous emission in the spectra. Though the amplification process in this experiment appears satisfactory, the gain and final output is not large. These are mainly limited by the properties of the gain fiber. Standard

Yb-doped fiber cannot provide enough gain and output in high power, high pulse energy amplification systems.

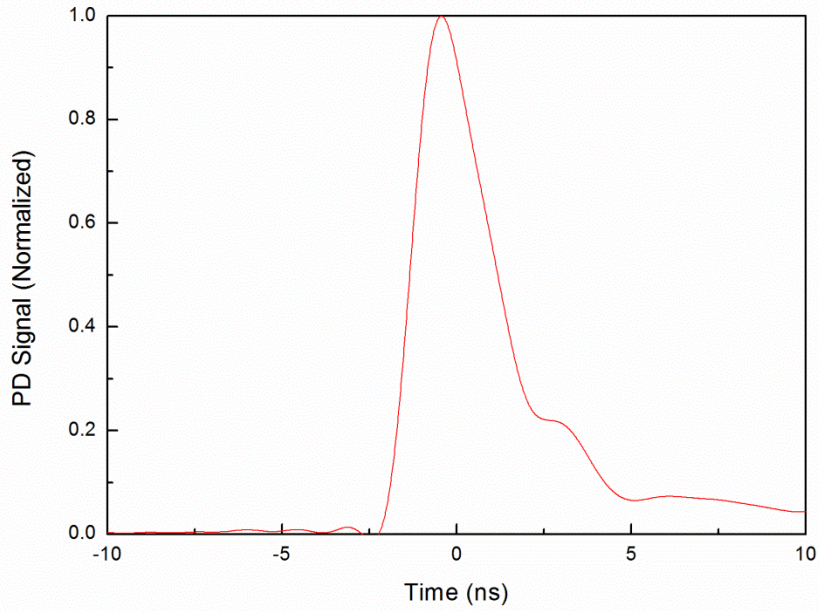


Figure 4.11 PD signal of the pulse with 3 ns pulse width.

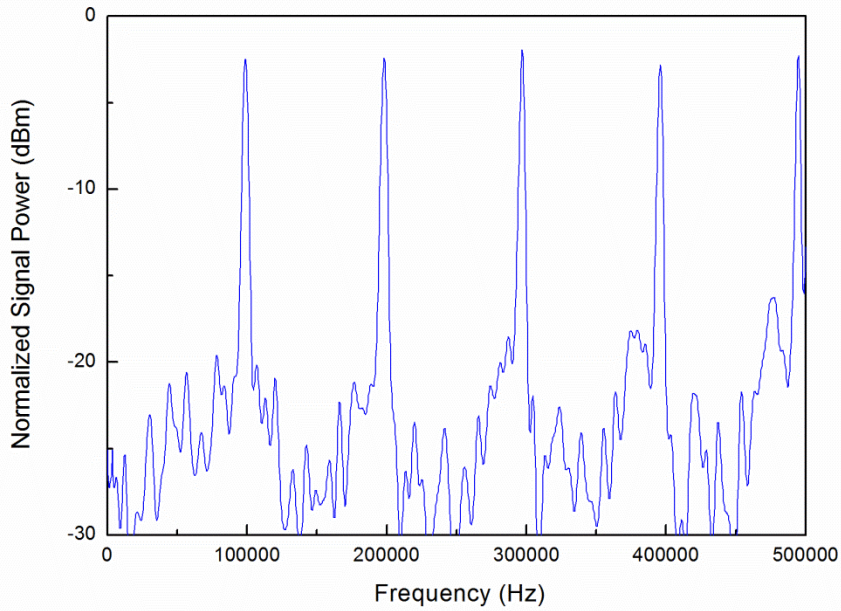


Figure 4.12 Electrical spectrum of the pulsed laser output.

Figure 4.11 pulsed laser signal as obtained with an ultrafast photodetector. The pulse width is 3 ns. Figure 4.12 is the pulse train as determined by an electrical spectrum analyzer. The repetition rate of the pulsed laser is 100 kHz.

To briefly summary the results of the experiments, we find that although amplification process is adequate, the coupling losses and the low gain of the standard fibers would make it difficult to construct an acceptable high power, high pulse energy amplification system.

4.2 Issues of Amplification

The two classes of fiber amplification systems introduced using standard fibers highlight the need to find alternative fibers for high power, high pulse energy amplification. In the following we discuss some of issues before build presenting the experimental work on high power, high pulse energy Yb-doped fiber amplifiers using a new fiber type.

4.2.1 Coupling and slope efficiency

Laser beam coupling into and from fibers is always the most challenging aspect of working with fiber amplifiers. As discussed in Chapter 2, the simultaneous coupling of seed light and the pump into a double clad fiber structure is very unusual.

The pump laser, which is generally multimode, is coupled into a pump area that is hundreds of microns in diameter. The numerical aperture of the cladding is usually

about 0.48, which is straight forward to couple into. A common three-axis coupler is good enough for coupling the pump laser. The real challenge and difficulty is coupling the seed; the process can be inefficient because of high losses. Coupling of single spatial mode beam can be described by the following equation [1]:

$$f = D \left(\pi \omega / 4 \lambda \right) \quad (4.1)$$

In order to couple light of wavelength λ from a collimated laser beam with beam diameter D into a fiber of mode field diameter ω , the focal length of the coupling lens must be chosen to be f . For collimated infrared laser beams, the beam diameter has to be at least 1 mm to minimize beam divergence. In this case, a large mode field diameter and large focal length would provide a good coupling efficiency. To increase the coupling efficiency, a five-axis coupler is usually used with a three-axis mounting platform. The three-axis platform provides a rough adjustment of the beam position. The five-axis coupler can do the precise adjustment in any common three-axis direction. In addition, this type of coupler can tune the angle of the beam accurately to better couple the single mode beam to the fiber.

Slope efficiency is a very important parameter of fiber amplification. It determines the power conversion between the pump laser and seed light. To increase slope efficiency, the doping concentration of a fiber should be high. A larger core area therefore would allow a larger dopant volume in unit length of fiber. When an efficient coupling process and a high slope efficiency conditions are created, one can successfully build a high power, high pulse energy laser amplifier.

4.2.2 Amplified spontaneous emission

The rare-earth doped fibers have been used as the gain media in fiber lasers and fiber amplifiers for many years. The excellent properties of these rare-earth doped fibers have brought in a variety of applications in different areas. However, amplified spontaneous emission has always been a problem during the amplification process in the fiber amplifiers, especially in high power, high pulse energy amplifiers. Amplified spontaneous emission is effected by several complicated factors. Pump laser power and fiber length, for example, may strongly effect amplified spontaneous emission. In this work, we investigate Yb-doped fiber amplifiers because of their outstanding conversion efficiency [2]. Amplified spontaneous emission in Yb-doped fiber amplifiers is usually very obvious when the pumping sources are of high power. Unfortunately, this may limit the conversion efficiency in the amplifier. In this section, we analyze amplified spontaneous emission in Yb-doped fibers under different situations, especially under unsaturated gain conditions in strongly-pumped fibers with different lengths.

Considering the energy level structure of Yb in silica together with the absorption and emission cross-sections, one generally chooses the pumping wavelength for the fiber amplifiers be 976 nm [2]. The issue of unsaturated gain regime in Yb-doped fiber has been under investigation for many years. We introduced the modeling of this situation earlier in Chapter 3 [8]. For the unsaturated gain regime, the emission cross-section represents the intensity of the spontaneous emission at various wavelengths in Yb-doped fibers [8]. In a simple model, amplified spontaneous

emission generation in Yb-doped fibers can be considered as emission of the fiber amplifier without the seed light. With these considerations, one can easily evaluate amplified spontaneous emission in unsaturated Yb-doped fibers.

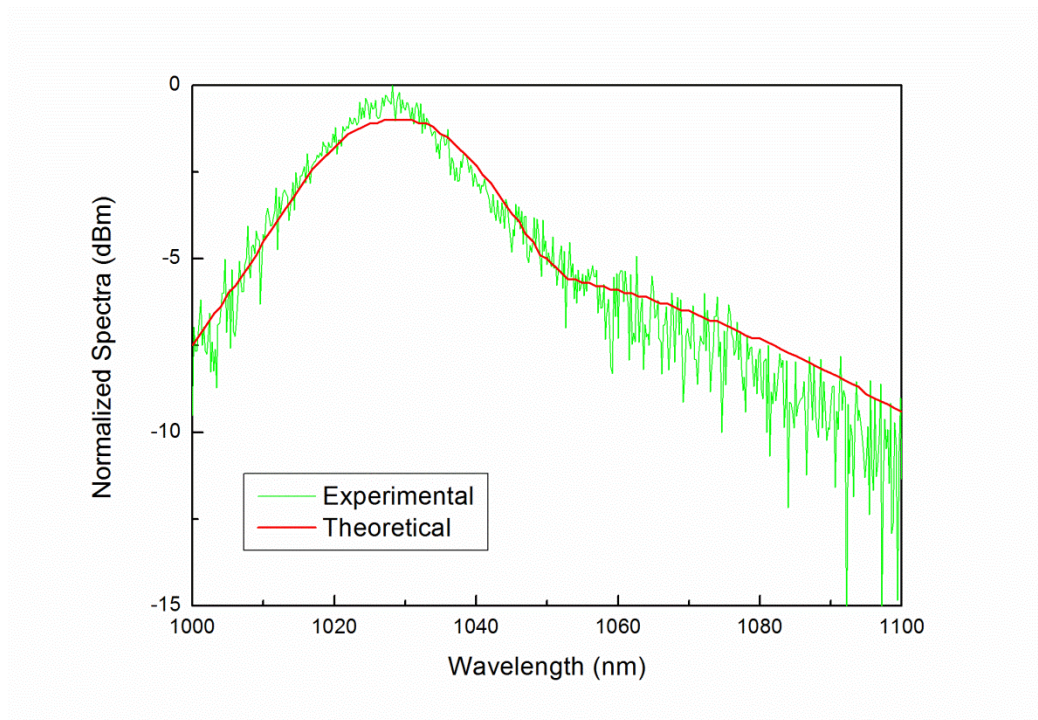


Figure 4.13 Comparing between theoretical and experimental results for backward ASE generated in 2 m long Yb-doped fiber with 2 W pumping.

Figure 4.13 shows the spectrum of backward amplified spontaneous emission between 1000 and 1100 nm. The theoretical results from the model referenced above closely follow the experimental result, with both the spectra having the largest intensity around 1030 nm, which is also the wavelength with the largest emission cross-section [2]. To experimentally investigate the nature of amplified spontaneous emission in Yb-doped fibers, we built the system shown in Figure 4.14.

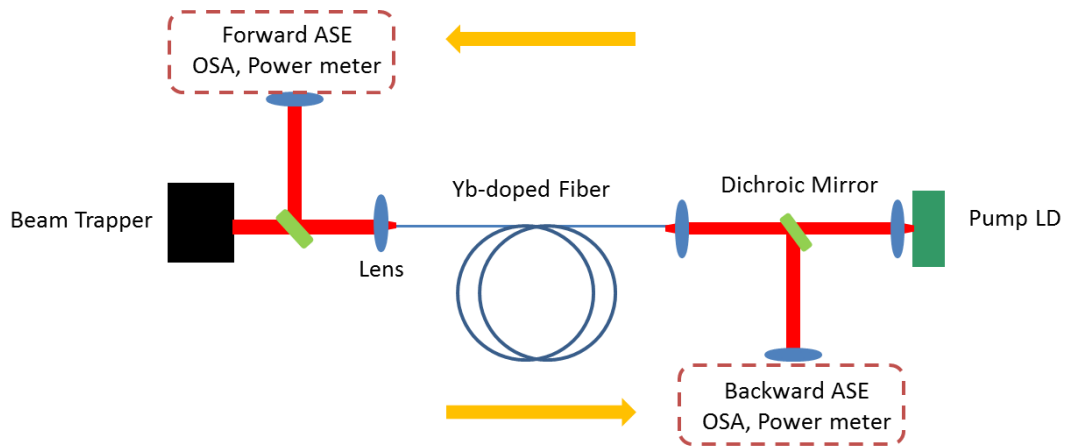


Figure 4.14 Amplified spontaneous emission generation in Yb-doped fiber.

As in all experiments in this thesis, we use backward pumping. The emission spectra are measured with an optical spectrum analyzer (OSA), while the power is measured with a thermal power sensor or a power meter with a calibrated photodetector. In the Yb-doped fibers, amplified spontaneous emission is generated in two directions: forward and backward. In unsaturated rare-earth doped fibers, backward amplified spontaneous emission is stronger than forward amplified spontaneous emission because of better absorption [31]. As pump power increases, the intensity of the amplified spontaneous emission also increases until the Yb-doped fiber saturated. The Yb-doped fibers used in this experimental set up are the same as those used in the two-stage fiber amplification system discussed earlier.

The amplified spontaneous emission spectra of Yb-doped fibers of different lengths are quite similar when the fibers have just reached saturation (Figure 4.15). To obtain the saturated amplified spontaneous emission spectra shown in Figure 4.15, the different pumping levels are used for different fiber lengths. Since longer fiber provides better absorption, it is easier saturate. Just at the point of saturation, the upper level atomic population of Yb-doped fibers is highest; the intensities of the

amplified spontaneous emission at the different wavelengths therefore related to the special emission cross-sections. Generally, the amplified spontaneous emission spectra follow the shape of the emission cross-section closely in this situation [35]. However, as the pump power grows, the spectra of the amplified spontaneous emission can be quite different.

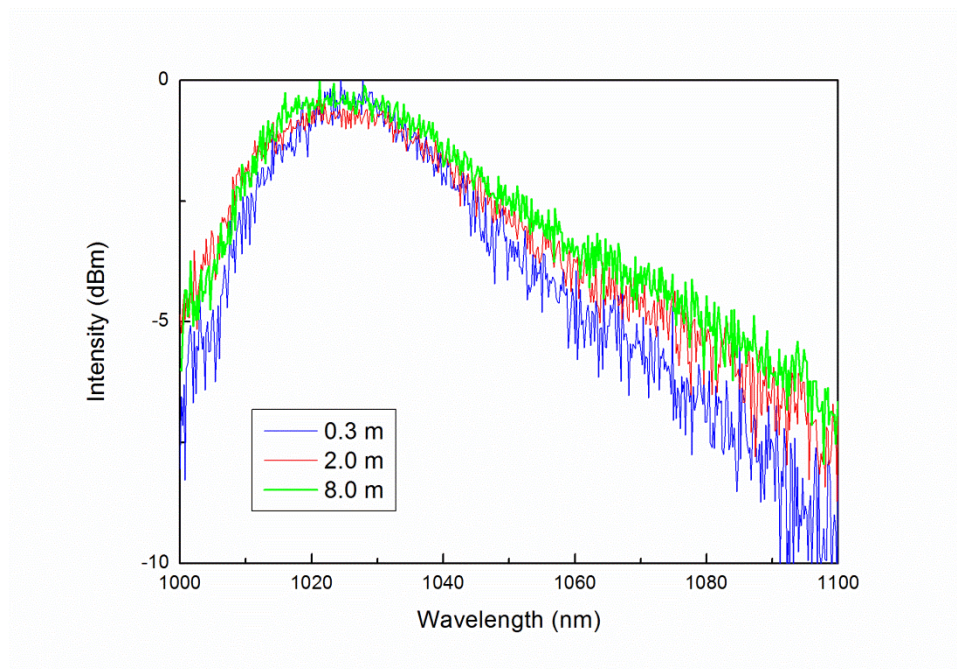


Figure 4.15 Amplified spontaneous emission spectra in Yb-doped fibers (0.3, 2, & 8 m) reaching saturation.

The fiber configuration for investigating amplified spontaneous emission (Figure 4.14) is similar to that of a fiber laser without cavity. Perpendicularly cleaved fiber ends can provide, through Fresnel reflection, feedback for laser oscillation [35]. Increasing the pump power can lead to an inverted population that is large enough to set the system into lasing mode. The spectra for amplified spontaneous emission and for lasing in Yb-doped fibers (with lengths of 0.3, 2 and 8 meters) are shown in Figure 4.16. The general characteristic of the spectra follow the trends of the spectra in

Figure 4.15. Specific lasing peaks occur at certain wavelengths that are dependent on the length of the fiber. This dependency is caused by the properties of the energy levels of Yb^{3+} (Figure 4.17), the dopant in the fibers [2].

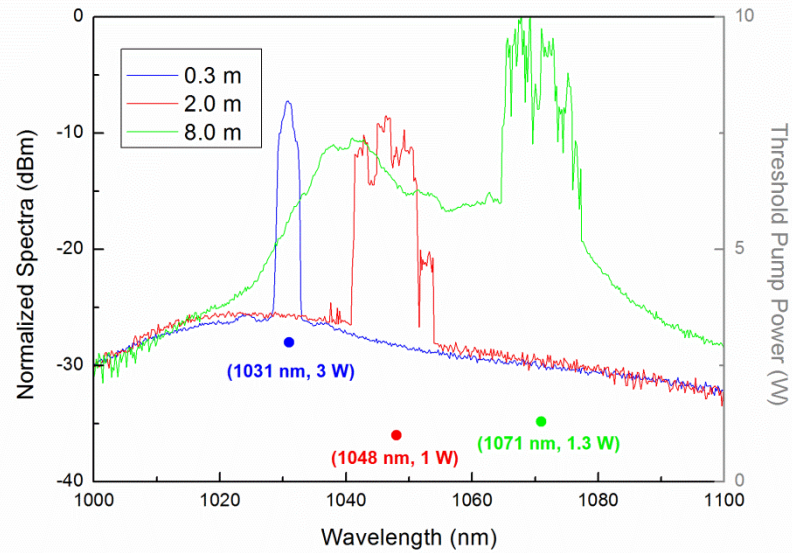


Figure 4.16 Amplified spontaneous emission and lasing wavelength shifting in Yb-doped fibers with different fiber lengths and threshold pump powers.

The energy level structure of Yb^{3+} , shown in Figure 4.17, is quite simple and consists of two manifolds: the ground state manifold $^2F_{7/2}$ (with four Stark levels labeled L_0-L_3) and the excited state manifold $^2F_{5/2}$ (with three Stark levels labeled U_0-U_2), around 10000 cm^{-1} above the ground level [1]. Strong absorption in Yb-doped fibers occurs when the fiber is pumped at a wavelength close to 976 nm. Common amplified spontaneous emission spectra follow the fluorescence spectra of Yb^{3+} . In the strongly pumped regime, the population structure is complicated. In a short fiber (0.3 m), lasing is due to a three-level system. The central wavelength is around 1031 nm, and the bandwidth is very narrow. In the 2-m long fiber, light is emitted from a quasi-three-level system, leading to a broad bandwidth from 1040 to 1052 nm. The

spectrum for the 8-m long fiber is quite complicated: there is a wide steep peak from 1065 to 1078 nm; note also that a gradual peak of amplified spontaneous emission occurs and is centered at 1040 nm. It appears that amplified spontaneous emission follows the absorption and emission cross-sections over an entire spectral range [1], [2]. Fiber length appears to have no impact on the amplified spontaneous emission spectra. However, varying the fiber length can lead to dramatic changes in the lasing wavelengths as shown in Figure 4.16. Longer fiber length tends to red-shift the lasing wavelength. This phenomenon is not affected by pump power level.

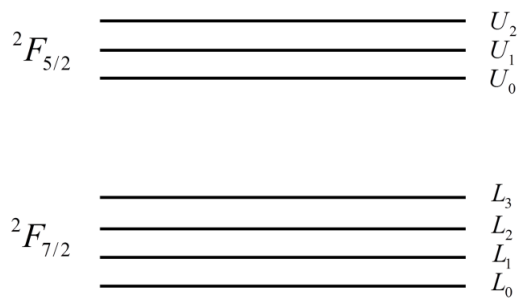


Figure 4.17 Energy level diagram of Yb³⁺.

Figure 4.16 also shows the shift in wavelength and change in pump threshold for Yb-doped fibers. Similar phenomena are observed in Er-doped and Tm-doped fibers [1]. These quasi-three-level media (like Yb-doped, Er-doped and Tm-doped fibers) have a lower laser level close to the ground state [1]. There is a large population at this lower laser level at thermal equilibrium at operating temperatures, leading to some reabsorption loss at the lasing wavelengths [36]. For longer fiber lengths, the reabsorption loss at short wavelengths is strong, while the relaxation of the inverted population generates photons at longer wavelengths. Thus the lasing wavelength,

including the lasing bandwidth, starts red-shifting with fiber length. The threshold pump level also changes for different fiber lengths. For the fibers we investigated, this power is generally below 1.5 W for fiber lengths longer than 2 m. Threshold pump power may gradually increase with fiber length to overcome increased reabsorption losses. For a 0.2-meter fiber length, the threshold pump power can be as large as 3 W to strongly invert Yb ions and to overcome cavity losses. Tm-doped fibers behave in a similar manner [37].

Fiber length has a strong influence on the stability of the energy diagram sublevels (Figure 4.18). For the fiber lengths of 0.3 or 2 m, the peaks of the lasing spectra remain similar during different measurement periods. On the other hand the peaks of the lasing spectra temporally vary for the 8-m long fiber. As already mentioned, longer fibers emit photons of longer wavelengths and less energy. Therefore heat generated in the longer fiber is higher and strongly affects the stability of the structure of energy sub-levels. This will have a negative impact on performance fiber lasers with long lengths.

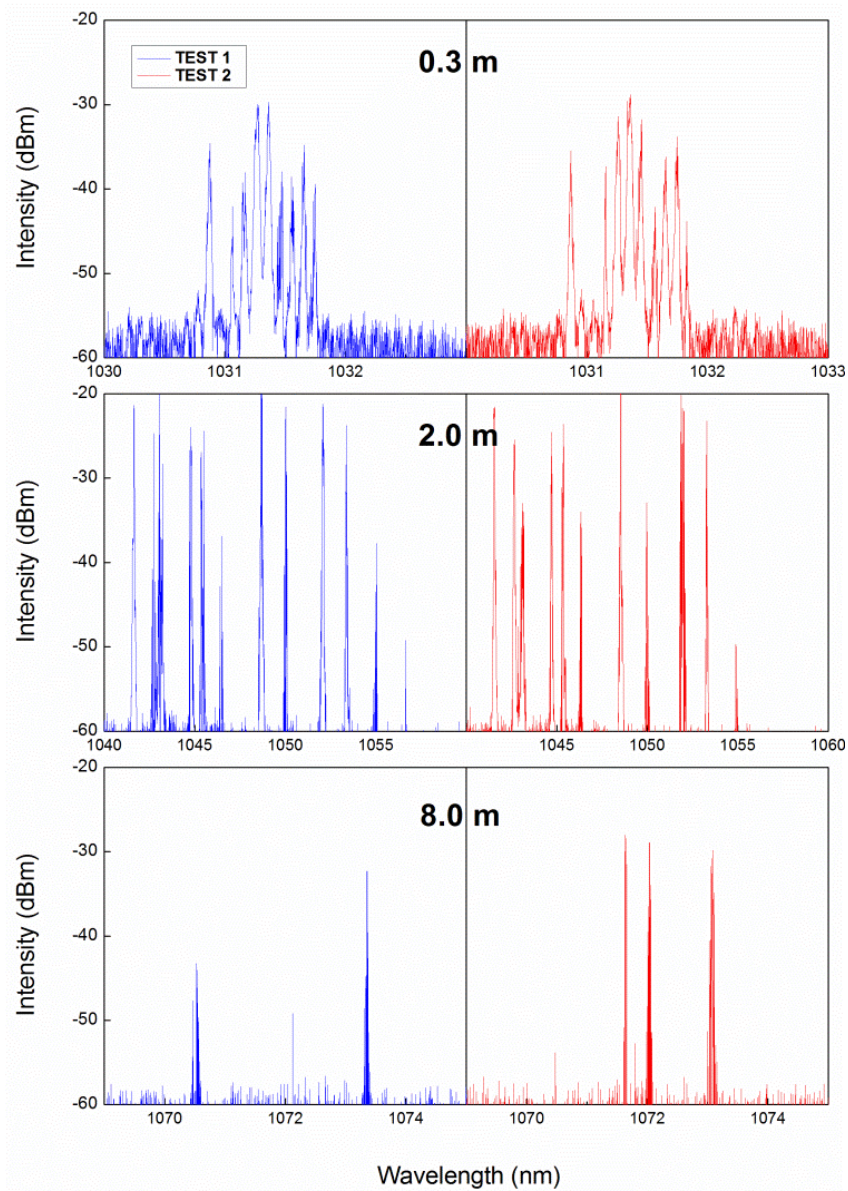


Figure 4.18 Lasing peak instability spectra comparison in 0.3, 2 & 8 m long fibers.

The analysis of amplified spontaneous emission indicates that the two major causes of amplified spontaneous emission are accumulation of inverted population and strong reflected spontaneous emission light.

Longer fiber length can provide larger gain but then the threshold power for generating amplified spontaneous emission would also be lower as shown in Figure 4.16. Any multi-stage amplifier configuration should therefore avoid the accumulation of inverted population while keeping the gain high. Another method to

lower the inverted population is to increase the input seed power. With a higher input seed power, the excited state population in the higher energy levels quickly relaxes to the lower energy levels. Thus the accumulated inverted population cannot reach the threshold levels to generate strong amplified spontaneous emission. Adding spectral filter is another approach to controlling amplified spontaneous emission. Since the wavelength band for amplified spontaneous emission in Yb-doped fibers is below 1050 nm, and most high power lasers are at 1064 nm adding a high pass filter would limit transmission of the forward amplified spontaneous emission. Isolators between different amplifier stages can also be used to limit transmission of backward amplified spontaneous emission. A combination of these approaches can constrain the factors that lead to amplified spontaneous emission.

To control reflected spontaneous emission, one can use anti-reflection coatings on the lenses in the optical path. This would limit reflection of the light during coupling and collimation. Furthermore, the fiber ends should be cleaved at an 8-degree angle. This would prevent the reflected beam from being coupled back into the fiber core.

4.3 Summary

This Chapter discussed standard Yb-doped fiber amplifiers and introduced the two types of seed lasers (continuous-wave and pulsed) used in this work. The performance of these sources were discussed and analyzed. The results brought out the important issues relevant for the high power amplification. One of these issues is amplified spontaneous emission. The relationship of amplified spontaneous emission/lasing wavelengths to fiber lengths is

discussed and theoretically explained. Finally, we suggest several methods to control amplified spontaneous emission.

5. HIGH POWER HIGH PULSE ENERGY YTTERBIUM-DOPED LASER SYSTEMS

In this Chapter, we discuss a high power, high pulsed energy master oscillator power amplifier system (MOPA) constructed from chirally-coupled core (3C) Yb-doped fibers. . The system consists of a computer controlled seed laser and a two-stage fiber amplification system as shown in Figure 5.1.

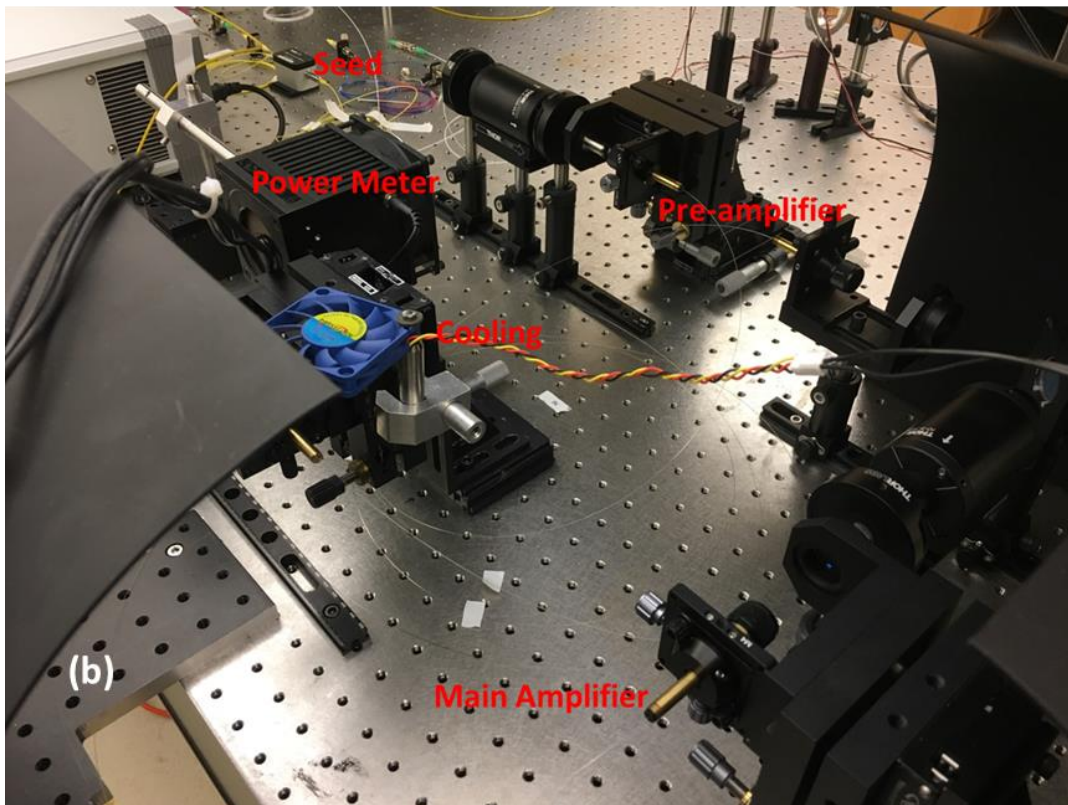
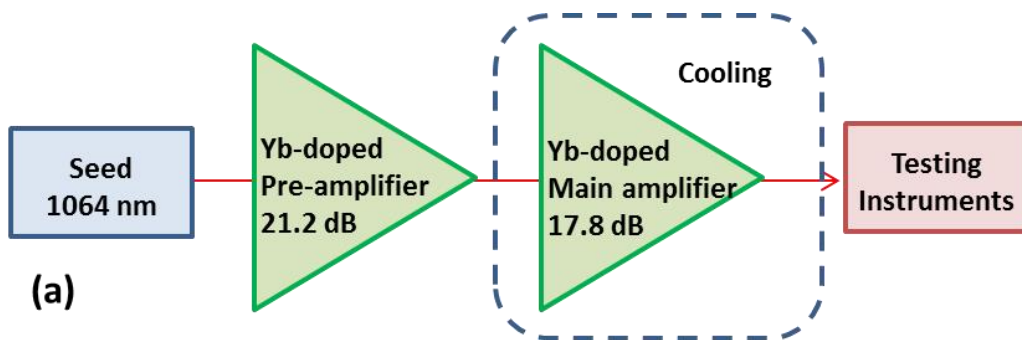


Figure 5.1 3C Yb-doped high power high pulse energy laser system.

The laser system emits at a wavelength of 1064 nm and is capable of delivering a

high quality beam ($M^2 < 1.2$) with an average power of up to 121.4 W at a repetition rate of 100 kHz; each 25-ns pulse has a pulse energy of 1.2 mJ. The power and energy performance specifications are limited by the available pump power. The total gain of the amplification system is 39 dB, which is outstanding among high power high, high pulse energy lasers. The slope efficiency of the system is 82 %, which is also remarkable compared other type large mode area (LMA) fiber amplifiers.

5.1 Seed Laser

As mentioned in Chapter 1 and Chapter 4, to build a fiber amplifier, one needs a seed signal light source, a fiber gain medium, and a pump laser.

As discussed in Chapter 4, there are two approaches to building a pulsed seed laser with Yb-doped fibers. The first approach involves use of a short pulse mode-locked laser with a fixed pulse width and a constant repetition rate that cannot be changed. The second approach to building a pulsed seed laser is to use master oscillator power amplifier as shown in Figure 5.2. This all-fiber seed laser system has an input from a diode laser that is fed to a two-stage amplification system. The initial input light is from a computer-controlled laser diode emitting at 1064 nm. The pulse width and repetition rate of the diode laser can be precisely set and controlled by the computer. Since the emission wavelength of the diode is different from the nominal peak emission wavelength of 1030 nm for Yb-doped fiber discussed in Chapter 4, we will require a longer length for amplification. For the first gain medium, we use a 35-cm long Yb-doped fiber whose core diameter is 4 μm , surrounded by a 125- μm cladding.

A wavelength division multiplexer (WDM) is used to combine the pump laser and the diode seed light before feeding this into the gain fiber. An optical (diode) isolator controls the beam propagation direction; the isolator also connects the first gain stage to the second gain stage which is a 50-cm long Yb-doped fiber of similar diameter and cladding. The output of this system is the amplified seed, which through a collimator can be coupled through free space to the pre-amplifier system.

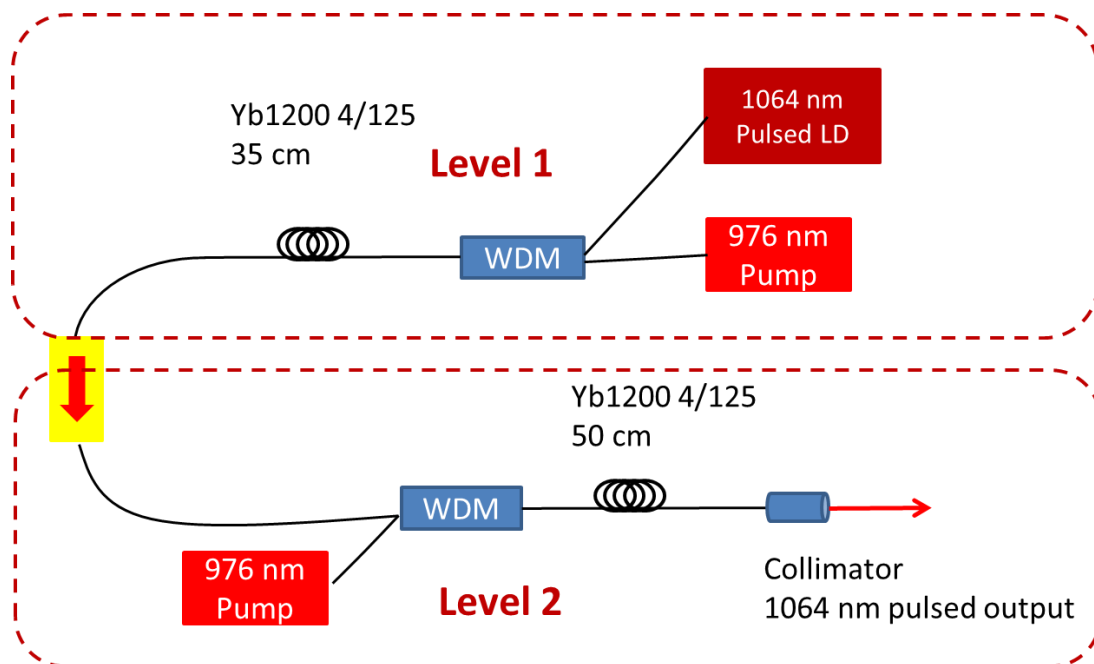


Figure 5.2 Configuration of seed laser.

The output of the computer-controlled laser diode is below 100 μ W, which is too low for the large signal pre-amplifier and amplifier system. However, after the two-stage seed amplification process, the output is slightly over 20 mW, which is large enough to be coupled to any multi-stage fiber amplifier system.

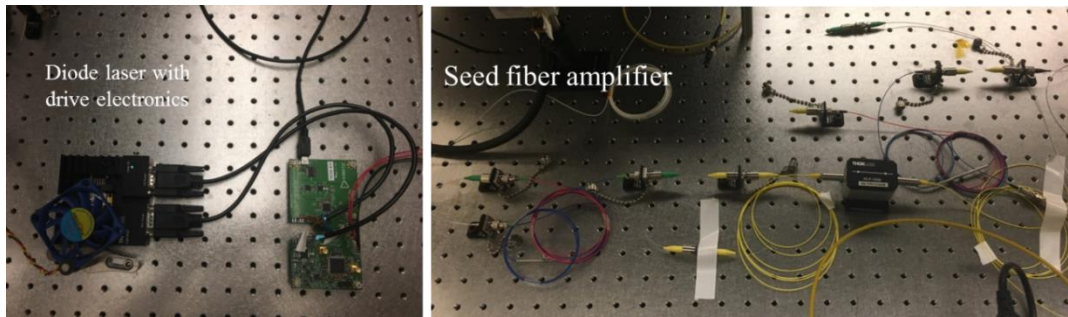


Figure 5.3 Actual size of seed laser.

The actual foot print of the pulsed seed laser system is shown in Figure 5.3. Other than the diode laser, all the other parts of the seed system are comprised of fiber, thus making the system very compact. The diode laser, which is mounted on a thermo-electrically cooled fixture with a fan on it, is driven by a high-precision electrical board.

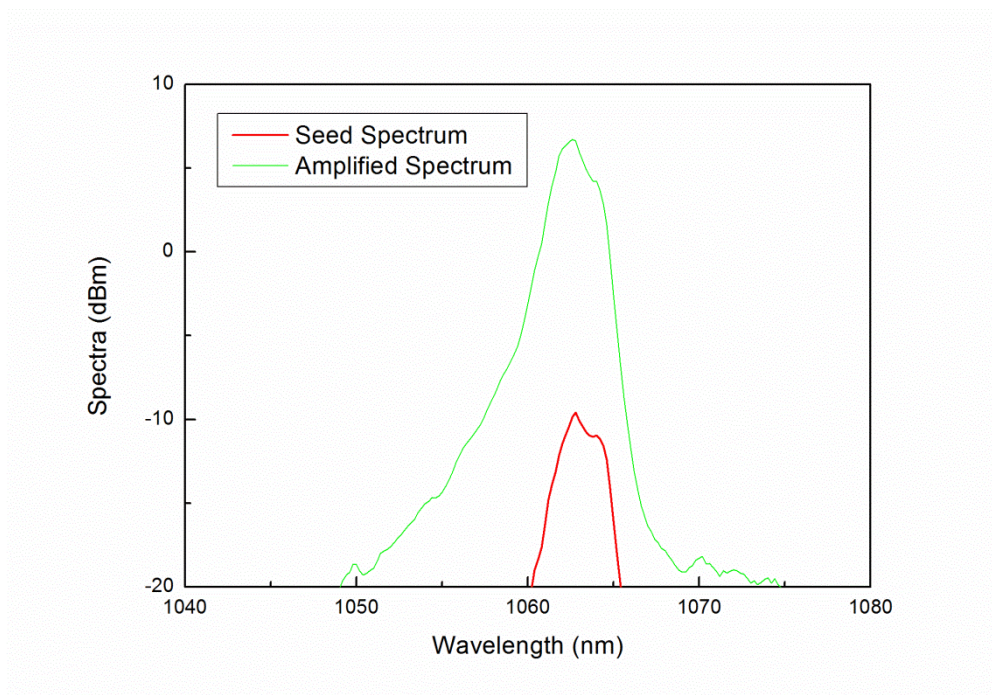


Figure 5.4 Spectra of the pulsed seed laser.

Figure 5.4 shows the spectrum of the initial diode seed light and the spectrum of the fiber-amplified replica of the seed. The fiber output is 20 mW centered at 1064 ± 2 nm. This spectral linewidth is narrow enough for high power, high pulse

energy amplification. The temporal pulse width is set to 25 ns, while the repetition rate is set to 100 kHz as shown in Figure 5.5.

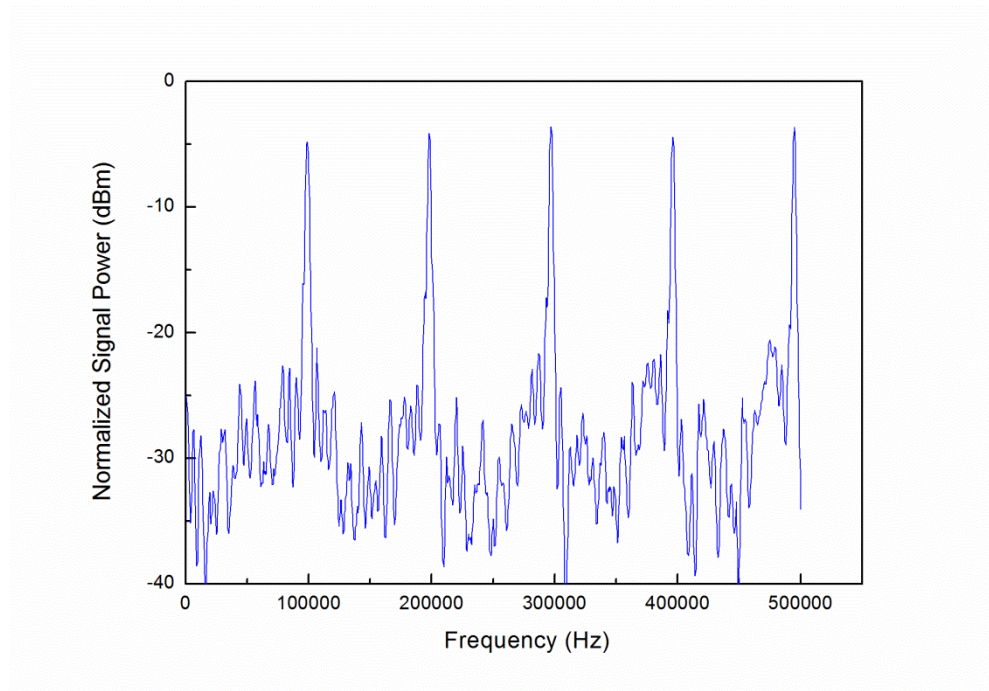


Figure 5.5 Electrical spectra of the pulsed seed laser.

5.2 Two-stage High Power Chirally-Coupled-Core Fiber Amplification System

The high power amplification system is designed as a two-stage structure shown in Figure 5.6. Both the pre-amplifier and the main amplifier use chirally-coupled core (3C) fibers as the gain media. The 3C fiber can be tightly coiled as well as spliced with standard fibers to minimize spatial volume. The core diameter of the 3C fibers is 34 μm and the pumping cladding diameter is 250 μm . The large core and cladding diameters are designed to allow for single mode coupling and high pumping intensity. Since Yb-doped fibers have their highest absorption at 976 nm, we use this wavelength as the pump wavelength. For a 2.5-meter fiber length, the pre-amplifier

provides a gain of 21.2 dB, and for 3-meter fiber length, the main amplifier provides a gain of 17.8 dB. The average output of the pre-amplifier is 2.03 W, resulting in total final output of 121.4 W at the main amplifier. The entire amplifier system is designed to be very compact. In a pilot prototype, it could be made even more compact when the coupling optical elements are replaced with spliced fiber connectors. In practice, the size of this all-fiber configuration, including the power supplies, could be as small as the size of hard box laptop carrier.

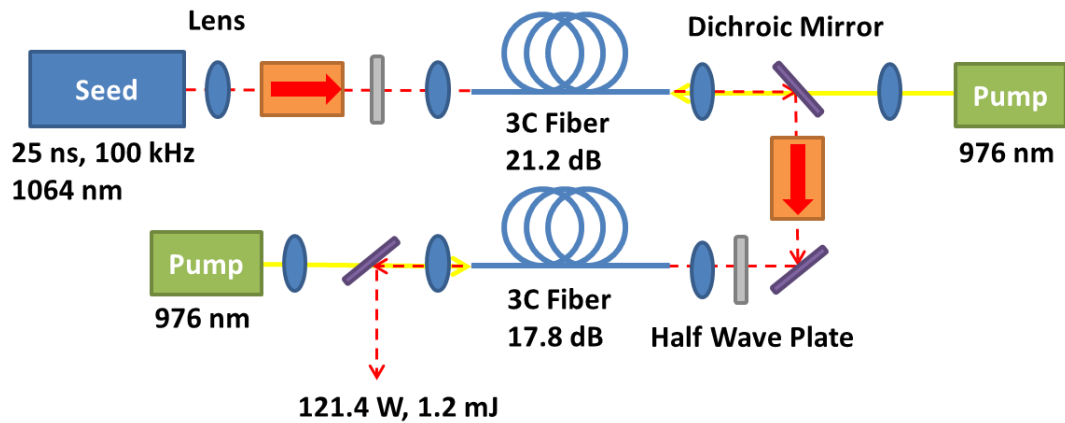


Figure 5.6 Configuration of the whole amplification system.

5.2.1 System design and configuration

We now discuss the details of the two-stage amplifier system. Because the magnitude of the input seed light is sufficiently high, and optical (diodes) isolators are used in the system, amplified spontaneous emission is not expected to be a problem that could limit amplification. To achieve better conversion efficiency, both the pre-amplifier and booster amplifiers are backward-pumped.

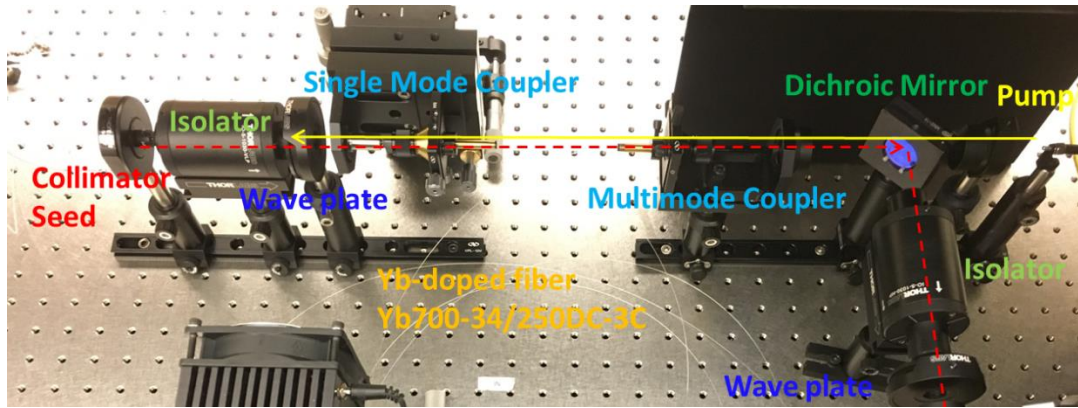


Figure 5.7 Configuration of the pre-amplifier.

The photograph of Figure 5.7 shows the configuration of the pre-amplifier. The structure is similar to the pre-amplifier introduced in Chapter 4. The red dashed line shows the direction of propagation of the seed, while the yellow solid line shows the direction of propagation of the pump. The beam diameter after exiting the collimator at the output of the seed system is about 500 μm . An isolator after the collimator is used to enforce the direction of beam propagation and to limit the amount of backward amplified spontaneous emission. The half-wave plate is used for polarization control. We use a single mode coupler for coupling a small aperture laser mode into the fiber core area. This five-axis coupler is mounted on a three-axis position platform; this mode-coupling process is precisely controlled. A multimode coupler is used for coupling the backward multimode pump laser light into the cladding area of the fiber. As already mentioned previously, the cladding diameter is 250 μm with a NA of 0.48. The large numerical aperture readily facilitates the coupling of the pump. We use a dichroic mirror to transmit the 976-nm wavelength seed laser light and reflect the 1064-nm wavelength pump laser light. This means the backward pumping laser light is easily transmitted, while the seed beam is reflected

into the main amplifier. The fiber in the pre-amplifier is a 2.5-meter chirally-coupled core fiber that can be coiled to a 30-cm diameter structure to suppress high-order modes.

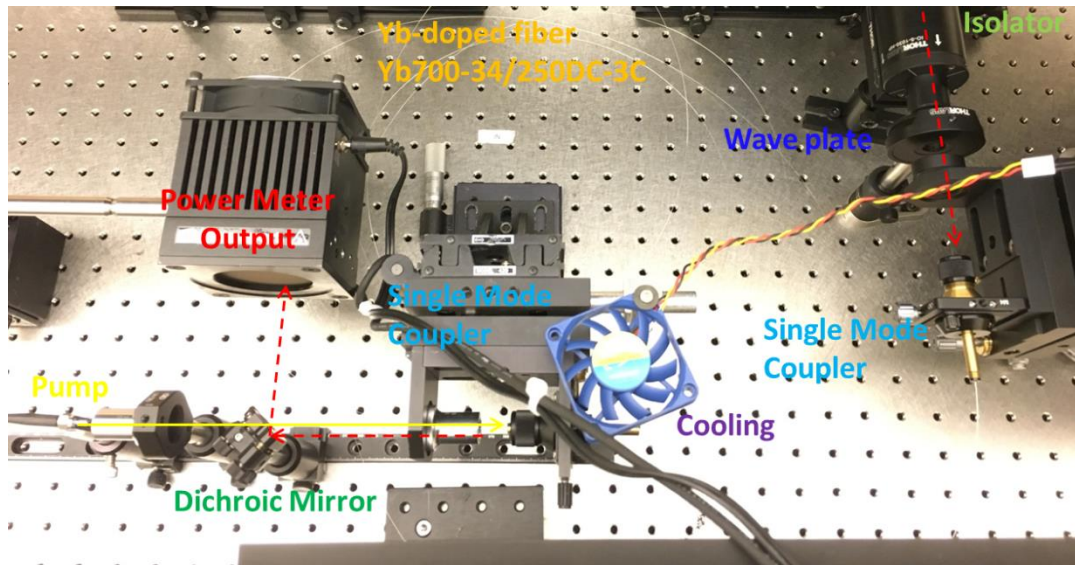


Figure 5.8 Configuration of the main amplifier.

To minimize the beam divergence and increase coupling efficiency, the beam diameter of the seed laser light is made as large as 2 mm. Before the collimated seed beam enters the pre-amplifier, it passes through an isolator and a half-wave plate for propagation direction and polarization control. These components ensure that the laser light entering the 3-m long Yb-doped fiber of the main amplifier has almost the same characteristics as the single mod beam coupled into the pre-amplifier. To further boost the power of amplified seed in the main amplifier requires high pump power. This high pump power is coupled from a multimode pump source. A dichroic mirror similar to the one in the pre-amplifier transmits the 976-nm wavelength pump beam while reflecting the 1064-nm wavelength seed laser light. As a crude but effective thermal management scheme, we use a fan to circulate the air and thus to cool the

copper chuck on which the fiber is mounted. This scheme effectively protects the fiber and its associated parts from burning as discussed in Chapter 2. Following the construction of the two-stage amplifier system, we built sub-systems for measuring and testing power, spectra, pulse width, and the repetition rate.

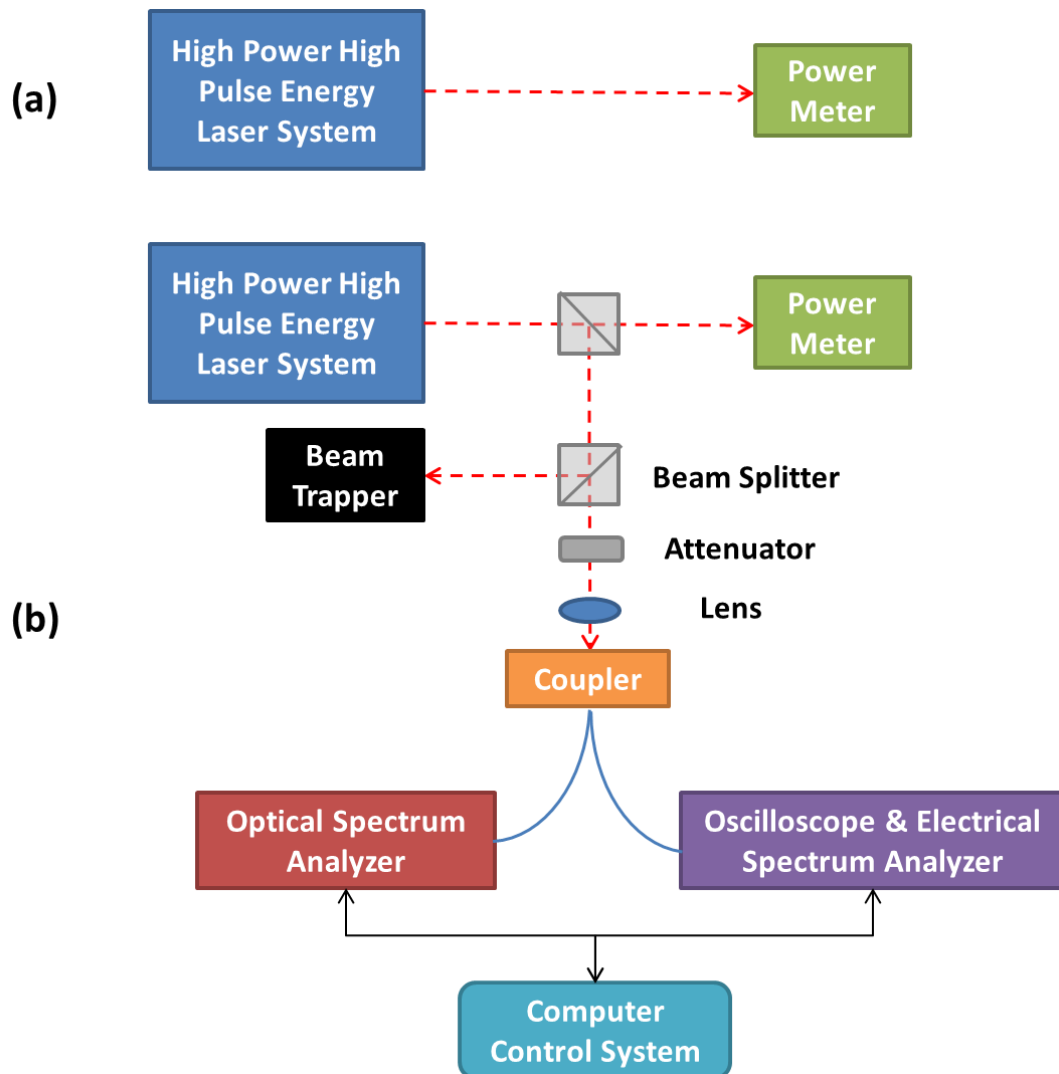


Figure 5.9 Configuration of testing system for (a) average power and (b) spectra, pulse width and repetition rate.

Figure 5.9 shows the sub-systems for characterization of the key performance parameters of the final laser output. There are a number of challenges to measurement and characterization of high power, high pulse energy laser systems. We measure the average power of the laser output with sub-system shown in Figure 5.9 (a). The

configuration is straight forward as only involves a power meter inserted in directly in the beam path. Because of the high output powers, normal silicon or GaAs detectors would be saturated or destroyed by the beam. There a thermopile detector was to measure the average power. To protect the thermopile detector and improve the accuracy of the measurement, the detector is mounted in an air-cooled system. Such a measurement system can handle laser beam average powers of up to 200 W.

The spectral characterization of the laser beam, is performed using an optical spectrum analyzer whose range extends from 600 to 1600 nm. We use an ultrafast oscilloscope (6 GHz) that has an embedded electrical spectrum analyzer it for measuring nanosecond-pulse width-level pulses with repetition rates in the hundreds of kilohertz range. These instruments, however, cannot be used under such high power conditions. The system is the re-configuration for the spectral, pulse width and repetition rate measurements as shown in Figure 5.9 (b). It is generally not advisable to measure the output of high power, high pulse energy laser systems directly. Here, we use two beam splitters to lower the beam intensity. The first beam splitter reflects about 30 % of the laser beam, leaving about 70 % of the beam for the power meter.. The second beam splitter transmits 10 % of the power to measurement instrument, allowing 90 % of the reflected beam to be blocked by the beam trapper. A 20-dB attenuator is imposed in the path of the second beam splitter, allowing mW-level power to be available for the final measurement. This beam is transported by a 50/50 fiber coupler to the optical spectrum analyzer and to oscilloscope where an ultrafast photodetector converts the optical beam into electrical signals that can be acquired by

the oscilloscope. All of the measurement instruments are computer-controlled through LabView program. This means we are able to synchronize the measurements.

5.2.2 Analysis of pulse amplification in high power laser systems

In this section we use the theoretical tools developed in Chapter 3 to analyze the configurations of the amplifier systems constructed in this Chapter.

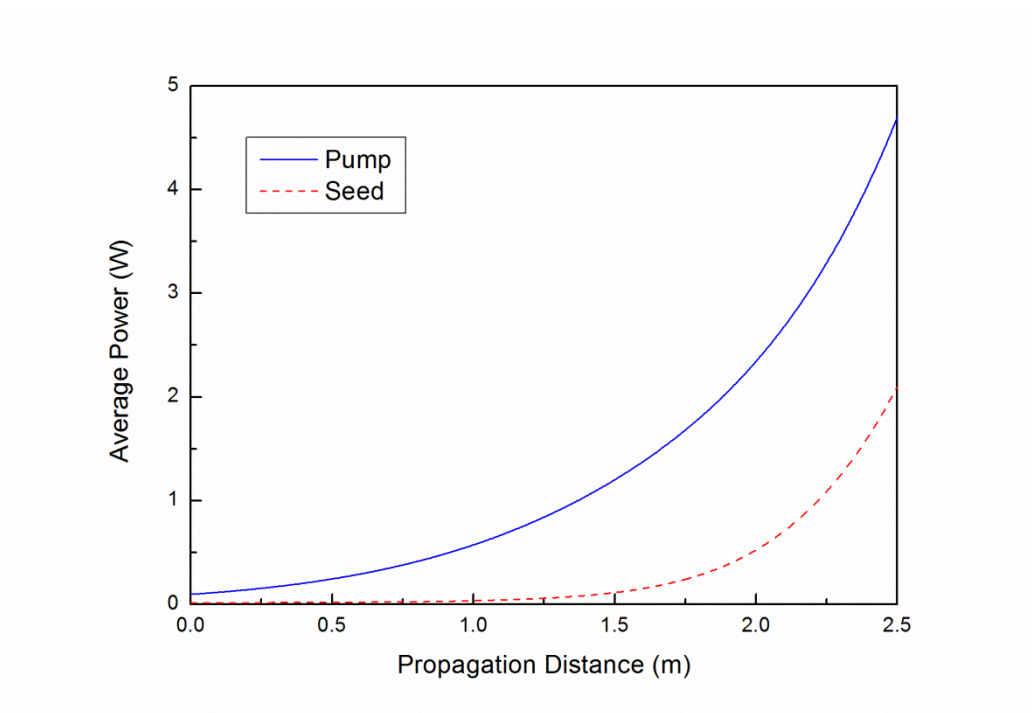


Figure 5.10 Simulated average power of the pre-amplifier.

Figure 5.10 shows the average power at different propagation lengths along the gain fiber of the pre-amplifier. Here the pump power is 4.5 W and the initial seed power is around 15 mW. For a 2.5-m long fiber, the seed light can be amplified to values larger than 2 W, which are sufficient to serve as input for the main amplifier. Because the initial input seed light to the pre-amplifier is low, the transmission efficiency in the pre-amplifier is not very high. The pump power decreases aggressively from the input

side to output side of system. Nearly all the pump power is absorbed by the fiber. Nevertheless, over 2 W pump power has not been converted to the seed laser light power, and the expected slope efficiency should be around 50 %. The pump power leads to large gain in the 3C fiber as shown in Figure 5.11.

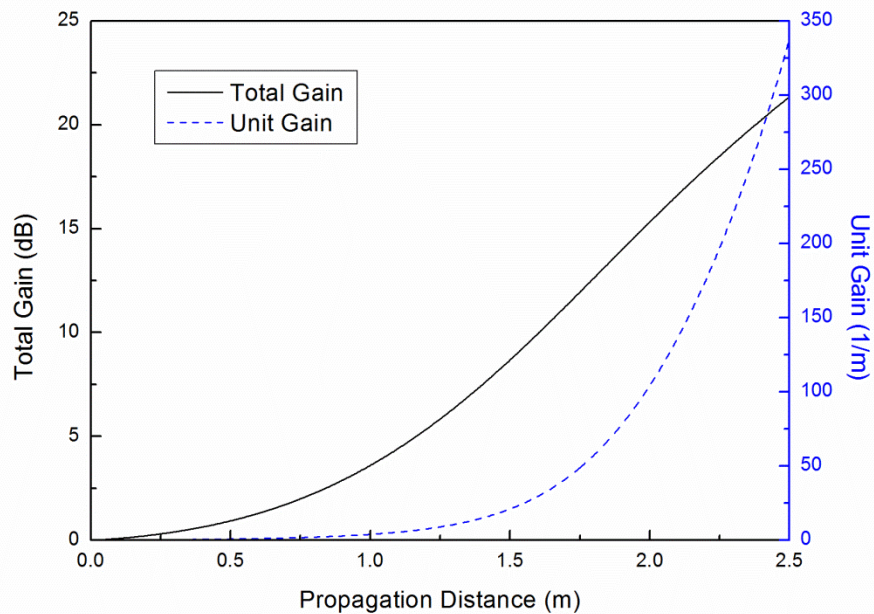


Figure 5.11 Simulated total gain and unit gain of the pre-amplifier.

With even more pump power, the 2.5-m Yb-doped 3C fiber generates about 22 dB of gain. There is virtually no amplified spontaneous emission. Figure 5.11 shows that the total gain in the initial part of the fiber is not very large. With the backward-pumping scheme, the inverted population in the initial part of the fiber is relatively low and thus cannot support high gain. On the other hand, the inverted population in the section of the fiber closest to the entrance of backward pump is high. The gain therefore increases very rapidly. This pattern of total gain and unit gain helps the low initial seed power to quickly overcome fiber loss and to rapidly increase

power in a short fiber length. Both the inverted population and the power of the seed light are large at the same fiber position, thus helping to suppress amplified spontaneous emission. Overall, one obtains high gain with limited amplified spontaneous emission in the pre-amplifier section of the system.

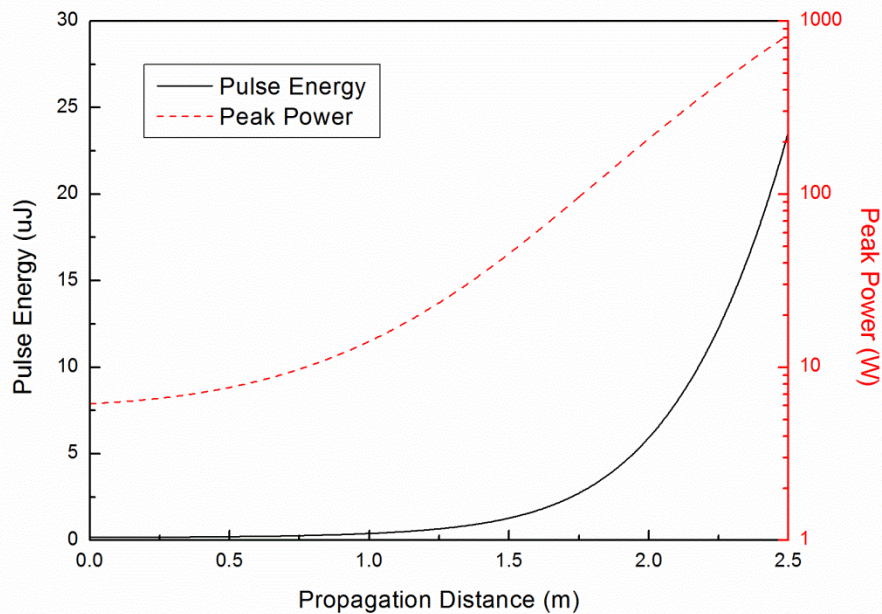


Figure 5.12 Simulated pulse energy and peak power of the pre-amplifier.

As shown in Figure 5.5, the repetition rate of the pulsed seed laser is 100 kHz. With 22 dB of gain, the pulse energy is amplified to 23 uJ. The pulse energy increases rapidly after propagating about 2-m of the Yb-doped fiber. The high unit gain in the fiber boosts the pulse energy within a short propagation distance. With a pulse width of 25 ns, the peak power of the output pulse is close to 1 kW. Figure 5.12 shows the rapid increase in peak power from below 10 W to 1 kW. Although the increase in peak power is very high, it is still well below the threshold for onset nonlinear effects.

In summary, with a pre-amplifier gain of 22 dB, the seed laser light can be

amplified to over 2 W which corresponds to pulse energy of 23 μJ . This amplified seed laser light becomes the input to the 3-meter long Yb-doped main amplifier described in the next paragraph.

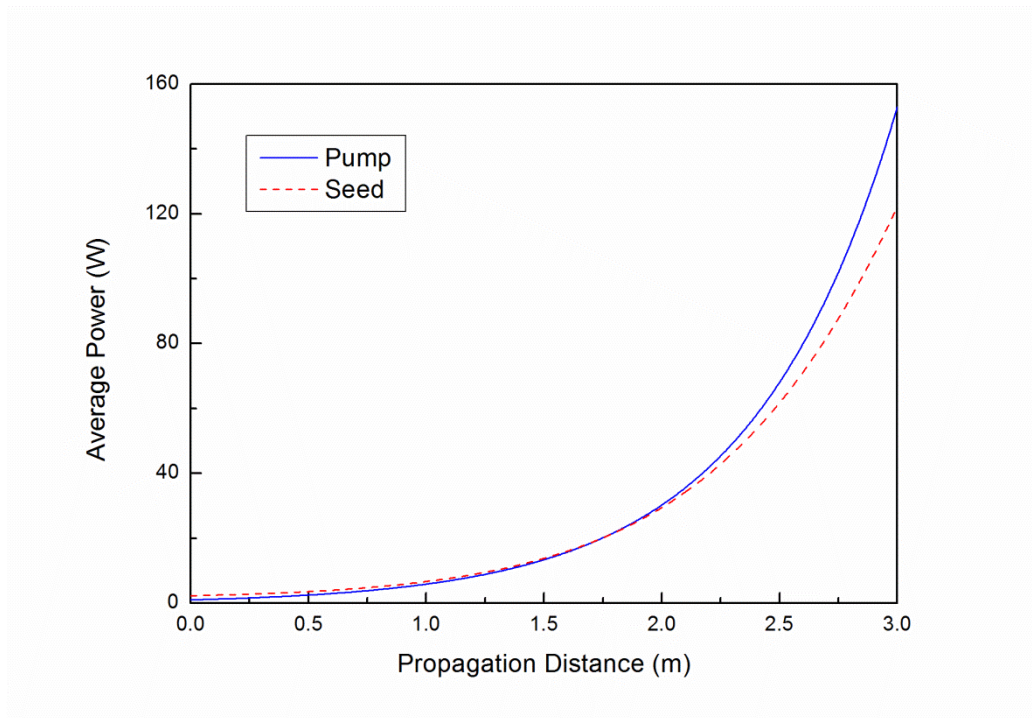


Figure 5.13 Simulated average power of the main amplifier.

Figure 5.13 shows the average power at different propagation lengths along the 3-m long Yb-doped fiber of the main amplifier. The input to this section of the amplifier is the amplified seed with over 2 W of average power and 23 μJ of pulse energy. The backward pump power is > 150 W. The average output power from this section of the amplifier is larger than 120 W. The transmission efficiency in the main amplifier is high. The growth of the amplified seed light in the main amplifier closely follows the increase of the pump power; there is very little residual power left in backward directed pump. The majority of the pump power is converted to amplified seed power. At this point, the conversion efficiency between the pump light and the seed light is

over 75 %, which represents an ideal amplification process. This ideal amplification condition is shown in Figure 5.14.

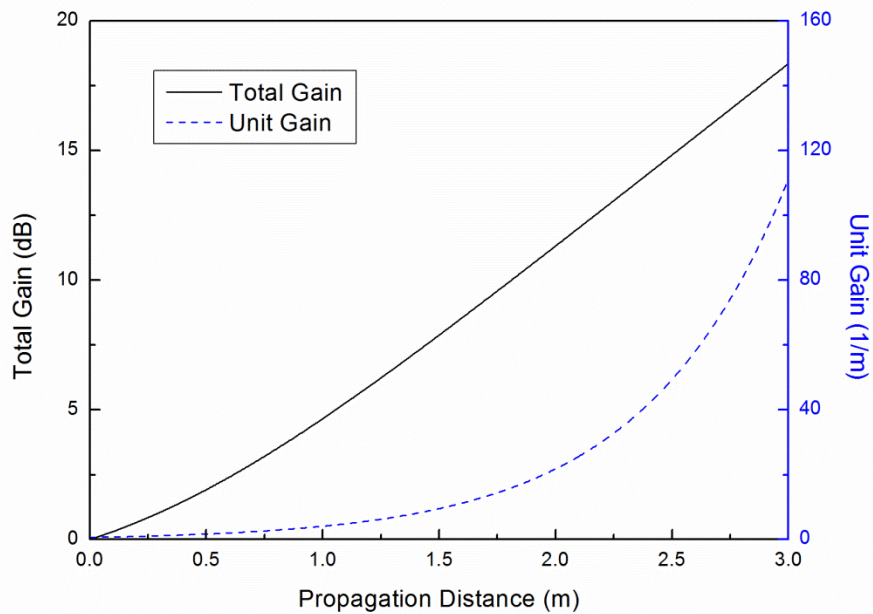


Figure 5.14 Simulated total gain and unit gain of the main amplifier.

With a power conversion efficiency of over 75 %, the 3-m Yb-doped fiber generates a gain of about 18 dB. The figure 5.14 shows the steady total gain increase along the propagation length. The total gain curve is almost linear. Because of the backward pumping scheme, the unit gain in the initial section of the fiber is small. Meanwhile, the unit gain in the section of the fiber closest to the backward pump increases rapidly. This pattern of the total gain and unit gain provides steady and continuous amplification of the seed light. There is no obvious sign of gain saturation in the amplification process. Both the gain and power of the seed light are increasing at the same pace, which tends to suppress amplified spontaneous emission. The high power conversion efficiency also tends to suppress amplified spontaneous emission.

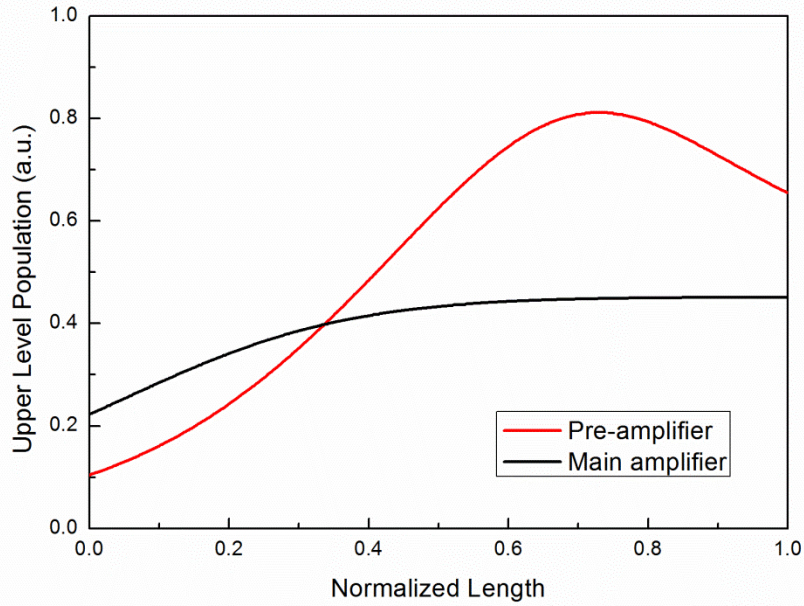


Figure 5.15 Simulated upper level population in both pre- and main amplifiers.

Gain is generally strongly related to the upper level population. Figure 5.15 shows the upper level population distribution in both the pre-amplifier and the main amplifier. Since the backward pumping method is utilized in two amplifiers, the upper level populations in the initial sections of the fibers are relatively lower. For the pre-amplifier, the upper level population increases dramatically along the fiber length. At the end of the fiber, the upper level population decreases slightly. From Figure 5.10, we note that the seed power increases dramatically in a short fiber length at the end of the fiber. The intensely amplified seed light leads to population relaxation from the upper level. For the main amplifier, the upper level population keeps increasing steadily along the whole length of the fiber. Similar results are computed in Figure 5.13 and 5.14. The amplification process in the main amplifier is steady, and the average power increases gradually. The stable total gain in the main amplifier is

generated from the even distribution of the upper level population along the fiber.

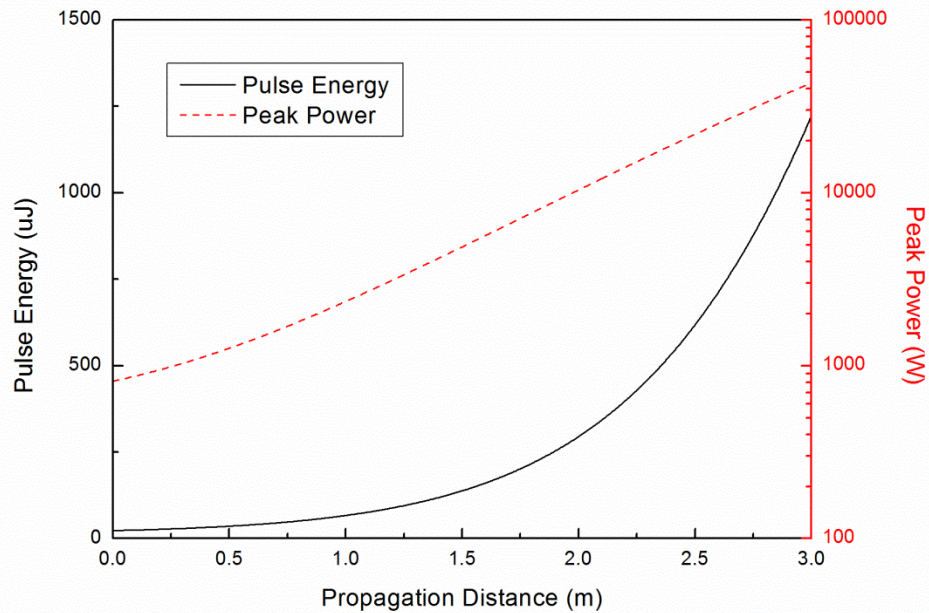


Figure 5.16 Simulated pulse energy and peak power of the main amplifier.

As already stated, the repetition rate of the pulsed seed laser is 100 kHz as shown in Figure 5.5. With an 18-dB gain in the main amplifier, the amplified seed pulse energy is boosted to 1.2 mJ. This pulse energy increases very rapidly after propagating in the 2-m section of the seed amplifier. The strong unit gain at the later section of the fiber boosts the pulse energy in 1 m. With a 25-ns pulse width, the corresponding peak power at the output is about 50 kW. As shown in Figure 5.16, the curve for the peak power is nearly a straight line, representing a steady amplification process. Close to the output end of the fiber, the peak power shows no sign of gain saturation. Based on the increasing tendency of the average power, the total gain, and the pulse energy, one can say that the amplification process in the main amplifier is steady and clean. There is no obvious evidence of amplified spontaneous emission in the main amplifier. The

measured output power supports the simulation results.

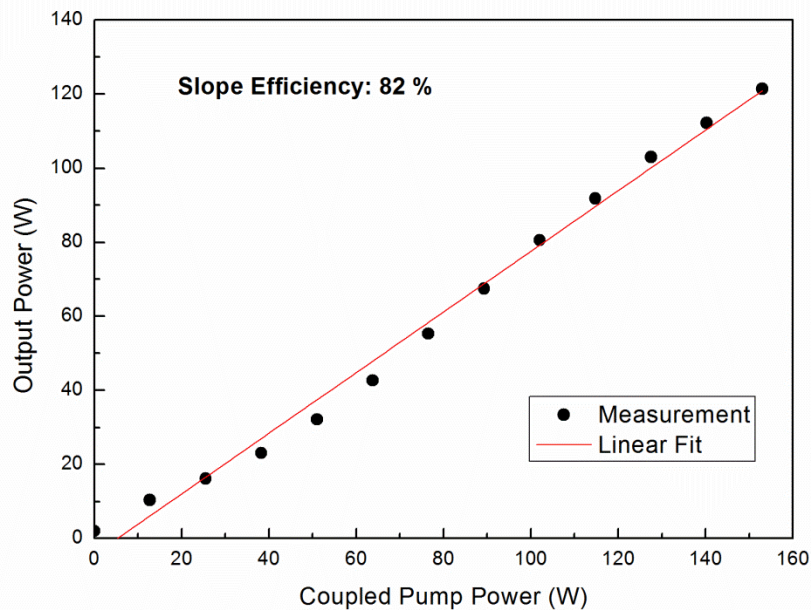


Figure 5.17 Tested output power and slope efficiency in main amplifier.

With the quantitative model introduced earlier, we have been able to faithfully reproduce the key performance characteristics of the system constructed in this thesis. Again, with an average initial seed power of 15.4 mW, we obtain an output of 2.03 W from the pre-amplifier, which is close to what is obtained from the simulation. The output power and slope efficiency of the main amplifier are shown in Figure 5.17. For a coupled pump power of 153 W, we obtain an output average power of 121.4 W from the main amplifier. This output is only limited by the available pump source power. The measured slope efficiency is 82 %, which is excellent compared to other high power lasers. As can be seen from Figure 5.17, the output power and coupled pump power have a nearly linear relationship. The highest pulse energy derived from these measurements is > 1.2 mJ. One begins to notice some gain saturation at this

large pulse energy. The measured power and pulse energy results agree with the results obtained by simulations.

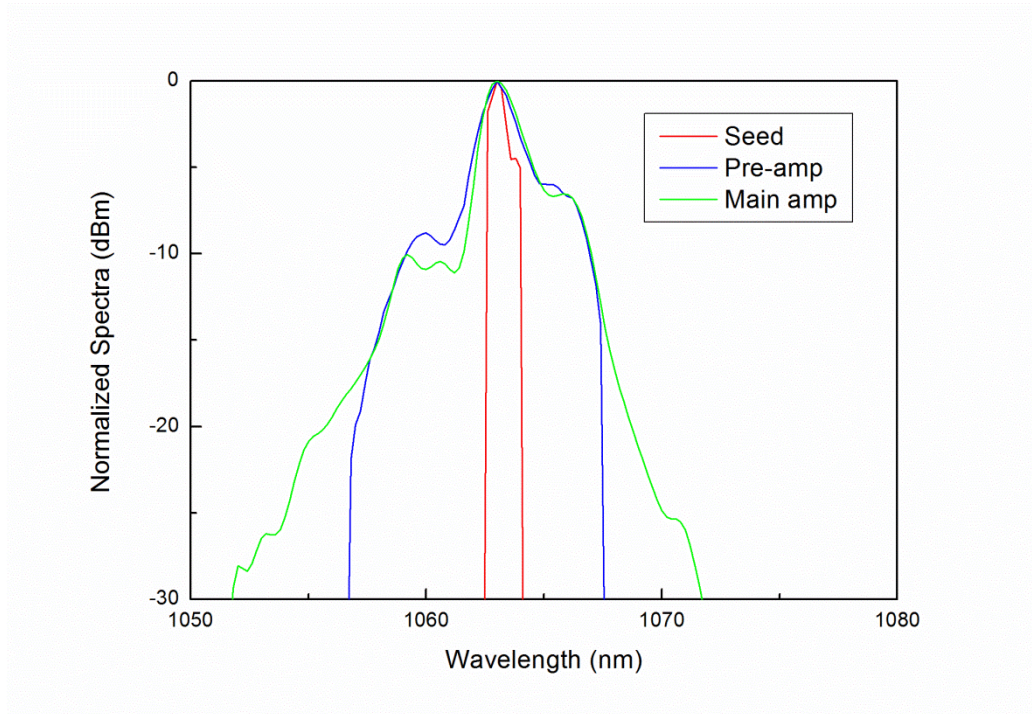


Figure 5.18 Tested spectra of the pulsed laser amplification process in the whole amplification system.

The spectral evolution of the seed laser light as well that of the amplified copies of it along the amplifier system is an important consideration in high power, high pulse energy lasers. We use an optical spectrum analyzer to measure the spectra of the seed system output, pre-amplifier, and the main amplifier. Figure 5.18 shows the normalized spectra from the outputs of the seed, the pre-amplifier, and the main amplifier. The seed spectrum is narrow and is centered at 1064 ± 1 nm. After amplification in the pre-amplifier and the main amplifier, the seed light spectrum broadens as shown in Fig 5.18. Due to high pump power and large gain, one expects side energy levels around the central emitting energy level to be excited. This would explain the spectral broadening observed in the outputs of the pre-amplifier and the

main amplifier. Note that the pre-amplifier and amplifier spectra broaden at about an intensity level below -10 dBm, which is much smaller than the intensity of the central peak.

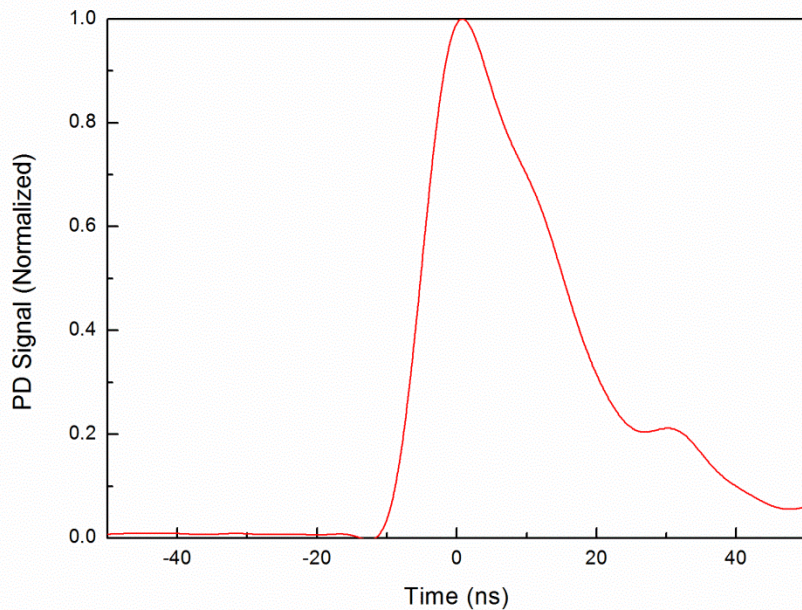


Figure 5.19 PD signal of the pulse with 3 ns pulse width.

As we have already stated, the initial pulse width of the seed laser is 25 ns. This is verified in Figure 5.19 which shows the detected seed light pulse. Measurement of the pulse characteristics after it has been amplified by the pre-amplifier and the amplifier, however, requires care because of the extremely high out power from the booster amplifier. The simplest approach is split off a small fraction of the output beam and using this as input to an ultrafast photodetector.

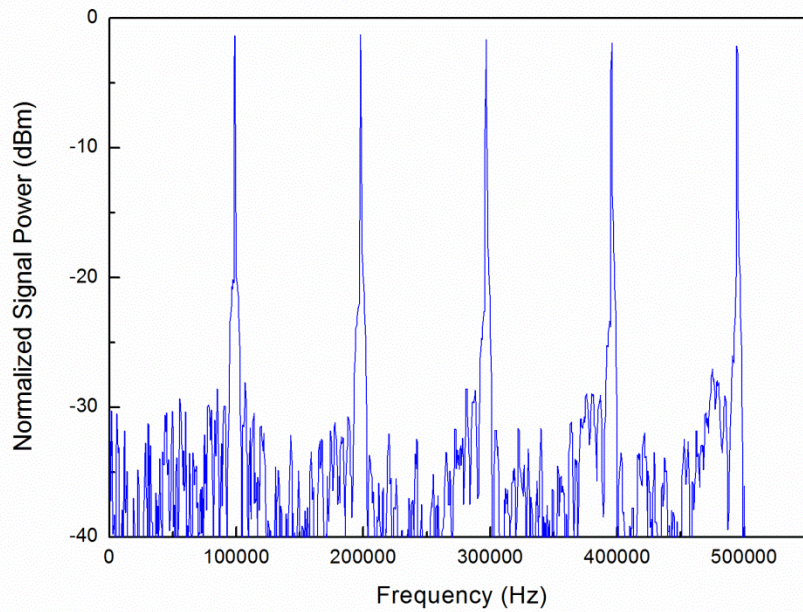


Figure 5.20 Electrical spectrum of the pulsed laser output.

The electrical spectrum of the pulse is measured using an electrical spectrum analyzer. Figure 5.20 shows the electrical spectrum of the output pulsed laser beam. Note that the peaks occur every 100 kHz, which represents the 100 kHz repetition rate of the pulsed seed laser. The contrast between the signal peak and background noise is over 30 dBm; no large random peaks occur between the signal peaks. There is very little noise in the pulse train which means the optical pulse train should emerge with little noise after amplification.

One other parameter for assessing the quality of an optical beam is its spatial intensity distribution otherwise known as the M^2 parameter, which is a measure of the intensity distribution at the beam waist.

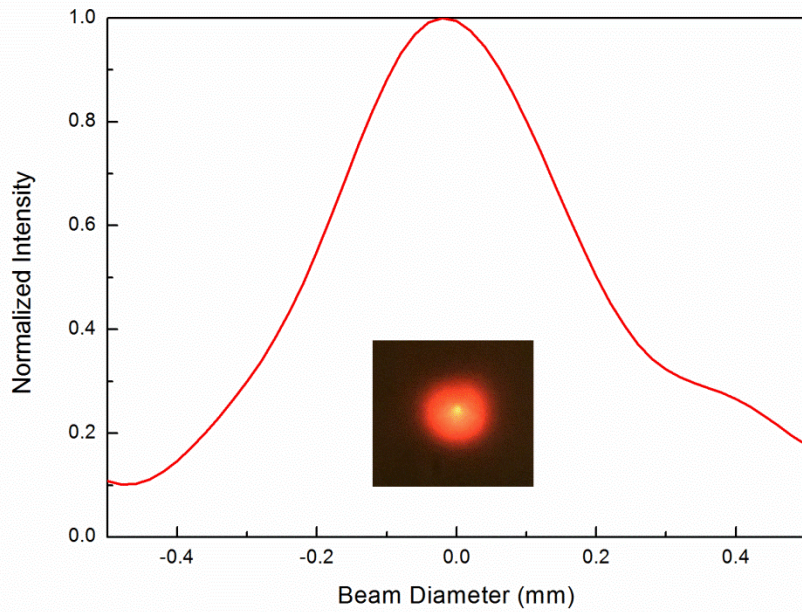


Figure 5.21 Intensity distribution of the single mode seed beam.

As shown in Figure 5.21, the beam intensity approximates a Gaussian distribution, which for the particular power level it was measured at has a beam diameter of about 0.8 mm at its waist. In terms of the M^2 factor, the measured value is $M^2 < 1.2$. The photograph in the inset supports the conclusion that the output is a single spatial mode.

To estimate the nonlinearity during the amplification process, the B-Integral introduced in Chapter 3 is calculated. We show in Figure 5.22, the computed B-Integrals for both pre-amplifier and main amplifier. As can be seen from the figure, along the whole length of the pre-amplifier, the value of the B-Integral is fairly small given the relatively low power and pulse energy in this part of the amplifier system. In the main amplifier, however, because the pulse energy is over 1.2 mJ, the value of the B-Integral gradually increases along the length of the main amplifier is definitely

much higher than that of the pre-amplifier along the entire amplifier length. The accumulated value of the B-Integral is about 3 (below 5); the small nonlinearity that is generated is not strong enough to cause obvious nonlinear phenomena in the fiber.

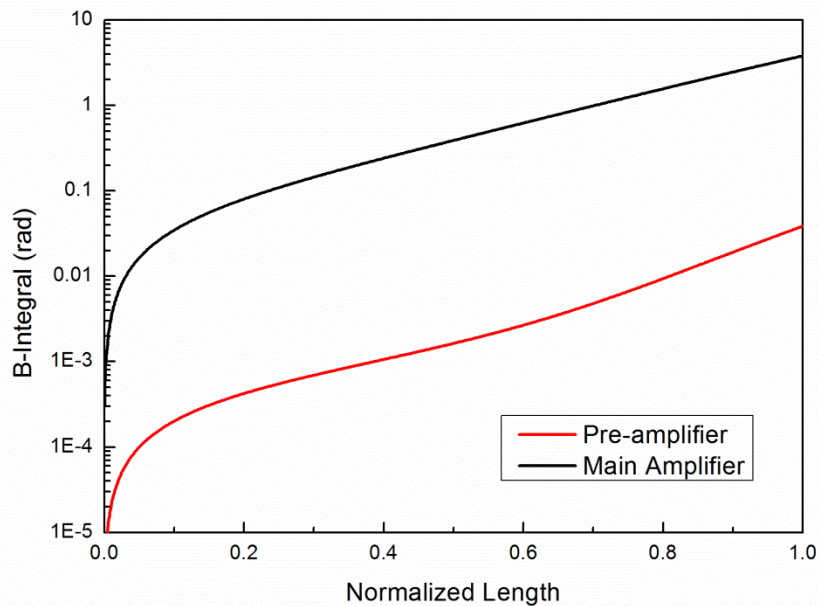


Figure 5.22 Simulated B-Integrals of the pre- and main amplifiers.

5.3 Applications of the high power laser system

High power, high pulse energy lasers are important for scientific research and industrial applications. This type of laser can be used in materials processing since it can provide an extremely intense beam in a small area in a short burst of time. In fact, prototype fiber amplifiers with 100-W average power and 1 mJ pulse energies have been successfully deployed for micromachining applications in manufacturing environments [16].

While the high power and high pulse energy attributes of a fiber laser are important

for many applications, another equally important attribute is the compact size of these systems. Laser systems constructed from the chirally-coupled core fiber discussed in this thesis can therefore provide a portable light source capable of delivering high power and high pulse energies, which are important in a number of important applications.

5.4 Summary

This Chapter discussed the Yb-doped 3C fiber amplifier system for generating high power and high pulse energies in a compact configuration. The fiber seed light source with an average output of 15 mW was constructed from a computer-controlled, pulsed semiconductor diode laser emitting at 1064 nm; the pulse width and repetition rate of this laser can be varied from 3 to 100 ns and from 1 to 500 kHz, respectively. The pulse width of 25 ns and the repetition rate of 100 kHz were selected for the experiments whose results are reported in this thesis.

The configuration of the two-stage fiber amplifier investigated in this work was constructed from 2 lengths of fibers. The first stage of the system is the pre-amplifier comprised of 2.5 meters of chirally-coupled-core fiber, followed by the main amplifier comprised of another 3 meters chirally-coupled-core fiber. The core of each fiber has a diameter of 34 μm and a cladding whose diameter is 250 μm . The system is pumped with 976-nm diode pump sources. In operation, the pre-amplifier can provide a gain of ~ 21.2 dB in its 2.5-m long section, while the main amplifier can provide ~ 17.8 dB of gain in a 3-m long fiber for a cumulative system

gain of 39 dB. The average output of the pre-amplifier is ~2.03 W and that of the main amplifier is 121.4 W.

Finally, the experimental results reported in this Chapter were analyzed using a quantitative modeling simulation scheme developed in Chapter 3.

6. CONCLUSION AND OUTLOOK

In this dissertation, we explored approaches to constructing high power, high pulse energy fiber laser systems, and made two major contributions in theory and technology. We developed a new quantitative modeling and simulation method for rare-earth doped fiber amplifiers. The method is capable of handling most operating conditions for rare-earth based fiber amplifiers. In technology, we designed, constructed, and demonstrated the operation of a high power, high pulse energy amplifier system based on chirally-coupled-core Yb-doped fibers.

6.1 Summary of the Dissertation

The key element of a fiber amplifier is the fiber gain medium. Traditional standard fibers and photonic crystal fibers are generally not suitable for compact high power, high pulse energy laser systems. It is difficult to manage or prevent the onset of high-order modes in standard fibers as core sizes are increased to accommodate high power, high pulse energy operation. While photonic crystals may be designed with large core sizes to enable high power, high pulse energy operation, inclusion of the air-hole structure in them makes it difficult to coil or bend the fibers to minimize the size of the amplifier. In addition, this type of fiber develops thermal mode instabilities during high power operation. A new gain medium, the chirally-coupled core fiber, solves most of these problems. In this type of fiber, one or several helical side-cores around a Yb-doped central core extracts the higher order modes from the central core and radiates their energy away from the central guide. By adjusting the parameters of the helical side core(s), the central core of a 3C fiber can be enlarged and still

maintain a single transverse mode. In this work, we discussed the advantages and disadvantages of the three major types of Yb-doped fibers. We then explained the principles of operation of the chirally-coupled-core fiber, particularly the mechanism by which it suppresses high-order modes in the presence of its large gain. To better understand the amplification process in high power, high pulse energy systems, we developed a new quantitative modeling and simulation method for rare-earth doped fiber amplifiers. The method is based on a combination of the rate equations and the nonlinear Schrödinger equation. In the new approach, gain is calculated from the rate equations and the pulse evolution is analyzed using the nonlinear Schrödinger equation. Simulation results based on the new unified model are compared with experimental results to verify the fidelity of the method. The advantages of the new method are shown through comparison with the traditional simulation methods. Simulation results obtained by this method provide guidance for construction of compact high power, high pulse energy laser systems. Before building the high power amplifier system with the new 3C fibers in this work, we constructed amplifiers with standard Yb-doped fibers. These were used for understanding the limitations and issues associated with these type fibers. One of the issues uncovered was amplified spontaneous emission; methods for resolving are suggested and implemented.

To achieve high power and high pulse energy operation, we designed a two-stage amplifier. Its operating characteristics are thoroughly analyzed and explained. The final system designed and built operated the wavelength of 1064 nm in pulsed mode with excellent beam quality ($M^2 < 1.2$). The highest average power was 121.4 W, limited only the available pump power source. For the pulsed system with 25-ns pulses with a repetition rate of 100 kHz, the pulse

energy was as high as 1.2 mJ. The overall gain of the amplifier system was 39 dB, with a slope efficiency of 82 %.

6.2 Outlook

Based on the measured experimental and simulated results, we believe better performance from the system we have constructed is possible.

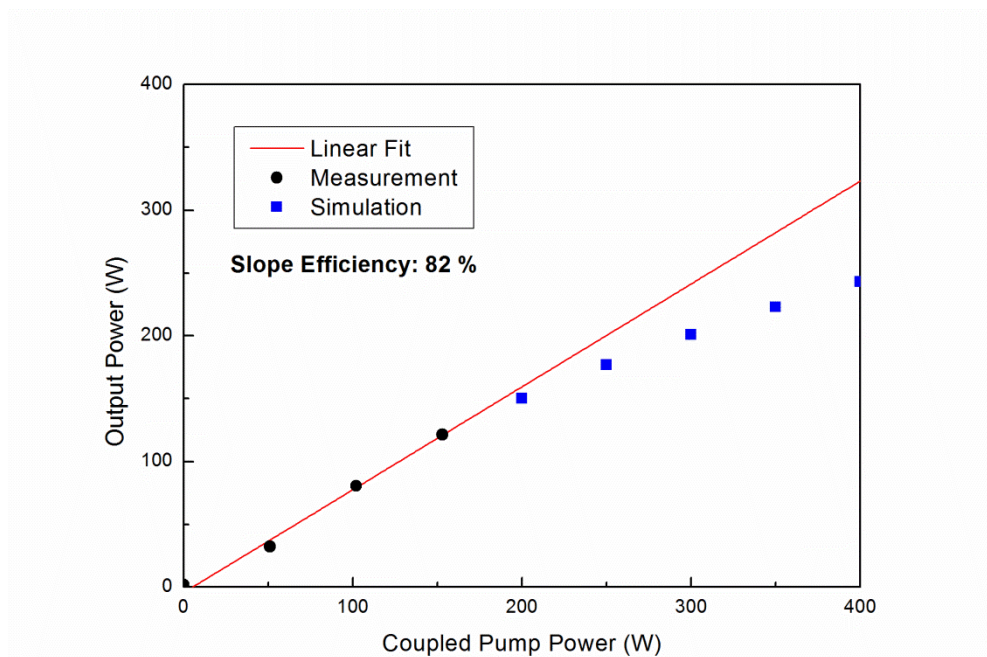


Figure 6.1 Potential output power from the current laser system.

Figure 6.1 shows the measured and simulated results of the amplifier system; a clear extrapolation shows that it is possible to obtain even higher output powers with stronger pumping. Based on the simulations, we note from Fig. 6.1 that for pump power levels larger than 300 W, the output no longer follows the linear fit closely. The decrease in the average output power is caused by gain saturation as shown in Figure 6.2.

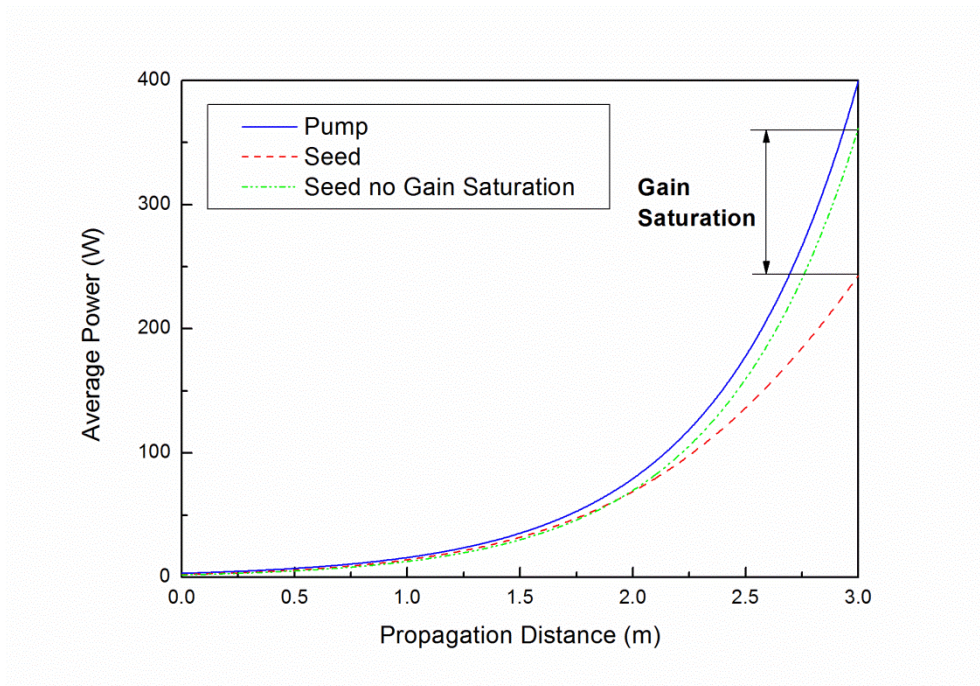


Figure 6.2 Potential output power and gain saturation with 400 W coupled pump power.

The curve without gain saturation is calculated using the traditional modeling method (which is incorrect), while the curve with gain saturation taken into consideration is calculated using the new modeling method developed in this thesis. Because of gain saturation, there is a 100-W output power difference in output for 400 W of coupled pump power. At the onset of gain saturation, the amplification process is no longer efficient. Based on our simulations we predict that optimal amplification is obtained for coupled pump power levels between 150 and 300 W for the two-stage amplifier configuration discussed in this work. Beyond this, the design configuration and gain medium parameters may need to be appropriately adjusted to obtain even better performance.

Finally, by combining theoretical modeling and simulation methods we have demonstrated that high power, high pulse energy amplifier systems can be designed and constructed. The key to success has been use of the modeling and simulation methods to guide the design of the amplifier system.

REFERENCE

- [1] M. J. F. Digonnet, ed., *Rare Earth Doped Fiber Lasers and Amplifiers* (Dekker, 1993).
- [2] R. Paschotta, J. Nilsson, A. C. Tropper, and D. C. Hanna, "Ytterbium-doped fiber amplifiers," *IEEE J. Quantum Electron.* 33, 1049-1056 (1997).
- [3] P. Russel, "Photonic crystal fibers," *Science* 299, 358-362 (2003).
- [4] F. Stutzki, F. Jansen, T. Eidam, A. Steinmetz, C. Jauregui, J. Limpert, and A. Tünnermann, "High average power large-pitch fiber amplifier with robust single-mode operation," *Opt. Lett.* 36, 689-691 (2011).
- [5] S. Pierrot and F. Salin, "Amplification and compression of temporally shaped picosecond pulses in Yb-doped rod-type fibers," *Opt. Express* 21, 20484-20496 (2013).
- [6] A. Hardy and R. Oron, "Signal amplification in strongly pumped fiber amplifiers," *IEEE J. Quantum Electron.* 33, 307-313 (1997).
- [7] A. C. Peacocka, R. J. Kruhlaka, J. D. Harveya, and J. M. Dudleyb, "Solitary pulse propagation in high gain optical fiber amplifiers with normal group velocity dispersion," *Opt. Commun.* 206, 171-177 (2002).
- [8] C. H. Henry, "Theory of Spontaneous Emission Noise in Open Resonators and its Application to lasers and Optical Amplifiers," *J. Lightwave Technol.* LT-4, 288-297 (1986).
- [9] A. Hasegawa, and F. Tappert, "Transmission of stationary nonlinear optical pulses in dispersive dielectric fibers. I. Anomalous dispersion," *Appl. Phys. Lett.* 23, 142-144 (1973).
- [10] D. Strickland, and G. Mourou, "Compression of amplified chirped optical pulses," *Opt. Commun.* 55, 447-449 (1985).
- [11] D. Hand, J. Entwistle, R. Maier, A. Kuhn, C. A. Greated, and J. DC Jones, "Fibre optic beam delivery system for high peak power laser PIV illumination," *Meas. Sci. Technol.* 10, 239-245 (1999).

- [12] T. Eidam, et al. "Fiber chirped-pulse amplification system emitting 3.8 GW peak power," *Optics Express*, Vol. 19, No. 1, pp.255-260, 2010.
- [13] K. Saitoh, Y. Tsuchida, M. Koshiba, and N. A. Mortensen, "Endlessly single-mode holey fibers: the influence of core design," *Opt. Express* 13, 10833-10839 (2005).
- [14] J.C. Knight, J. Arriaga, T. A. Birks, A. Ortigosa-Blanch, W. J. Wadsworth, and P. St J. Russell, "Anomalous dispersion in photonic crystal fiber," *Photon. Technol. Lett.* 12, 807-809 (2000).
- [15] B. Ward, C. Robin, and I. Dajani, "Origin of thermal modal instabilities in large mode area fiber amplifiers," *Opt. Express* 20, 11407-11422 (2012)
- [16] T. Sosnowski, A. Kuznetsov, R. Maynard, X. Ma, C. Zhu, I. Hu, A. Galvanauskas, J. J. Koponen, and T. S. McComb. "3C Yb-doped fiber based high energy and power pulsed fiber lasers." In *SPIE LASE*, pp. 86011M-86011M. International Society for Optics and Photonics, (2013).
- [17] Liu, Chi-Hung, Guoqing Chang, Natasha Litchinitser, Almantas Galvanauskas, Doug Guertin, Nick Jakobson, and Kanishka Tankala. "Effectively single-mode chirally-coupled core fiber." In *Advanced Solid-State Photonics*, p. ME2. Optical Society of America, 2007.
- [18] Galvanauskas, Almantas, M. Craig Swan, and Chi-Hung Liu. "Effectively single-mode large core passive and active fibers with chirally coupled-core structures." *Conference on Lasers and Electro-Optics*. Optical Society of America, 2008.
- [19] Xiuquan Ma, Chi-Hung Liu, Guoqing Chang, and Almantas Galvanauskas, "Angular-momentum coupled optical waves in chirally-coupled-core fibers," *Opt. Express* 19, 26515-26528 (2011)
- [20] S. K. Turitsyn, A. E. Bednyakova, M. P. Fedoruk, A. I. Latkin, A. A. Fotiadi, A. S. Kurkov, and E. Sholokhov, "Modeling of CW Yb-doped fiber lasers with highly nonlinear cavity dynamics," *Opt. Express* 19, 8394-8405 (2011).
- [21] R. Paschotta, *Encyclopedia of Laser Physics and Technology* (Wiley-VCH, 2008).

- [22] L. Allen and G. I. Peters, "Amplified spontaneous emission III. Intensity and saturation," *J. Phys. A* 4, 564-573 (1971).
- [23] J. Bai, and E. Towe, "Unified model for analysis of light amplification in rare-earth doped fibers," *J. Opt. Soc. Am. B*, 31, 2809-2816 (2014)
- [24] A. E. Siegman, *Lasers* (University Science Books, 1986).
- [25] E. Desurvire, *Erbium-Doped Fiber Amplifiers: Principles and Applications* (Wiley, 1994).
- [26] C. R. Giles and E. Desurvire, "Transient gain and cross talk in erbium-doped fiber amplifiers," *Opt. Lett.* 14, 880-882 (1989).
- [27] L. M. Frantz and J. S. Nodvik, "Theory of pulse propagation in a laser amplifier," *J. Appl. Phys.* 34, 2346-2349 (1963).
- [28] F. Röser, T. Eidam, J. Rothhardt, O. Schmidt, D. N. Schimpf, J. Limpert, and A. Tünnermann, "Millijoule pulse energy high repetition rate femtosecond fiber chirped-pulse amplification system," *Opt. Lett.* 32, 3495-3497 (2007).
- [29] D. J. Richardson, J. Nilsson, and W. A. Clarkson, "High power fiber lasers: current status and future perspectives," *J. Opt. Soc. Am. B* 27, B63-B92 (2010).
- [30] J. Nilsson, S. Alam, J. A. Alvarez-Chavez, P. W. Turner, W. Clarkson, and A. B. Grudinin, "High-power and tunable operation of erbium-ytterbium co-doped cladding-pumped fiber lasers," *IEEE J. Quant. Electron.* 39, 987-994 (2003).
- [31] E. Desurvire, "Analysis of gain difference between forward-and backward-pumped erbium-doped fiber amplifiers in the saturation regime," *Photon. Technol. Lett.* 4, 711-714 (1992).
- [32] E. Bourkoff, W. Zhao, R. I. Joseph, and D. N. Christodoulides, "Evolution of femtosecond pulses in single-mode fibers having higher-order nonlinearity and dispersion," *Opt. Lett.* 12, 272-274 (1987).
- [33] D. Strickland and G. Mourou, "Compression of amplified chirped optical pulses," *Opt. Commun.* 56, 219-221 (1985).

- [34] M. D. Perry, T. Ditmire, and B. C. Stuart, "Self-phase modulation in chirped-pulse amplification," *Opt. Lett.* 19, 2149-2151 (1994).
- [35] E. Desurvire, and J. R. Simpson, "Amplification of Spontaneous Emission in Erbium-Doped Single-Mode Fibers," *J. Lightwave Technol.* 7, 835-845 (1989).
- [36] T. C. Newell, .., P. Peterson, A. Gavrielides, and M. P. Sharma. "Temperature effects on the emission properties of Yb-doped optical fibers." *Optics communications* 273, no. 1: 256-259 (2007).
- [37] A. S. L. Gomes, de Araújo, C. B., Ainslie, B. J., & Craig - Ryan, S. P. "Amplified spontaneous emission in Tm³⁺-doped monomode optical fibers in the visible region". *Applied physics letters*, 57(21), 2169-2171. (1990).